DEVELOPMENT OF A DRUG DOSE-ADJUSTABLE TRANSDERMAL MICRONEEDLE SYSTEM

İLAÇ DOZU AYARLANABİLİR BİR DERİ İÇİ MİKROİĞNE SİSTEMİNİN GELİŞTİRİLMESİ

BUĞRA KAĞAN ÜNAL

ASSOC. PROF. DR. SONER ÇAKMAK

Supervisor

ASS. PROF. DR. FATİH ŞENTÜRK

Co-supervisor

Submitted to

Graduate School of Science and Engineering of Hacettepe University as a Partial Fulfillment to the Requirements for the Award of the Degree of Master of Science in Bioengineering.

2023

İthaf Sayfası

Yazarın İstediğine Bağlı olarak

ABSTRACT

DEVELOPMENT OF A DRUG DOSE-ADJUSTABLE TRANSDERMAL MICRONEEDLE SYSTEM

BUĞRA KAĞAN ÜNAL

Master of Science, Bioengineering

Supervisor: Assoc. Prof. Dr. Soner ÇAKMAK

Co-supervisor: Ass. Prof. Dr. Fatih ŞENTÜRK

July 2023, 91 pages

In the first wave of COVID-19 pandemic, it was seen that overcrowded hospitals and lack of personnels increased the risk of mortality. Dexamethasone is a corticosteroid recommended by the World Health Organization (WHO) for use in severe COVID-19 patients. Microneedle technology allows patients to take drugs painlessly with high bioavailability directly into the skin. Therefore, with the developments in this technology, this system which allows self administered without the need for any specialist will come forward in the future. Dosing systems ensure that the drug remains at the therapeutic level for a long time without side effects. Micropumps, which are defined as small devices capable of delivering the drug to the patient at a certain rate, have the ability to provide long-term therapeutic effects by adjusting the dosing on demand. When microneedle systems are combined with micropumps, more reliable, effective and hospital/expert-independent drug dosing/management can be achieved compared to traditional drug administration strategies.

Within the scope of this thesis, a micropump-assisted microneedle system with a drug reservoir, capable of dosing in the presence of a magnetic field, has been developed for the use of COVID-19 patients. Accordingly, the hollow polymeric microneedle array was produced from poly-L-lactic acid (PLLA) by solvent casting method in a single step within a suitable mold. The length, width and tip diameter (OD) of the microneedles were calculated as 1.4 ± 0.2, 0.9 ± 0.1 and 0.20 ± 0.03 mm, respectively and this system consists of 6 microneedles in a circular geometry and spaced at 1.8 mm intervals. As a result of the mechanical analysis, the failure force of the microneedles was found to be 2.9 ± 0.4 N per needle and the decrease in their length was $58 \pm 4\%$. Subsequently, to test the skin penetration abilities of the microneedles, *in vitro* studies were carried out with the skin model created from Parafilm®. In the Parafilm® test, 8 Parafilm® layers were folded on top of each other to create an artificial skin with a thickness of approximately 1 mm and it was determined to what extent the microneedles fixed to the mechanical analyzer could pierce the Parafilm® layers. It has been observed that the microneedles can effectively pierce the Parafilm® up to the 7th layer (~ 900 μm). Considering all these results, it has been shown that the microneedle array, which is capable of penetrating the skin painlessly with its length and mechanical properties, is suitable for the "poke and flow" approach for transdermal or intradermal applications.

The liquid drug reservoir was 3D printed from acrylonitrile-butadiene-styrene (ABS) with a diameter of 28 mm, a height of 8 mm, and a diameter of the filling port of 2 mm. It has been observed that the drug solution can be easily fillled into the reservoir with a hypodermic needle (21 gauge) and the fluid can be drained through the same opening. No leakage was observed in the reservoir.

Iron oxide (Fe_3O_4) particles were produced by co-precipitation to be used in the production of the magnetic membrane. Then, Fe_3O_4 particles and PDMS were mixed with a homogenizer at certain ratios (10, 20 and 30%, $w_{Fe3O4}/w_{membrane}$, %) by mass, and then coated on a glass substrate surface by dynamic spin coating method and cured at 90ºC for 3 hours. The saturation magnetization of the iron oxide particles was found to be 62.5 emu/g. The saturation magnetization of the thin magnetic membranes were measured as 5.5, 10.7 and 15.3 emu/g, respectively. The thickness of the magnetic membranes varies between 0.74 and 0.44 mm. The deflection of the membranes at applied voltages (10, 20

and 30 V) was analyzed. The resulting deflection values varied from 0.165 ± 0.014 to 1.1358 ± 0.1 mm. The amount of deflection are maximum at Fe_3O_4 ratio of 20% and minimum at 10% by mass.

Two different assembly processes were performed for the fabrication of the micropump-assisted microneedle array. The microneedle array and the reservoir were attached together by solvent bonding using dichloromethane, while the magnetic membrane was joined to the reservoir by the partial curing method. When the entire system was assembled, the total weight was measured as 4.6 g. Afterwards, the reservoir was filled with approximately 1.3 mL of dexamethasone solution and the dosing performance of the developed system at different voltages (30, 40, 50 and 60 V) was analyzed. The aqueous solution of dexamethasone 21-phosphate (0.2 mg/mL) was used as stock drug solution. For this, different voltage values (30, 40, 50 and 60 V) were applied to the system, but pumping did not occur because the deflection of the magnetic membrane alone was not sufficient. Afterwards, it was observed that the pumping was achieved by placing a cylindrical neodymium magnet of 10x1.5 mm size on the magnetic membrane. Accordingly, liquid pumping capacities ranging from 43 ± 17 to 115 ± 8 μL/s were achieved when each voltage between 30 - 60 V (10 V increment) was applied to the system alone, and between 32 ± 12 and 142 ± 45 μL/s were achieved when the system was operated in stages between 30 - 60 V (10 V increment, 2 s on, 2 s off). The system is capable of delivering a total of 52 μg dexamethasone in 16 seconds. It has also been shown that the system are capable of dosing in different volumes and perform multiple dosings according to the applied voltage values over time.

The micropump-assisted microneedle array produced in this study, may come forward as a 'proof of concept' system that patients can apply it directly on their own, adjust the drug dose, and make repeated dosing at a certain time interval. In addition, this developed system can be used successfully for other dosing applications where necessary besides dexamethasone.

Keywords: COVID 19, Microneedle, Microfabrication, Dexamethasone, Magnetic Micropump

ÖZET

İLAÇ DOZU AYARLANABİLİR BİR DERİ İÇİ MİKROİĞNE SİSTEMİNİN GELİŞTİRİLMESİ

BUĞRA KAĞAN ÜNAL

Yüksek Lisans, Biyomühendislik Anabilim Dalı

Danışman: Doç. Dr. Soner ÇAKMAK

Eş danışman: Dr. Öğr. Üyesi Fatih ŞENTÜRK

Temmuz 2023, 91 sayfa

COVID-19 pandemisinin ilk dalgasında hastanelerin aşırı kalabalık olması ve personel eksikliğinin ölüm riskini artırdığı görülmüştür. Deksametazon, Dünya Sağlık Örgütü (DSÖ) tarafından ağır COVID-19 hastalarında kullanımı önerilen bir kortikosteroidtir. Mikroiğne teknolojisi, hastaların ilaçları ağrısız ve biyoyararlanımı daha yüksek bir şekilde doğrudan deri içine salımı ile almasını sağlar. Dolayısıyla, bu teknolojideki gelişmelerle gelecekte hastaların herhangi bir uzmana ihtiyaç duymadan ilaçları doğrudan kendi başlarına alabilecekleri sistemler ön plana çıkacaktır. Doz ayarlı sistemler ilacın terapötik seviyede uzun süre kalmasını ve yan etkilerinin daha düşük olmasını sağlar. İlacı hastaya belirli bir hızda gönderebilen küçük cihazlar olarak tanımlanan mikropompalar, isteğe göre dozlamayı ayarlayarak uzun vadeli terapötik etki sağlama yeteneğine sahiptir. Mikroiğne sistemleri mikropompalar ile birleştirildiğinde geleneksel ilaç uygulama stratejilerine göre daha güvenilir, etkili ve hastane/uzmandan bağımsız ilaç dozlama/yönetimi sağlanabilir.

Bu tez çalışması kapsamında, COVID-19 hastalarının kullanımı için manyetik alan varlığında dozlama yapabilen, ilaç rezervuarına sahip mikropompa destekli bir mikroiğne sistemi geliştirilmiştir. Bu doğrultuda, içi boş polimerik mikroiğne dizisi, poli-L-laktik asitten (PLLA) çözücü döküm yöntemi ile uygun bir kalıp içerisinde tek adımda üretilmiştir. Dairesel bir geometride ve 1.8 mm aralıklarla yerleşmiş 6 adet mikroiğneden oluşan bu sistemde, mikroiğnelerin uzunluğu, genişliği ve uç çapı (OD) sırasıyla 1.4 ± 0.2, 0.9 ± 0.1 ve 0.20 ± 0.03 mm olarak hesaplanmıştır. Mekanik analizler sonucunda, mikroiğnelerin deformasyon kuvveti iğne başına 2.9 ± 0.4 N ve uzunluklarındaki azalış % 58 ± 4 olarak bulunmuştur. Devamında, mikroiğnelerin deri penetrasyon yeteneklerini test etmek için Parafilm®'den oluşturulmuş deri modeliyle *in vitro* çalışmalar gerçekleştirilmiştir. Parafilm® testinde, 8 adet Parafilm® tabakası üst üste katlanarak yaklaşık 1 mm kalınlığında bir yapay deri modeli oluşturulmuş ve mekanik analiz cihazına sabitlenen mikroiğnelerin Parafilm® tabakasını hangi katmanlara kadar delebildiği belirlenmiştir. Mikroiğnelerin, Parafilm® modelini 7. tabakaya kadar (~ 900 μm) başarılı bir şekilde delebildiği görülmüştür. Tüm bu sonuçlar göz önüne alındığında, cilde ağrısız bir şekilde nüfuz etme özelliğine sahip olan mikroiğne dizisinin, transdermal veya intradermal uygulamalar için "dürt ve akıt" yaklaşımına uygun olduğu gösterilmiştir.

Sıvı rezervuar, çapı 28 mm, yüksekliği 8 mm ve doldurma girişinin çapı 2 mm olacak şekilde akrilonitril-bütadien-stirenden (ABS) 3 boyutlu yazıcı ile üretilmiştir. Rezervuara, hipodermik iğne (21 gauge) ile ilaç çözeltisinin kolaylıkla doldurulabildiği ve yine aynı açıklıktan sıvının boşaltılabildiği görülmüştür. Rezervuarda herhangi bir sızıntı görülmemiştir.

Manyetik zarın üretiminde kullanılmak üzere Fe_3O_4 partikülleri ikili çöktürme yoluyla üretilmiştir. Daha sonra, Fe_3O_4 partikülleri ve PDMS kütlece belli oranlarda (% 10, 20 ve 30, k_{Fe3O4}/k_{Zar}, %) olacak şekilde bir homojenizatör aracılığıyla karıştırıldıktan sonra dinamik döndürerek kaplama yöntemiyle bir cam substrat yüzeyine kaplanmış ve 90ºC'de 3 saat boyunca kürlenmiştir. Demir oksit partiküllerin doygunluk manyetizasyonu 62.5 emu/g olarak bulunmuştur. Elde edilen ince manyetik zarların doygunluk manyetizasyonları ise sırasıyla 5,5, 10,7 ve 15,3 emu/g olarak ölçülmüştür. Manyetik zarların kalınlıkları 0,74 ve 0,44 mm arasında değişmektedir. Zarların, uygulanan voltaj değerlerindeki (10, 20 ve 30 V) yer değiştirmesi analiz edilmiştir. Elde edilen yer

değiştirmeler, 0,165 ± 0,014 ile 1,1358 ± 0,1 mm arasında değişmektedir. Yer değiştirme miktarları, kütlece %20 Fe_3O_4 içeren zarda en fazla, %10'da ise en azdır.

Mikropompa tabanlı mikroiğne dizisinin üretimi için iki farklı montajlama işlemi gerçekleştirilmiştir. Mikroiğne dizisi ve rezervuar, diklorometan kullanılarak çözücü bağlama yöntemiyle bir araya getirilirken, manyetik zar rezervuara kısmi kürleme yöntemiyle bağlanmıştır. Tüm sistem bir araya getirildiğinde toplam ağırlık 4.6 g olarak ölçülmüştür. Sonrasında, rezervuar yaklaşık 1.3 mL deksametazon çözeltisiyle doldurulmuş ve geliştirilen sistemin farklı voltaj değerlerindeki (30, 40, 50 and 60 V) dozajlama performansı analiz edilmiştir. Stok ilaç çözeltisi olarak deksametazon 21-fosfat sulu çözeltisi (0,2 mg/mL) kullanılmıştır. Bunun için, öncelikle sisteme farklı voltaj değerleri (30, 40, 50 ve 60 V) uygulanmış ancak manyetik zarın yer değiştirmesi tek başına yeterli olmadığı için pompalama gerçekleşmemiştir. Devamında, 10x1.5 mm boyutlarında silindirik neodyum mıknatıs manyetik zarın üstüne yerleştirilerek pompalama işleminin sağlandığı görülmüştür. Buna göre, sisteme 30 – 60 V arasında (10 V artış) her bir voltaj tek başına uygulandığında 43 ± 17 ile 115 ± 8 μL/s, 30 – 60 V arasında (10 V artış, 2 s açık 2 s kapalı) kademeli çalıştırıldığında ise 32 ± 12 ile 142 ± 45 μL/s arasında değişen oranlarda sıvı pompalama kapasitelerine ulaşılmıştır. Sistem 16 saniyede toplam 52 μg deksametazon verebilme özelliğine sahiptir. Bu veriler ışığında, sistemin uygulanan voltaj değerlerine göre farklı hacimlerde dozajlama yapabildiği ve bu dozajlamayı çoklu bir şekilde zamana göre gerçekleştirebildiği de gösterilmiştir.

Bu çalışmada üretilen mikropompa tabanlı mikroiğne dizisi, hastaların doğrudan kendi başlarına uygulayabileceği, ilaç dozunu ayarlayabilecekleri ve belli bir zaman aralığında tekrarlı dozaj yapabilecekleri bir 'proof of concept' sistem olarak ön plana çıkabilir. Ayrıca, geliştirilen bu sistem dozajlaması gerçekleştirilen deksametazonun yanı sıra diğer dozajlama uygulamaları için de başarılı bir şekilde kullanılabilir.

Anahtar Kelimer: COVID 19, Mikroiğne, Mikrofabrikasyon, Deksametazon, Manyetik Mikropompa

ACKNOWLEDGEMENTS

I would like to express my deepest appreciation to my supervisor, Assoc. Prof. Dr. Soner Çakmak for his unwavering support and guidance throughout my master's program, for his confidence, encouragement, and motivation. I would especially like to thank Dr. Soner Çakmak for introducing me to the topic of my thesis, on which I really enjoyed working. I would like to thank my co-supervisor, Dr. Fatih Şentürk for his support and motivation.

I am also grateful to Prof. Dr. Lokman Uzun for allowing me to benefit from his laboratory facilities as well as providing a friendly environment during my master studies. I am really honored to work with Biosmart Research Team. Special thanks to Tunca Karasu for his willingness to share his experiences. I would like to thank my other labmates, Sena Pişkin, Emrecan Yıldız and Ahmet Burak Berk for their support and friendship. I like to express my gratitude to Begüm Sargon for taking time to help me.

I would like to express my gratitude to the Scientific and Technological Research Council of Türkiye (TÜBİTAK), which provided financial support to my work as a scholar within the scope of the 2210-C Domestic Priority Fields Graduate Scholarship Programme.

I would also like to present my gratitude for the financial support provided by Scientific Research Projects Coordination Unit in Hacettepe University (BAP), project FKB-2022-19592.

Last but not least, I am deeply thankful to my parents and sister for their endless love, confidence and support.

TABLE OF CONTENT

LIST OF FIGURES

LIST OF TABLES

SYMBOLS AND ABBREVIATIONS

Symbols

HCl	Hydrochloric Acid
NaOH	Sodium Hydroxide
Fe_3O_4	Iron (II, III) Oxide
$FeCl_2.4H_2O$	Iron (II) Chloride Tetrahydrate
$FeCl_3.6H_2O$	Iron (III) Chloride Hexahydrate
v/v	Volume per Volume
w/v	Weight per Volume

Abbreviations

PDMS	Polydimethylsiloxane
ABS	Acrylonitrile-Butadiene-Styrene
SC	Stratum Corneum
DDS	Drug Delivery System
TDDSs	Transdermal Drug Delivery Systems
PMMA	Poly (Methyl Methacrylate)
PLGA	Poly (Lactic-co-Glycolic Acid)
PVP	Poly (Vinylpyrrolidone)
PLA	Poly (Lactic Acid)
PLLA	Poly(L-Lactide)
PVA	Poly (Vinyl Alcohol)
MEM	Micro-electromechanical Systems

N	Newton
mN	Millinewton
rpm	Round Per Minute
h	Hour
s	Second
min	Minute
V	Voltage
T	Tesla
mT	Millitesla
SEM	Scanning Electron Microscope
DSC	Differential Scanning Calorimetry
WHO	World Health Organization
FDA	Food and Drug Administration
g	Gram
mg	Milligram
µg	Microgram
ng	Nanogram
mm	Millimeter
µm	Micrometer
ml	Millilitre
UV	Ultra-violet
3D	Three-dimensional

1. INTRODUCTION

COVID 19 pandemic caused the death of almost 7 million people all over the world. Dexamethasone is a corticosteroid recommended by the World Health Organization (WHO) for use in severe COVID-19 patients. Dexamethasone can be taken by tablets or intravenous injection. While oral administration of dexamethasone has low bioavailability compared to intravenous injection. However, intravenous administration requires a medical expert and causing fear and pain for patient which may result in poor patient compliance.

Skin, the outermost layer of the body is a vital organ taking a role of protection, sensing and regulation in the body. In addition to these inborn functions, skin is also a promising site of drug delivery due to presenting a large area of administration whether to impart local or systemic effect in the body. However, stratum corneum, due to its dense integrity, forms the main barrier against the delivery of drugs into skin. Only drugs which have certain physicochemical properties are able to pass stratum corneum. There are many enhancement methods to overcome this barrier. Microneedles, one of the these methods, is used to improve transdermal and intradermal drug delivery. Microneedle technology allows patients to take drugs painlessly with high bioavailability directly into the skin. Therefore, with the developments in this technology, systems which allow self administered without the need for any specialist will come forward in the future. Micropumps are well known small devices used for controlled dosing. In this thesis, a hollow microneedle array was incorporated with electromagnetic micropump to provide adjustable dosing of dexamethasone for intradermal delivery.

In this thesis, microneedle array was fabricated from PLLA by solvent casting method. The liquid reservoir was 3D printed from acrylonitrile-butadiene-styrene (ABS). A thin magnetic membrane was fabricated from Fe_3O_4/PDMS composite by dynamic spin coating method. The microneedle array and the reservoir were attached together by solvent bonding using dichloromethane, while the magnetic membrane was joined to the reservoir by the partial curing method. In characterization studies, morphology, mechanical properties and penetration abilities of microneedle arrays were investigated.

Deflection capacity and magnetization of membranes were investigated. Lastly, dosing performance of micropump-based microneedle array was evaluated with single and multiple actuations.

2. GENERAL INFORMATION

In this part, general information related to this thesis was provided. At the beginning, the structure of skin was introduced. After that, transdermal drug delivery systems and their improvement strategies were explained. Then, microneedle technology was addressed according to structure, material and mechanisms. At the end, the features of poly lactic acid and dexamethasone were presented. In the final part, micropump systems were explained in detail with their classification mechanism, and features.

2.1. Structure and Function of Skin

Skin comprises approximately 15 % of adult human weight and covers an area of 1.5 – 2 m^2 [1]. There are many vital functions of skin for the body. Primarily, it serves as a protective barrier against ultraviolet radiation, microorganisms, chemicals and physical impacts. For the homeostasis, it takes the role in the regulation of body temperature and presents skin cells for the damaged areas. In addition, skin has different kinds of receptors providing the perception for the surrounding [2]. There are three sublayers of skin, namely epidermis, dermis and hypodermis (Figure 2.1). Each of these sublayers has distinct characteristics in terms of structural and functional aspects.

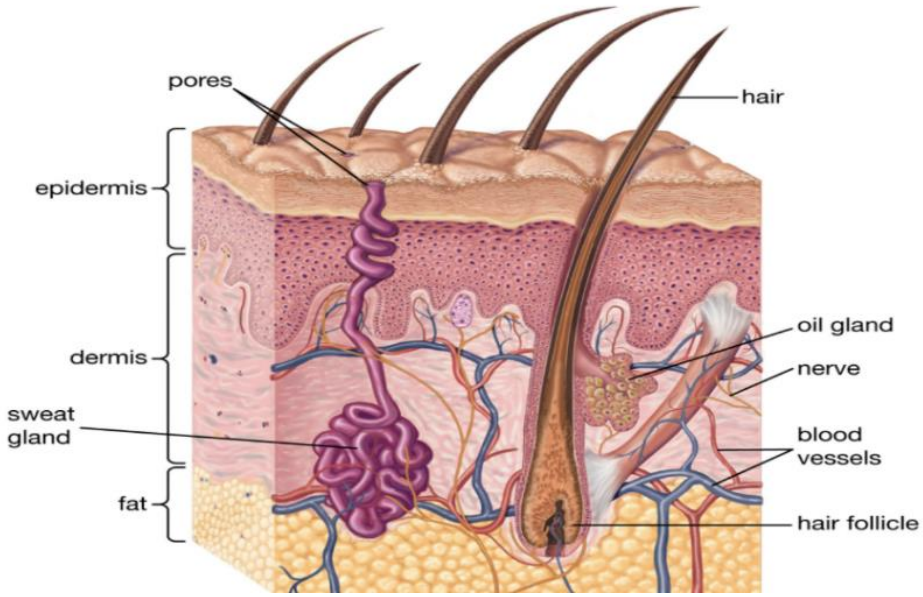

Figure 2.1. Human skin is demonstrated with its three layers and appendages [3].

2.1.1. Epidermis

Epidermis, the upper layer of skin, overlays the dermis. It includes mostly keratinocytes, but melanocytes, langerhans, merkel and stem cells are also avaliable together with keratinocytes [4]. The thickness of epidermis varies with respect to the age and sex of the individual as well as the region where it localizes throughout the body. While epidermis is the thickest on palms and soles by reaching up to 0.8 +/- 1.5 mm, it is the thinnest on eyelids with the depth of 0.05 mm [5]. Cells obtain the nutrients by diffusion due to the absence of blood vessels in epidermis. Generally, epidermis is divided into the five stacked layers based on the state of the cellular differentiation of keratinocytes, called 'Keratinization'. These layers are given below with a brief introduction as in sequence from the bottom to the top.

Stratum basale is the deepest layer of epidermis. This layer is composed of single layer columnar shaped stem cells, also called basal keratinocytes which are attached to the basal membrane with multi-protein complex called 'hemidesmosomes'. These basal keratinocytes are responsible to support homeostasis by producing keratinocytes into the body. Newly formed keratinocytes push the former ones upward through epidermis. During this movement, keratinocytes undergo distinct differentiation stages of keratinization until becoming mortar cells. In addition to keratinocytes, melanocytes and merkel cells also exist in stratum basale. Melanocytes are essential cells in the point of presenting the pigment called 'melanin' which protects the body from the adverse effects of UV radiation. Merkel cells, another existing cell in epidermis, provides the touch sensation by Piezo2-dependent transmission channels [5–7].

Stratum spinosum lies beneath stratum granulosum. Its name comes from spiky keratinocytes observed under histological examination. In the layer of stratum spinosum, keratinocytes start to keratinization. Characteristically, keratinocytes are interconnected with each other by desmosomes which contribute to the structural robustness of stratum spinosum. In addition to keratinocytes, Langerhans cells are also found in stratum spinosum. Langerhans cells are the skin immune cells, serve to induce sensitized T lymphocytes against pathogens by presenting antigen [8–10].

Stratum granulosum consists of grainy keratinocytes containing keratohyalin and lamellar granules. Keratohyalin granules are rich in histidine and cysteine, which function to

aggregate keratin filaments. Lamellar granules are secreted to extracellular space serving as a regulator for the cell integrity [7].

Stratum lucidum is a thin transparent layer, only observed in the thick areas of the skin such as palm and soles. In the layer of stratum lucidum, keratinocytes are dead and have flattened shape. This layer has a densely packed structure consisting of keratinocytes which contains the specific protein called ‘eleidin’ converted from keratohyalin. Eleidin supports to water barrier function of skin [8].

Stratum corneum (SC) is the superficial layer of the body. The average thickness of human SC varies in the range of 10 to 30 μm [11]. It is composed of corneocytes which are the form of keratinocytes that reached the last stage of cellular differentiation. Corneocytes, simply dead cells, have lack of nucleus or organelles. ‘Brick’ mortar model is commonly used in literature to explain the structure and organization of the components forming SC. Simply, ‘Brick’ stands for corneocytes, which were flattened through the differentiation. ‘Mortar’ stands for the extracellular lipid matrix consisting of lipid lamellae serving as the continuous phase of SC. Corneocytes are embedded within the intercellular lipid matrix; besides, they are linked with a glycoprotein called corneodesmosomes that contributes to the strength and function of this formed ‘brick wall’ layer. The total mass of SC consists of 70% of proteins, 15% of lipids and 15% of water. The large portion of lipids made of 50% of ceramides, 25% cholesterol and 15% free fatty acids. Stratum corneum has highly dense integrity, which efficiently prevents excessive water loss as well as keeps unwanted substances (e.g. pathogens and chemicals) away from the body [12–14]. Because of this firmly organized structure of SC, transdermal drug delivery systems have difficulties in the effective delivery as well. More detailed knowledge regarding the aspect of transdermal systems, is summarized in the following sections of this thesis.

2.1.2. Dermis

Dermis, the other main layer of skin, is located between epidermis and hypodermis. Differently from epidermis, dermis is connective tissue which includes fibroblasts as predominant cell type; furthermore, a wide range of skin components such as, sweat glands, free nerve endings, blood and lymphatic vessels are found in dermis [5, 15]. Dermis has an irregular fibrous structure composed of collagen and elastin fibers.

Collagen composes about 70% of dry weight of dermis; furthermore, the most abundant collagen type presented in unwounded skin is type I collagen [16]. While collagen fibers confer strength to skin, elastin contributes to flexibility of skin. Dermis has varied functions due to more skin components which it includes. One of those functions is the thermal regulation which is caused by the blood vessels and sweat glands. The sensation role comes along with the free nerve endings as well as other kinds of receptors. Dermis also serves as a supportive layer with its extracellular matrix (ECM) for the skin components. There are two separate sublayers of dermis, namely papillary and reticular dermis. Papillary dermis lies beneath SB. It has a loosely organized fibrous structure which is made of thin collagen and elastin fibers. Characteristically, papillary dermis extends with a finger-like ridges through epidermis. Those ridges, increasing the contact area between dermis and epidermis, enable oxygen and nutrients transferred to epidermis [17]. Reticular dermis forms the bottom layer of dermis which extends through hypodermis. Compared to papillary dermis, structural fibers of reticular dermis are thicker, densely organized, and outnumbered [18, 19].

2.1.3. Hypodermis

Hypodermis (subcutis) is the deepest layer of skin located beneath the dermis. It is a loose connective tissue attached to reticular dermis by collagen fibers [20]. Characteristically for hypodermis, it is composed of adipocytes which are organized in lobules. Hypodermis serves as an entry for systemic circulation of the substances by the blood vessels which are branched from dermis. Similarly to dermis, most of skin components are also found in hypodermis as well (e.g. blood vessels, sensing nerves, macrophages), so the functions of hypodermis is basically the same with dermis [5, 21].

2.2. Transdermal Drug Delivery Systems

Transdermal drug delivery is a method in which it targets the skin as a site of absorption of drug to impart systemic effect in a body.

2.2.1. Drug Delivery Systems

Drug delivery system (DDS) stands for the method which enables the presentation of the amount of drugs imparting therapeutic effect for targeted sites of the body [22, 23]. While

tablets, capsules and syrups are conventional examples of DDS, liposomes, nanoparticles, microneedles and micropumps are advanced systems.

There are primarily three types of drug releasing mechanisms employed by drug delivery systems, namely diffusion, erosion and swelling. In the diffusion mechanism, drug particles move randomly through the less concentrated areas due to Brownian motion. Brownian motion is an important phenomenon for the delivery of drug particles ranging from nanometre to millimetre in scale [24, 25]. Erosion mechanism is based on the physical dissolution of a drug carrier matrix (e.g. polymer) by enzymatic reactions or hydrolysis. According to the manner of the dissolution process, erosion mechanisms can be divided into the two sub-categories as bulk and surface erosion. While bulk erosion occurs homogeneously through the matrix, surface erosion, however, takes place only in the surface of the matrix [26]. Another mechanism is swelling. This mechanism relies on emergence of the channels for drug molecules to pass through, by swelling of the drug carrier matrix with fluid (e.g. water) [27]. Generally, the DDS are mostly designed with those releasing mechanisms, however, in novel drug delivery systems, magnetic field or ultrasound waves are also used to support drug release mechanisms [28, 29].

Ideally, it is expected from DDS to deliver the sufficient amount of drug to its target site, and then to produce therapeutic response; besides, DDS should function in the long term therapeutic range without causing any side effects [30]. According to the change of plasma drug level over time, the drug release profiles of DDS can be categorized as conventional, sustained and controlled. In conventional releasing systems (e.g. tablets, syrups), the drug molecules have rapidly released from systems. Due to this releasing profile, plasma drug levels also decrease rapidly, relative to other releasing systems. The main disadvantage of conventional releasing systems is that they require the administration repeatedly with short time intervals, which may lead to side effects and not sustain therapeutic plasma drug level in sufficient time to produce effective therapeutic response [31]. In sustained release systems, the drug releasing rate from the system is predetermined constant. Relatively to its conventional counterparts, those systems enable the drug molecules to be released slowly in more prolonged time by keeping their plasma concentration in the therapeutic range [32]. The controlled release systems have the zero order drug release profile, which lead to long term therapeutic

effect. These systems are advantageous to increase patient compliance and to avoid side effects of the drug [33, 34].

2.2.2. Routes of Drug Administration

Drug delivery system can be administered with a wide range of routes (e.g. oral and transdermal). The selection of the right route is related to the consideration of pharmacokinetics and pharmacodynamic properties of the drug as well as the ease of use and the convenience for patient conditions [35, 36]. According to the effect of the drug in the body, DDS can be designed to produce systemic or local therapeutic effects in the body. The common administration routes of DDSs which produce systemic effect, can be divided as parenteral and enteral routes. The main difference between them is that in a parenteral route, the drug molecules enter the systemic circulation by bypassing gastrointestinal tract. Parenteral routes (e.g. intravenous, transdermal, intramuscular) are administered through the skin. In parenteral routes, the drug molecules are not exposed to the first pass metabolism which arises through the GI tract and enter systemic circulation directly after the administration. Thus, parenteral routes are advantages over enteral routes regarding the higher bioavailability of drugs. Parenteral routes are preferred for the drug molecules, which are unable to be absorbed through GI tract and/or degrades in the harsh conditions of the GI tract (e.g. insulin). In some cases, parenteral routes can be used to produce local effects by injecting to organs. As disadvantages, parenteral routes may cause infection, pain and fear [35, 37, 38]. In enteral routes (e.g. oral, rectal, buccal and sublingual), the drug molecules enter systemic circulation by the absorption through the GI tract. The disadvantages of some enteral routes such as oral and rectal, is that drug molecules are exposed to the first pass metabolism which decreases bioavailability of the drug. Differently from oral and rectal routes, buccal and sublingual routes may be used to increase bioavailability, but only certain types of drugs, which have specific physicochemical properties such as small size and high solubility, can be administered by those routes. Enteral routes have disadvantages as resulting the lower bioavailability as well as being employed only for the limited number of drugs due to inefficient drug absorption, however, enteral routes as their advantage are considered as self-administrable, safe, cheap and offering higher patient compliance [35, 38–40]. Apart from systemic effects, DDS can be designed to produce local therapeutic effects. Local or topical drug administration routes aim to provide the concentration of the drug molecules, sufficiently enough to produce local effect at the specific site of the body. Skin and

mucous membranes (e.g. eye, mouth and nose) are the target sites of the body for the local administration. Local administration has advantages in regard to preventing side effects, being simple, non-invasive, and offering high patient compliance. Commonly, the forms of DDS such as patches, cream and spray, are used for those local routes [38, 41, 42].

2.2.3. Advancements in Transdermal Drug Delivery Systems

Drug delivery systems which benefit from the route of skin for delivery, is called transdermal drug delivery systems (TDDSs). Generally, these types of DDS are formulated with the adhesive carrier called 'patch' which has the ability of dosing in either controlled or sustained manner to produce systematic therapeutic effect [43,44]. Basically, TDDSs rely on the diffusion of the drug molecules through the epidermal layer of skin, and then the entrance to systemic circulation by the absorption from the blood vessels located in dermis [45].

Prausnitz and Langer [46] classified TDDSs into the three generations according to their development process. The first generation TDDSs depend on diffusion of the drug molecules through SC to enter systemic circulation. The pioneering products of this generation include the topical formulations (e.g. gel, spray and cream) besides transdermal patches. These systems are advantageous to improve patient compliance and increase bioavailability of the drug due to bypassing the first pass metabolism. However, due to rigid lipid structure of SC, only a limited number of drugs which are low molecular weight (<600 Da) and lipophilic (1> Log P value > 3), are appropriate for those systems. In addition, they are functional in low dosing applications. Second generation TDDSs emerged to overcome those deficiencies by employing the enhancement methods with TDDSs. Those strategies used with the second generation TDDSs, include chemical enhancers (e.g. liposome), iontophoresis and non cavitational ultrasound. Differently from previous ones, the enhancement methods in the third generation TDDSs, aim directly to SC by creating the conduits within or removing it reversibly without any damage in deeper tissue. Microneedles, electroporation sonophoresis, thermal ablation and microdermabrasion are example of these strategies. Due to that focus on SC, the third generation TDDSs enable more effective drug delivery, compared to other two generations of TDDSs [46, 47]. The following part of the thesis addresses the enhancing strategies in a detailed manner.

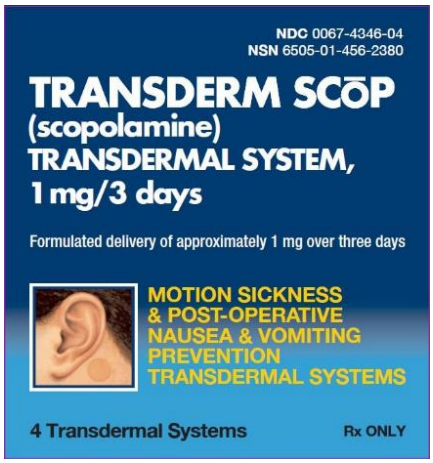

Figure 2.2. Transdermal Scōp® appeared as the first commercial product of TDDSs with the approval in 1979 by the FDA [46].

2.3. Enhancement Methods for Transdermal Drug Delivery

Another classification made on the enhancement methods, divides them into two main categories such as active and passive (Figure 2.3). All of these methods aims to increase the permeation of the skin for the drug molecules in order to enter the systemic circulation. While active enhancement methods benefit from the application of the external energy (e.g. heat, ultrasound and mechanical), passive enhancement methods are related to the improvements in the drug formulation or the modification of SC by the chemicals [36, 45, 48].

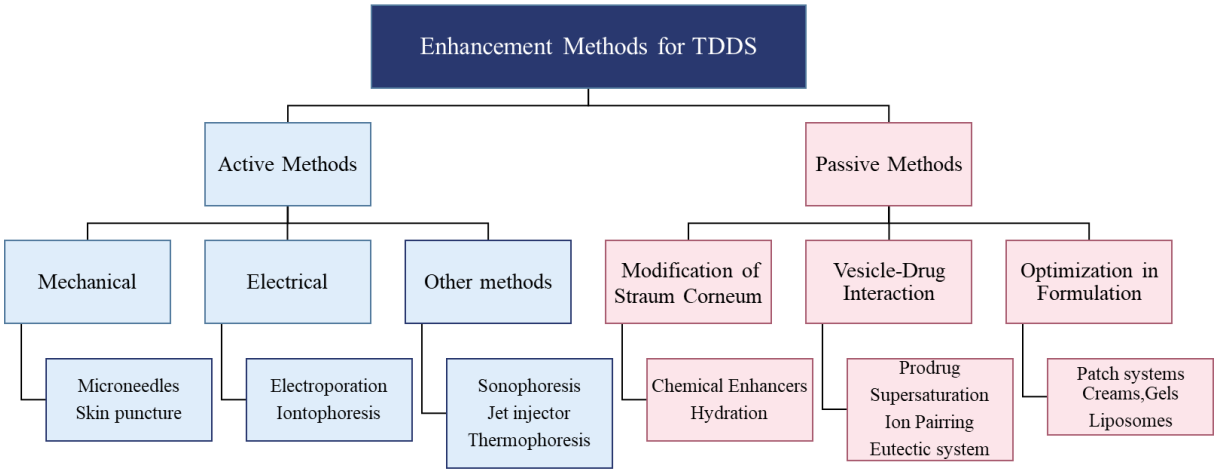

Figure 2.3. Classification of improvement methods used in TDDSs [36].

2.3.2. Passive methods

Passive methods include the strategies basically aiming to improve drug formulation or to increase the permeability of SC by applying chemicals. The penetration of drug molecules across SC follows the Fick'law as given below (Equation 2.1).

$$dM/dt = J = DC0P / \mathrm{h} \tag{2.1}$$

J is flux, the amount of drug passing through the membrane per unit area. D is the diffusion coefficient of the drug in SC. CO is the constant initial concentration of a drug. P is the partition coefficient of drug between the vehicle and SC. Lastly, h implies the thickness of SC [49]. Higuchi [50] reorganized in the form of Equation 2.2 as given below; a stands for thermodynamic activity of a drug in the formulation and γ is the effective activity of a drug in the membrane.

$$dM/dt = aD/\gamma h \tag{2.2}$$

Reversible disorganization of rigidly organized lipid structure of SC is one of the common strategies to increase diffusion coefficcient. The chemicals including alcohol (e.g. ethanol), fatty acids (e.g. oleic acid), sulfoxides (dimethyl sulphoxide), pyrrolidones (e.g. n-methyl pyrrolidone), surfactants (e.g. sodium lauryl sulphate) are the well known chemical enhancers used due to their ability to interact with structural components of SC, such as lipid bilayer and keratinized region. Apart from this role, another beneficial impacts are provided such as increasing solubility of the drug in the vehicle and the partition coefficient of drug [67, 68]. Increasing hydration level of SC results in the extension over the thickness, therefore increasing the permeability of SC [53]. Increasing thermal activity of drug is another strategy to increase the drug penetration. To achieve higher thermal activity, saturated or supersaturated drug formulation can be prepared by increasing the amount of drug or by reducing the solubility of drug in the solution. Supersaturated formulations are mostly prepared by co-solvent method, which require the addition of poor solvent into saturated drug solution [36, 67, 68].

Pro-drug approach is based on modifying chemical properties of a drug, generally by the addition of pro-moiety, which increases lipophilicity of the parent drug. Pro-drugs are inactive compounds but they have the ability of transformation to its parent form (active

drug) via chemical reactions in a body. In transdermal delivery, pro-drug approach is used to increase partition coefficient of drug, therefore increasing the penetration of active drug molecules [68, 70]. Ion pairing is similar with pro-drug approach in terms of modification of drug properties. Charged drug molecules do not penetrate SC easily. Therefore, these drugs require neutralizing by the addition of oppositely charged compound to the formulation. Differently, ion pairing is not formed by covalent bonds as being as in pro-drug approach, but electrostatic forces. Ion pairing is used to increase partition of drug in SC. After the ion pairing reached to the viable epidermis, the parent drug appears by removal of the paired ion [47, 71, 72]. As stated in the ideal solubility theory, lower melting point is consistent with good solubility. Eutectic systems can be applied to lower the melting point of the formulation, therefore increasing solubility in SC for the achievement of higher drug penetration. Simple eutectic systems are composed of two solvent which prevent each other to being crystallization, therefore lowering the melting point of the formulation [65, 68, 73]. Nanovesicles such as liposomes are used as a carrier to improve the penetration of a drug. Liposomes, the specific phospholipid-based vesicles, are commonly applied for the encapsulation of both hydrophobic and hydrophilic drugs. The purpose of using liposomes is to increase drug partition, solubility of drug in the formulation, besides distortion of lipid structure of SC. Liposomes are commonly applied in pharmacology due to those multiple beneficial effect for drug penetration as well as being biocompatible and biodegradable [46, 74].

2.3.1. Active Methods

Microneedle, sonophoresis, electroporation, iontophoresis and jet injector, thermal ablation, the well known examples of active methods, are addressed in this part.

Microneedle is a mechanical method. Basically, it is based on the formation of microchannels through epidermis by piercing (Figure 2.6a). The drug passes through these channels and then absorbed by the blood vessels in dermis [59]. Microneedles are made of a wide range of materials (e.g. polymer, metal, ceramic) with different shapes (e.g. cone, pyramid) [49, 50]. The length of microneedles varies from 25 to 2000 μm [47,61]. Due to their miniature structure, microneedles are considered as a minimally invasive and safe method in TDDSs applications. Differently from parental applications such as intravenous, microneedles are self administrable and painless, so it does not require any trained personnel and known as patient compliance. In addition, it is possible

to deliver drug molecules, which are large molecular weight (>600 Da) and hydrophilic (Log P value <1), by avoiding the first pass metabolism with microneedle-assisted TDDSs [45, 47, 49]. AdminPatch® 1500 microneedle array is one of the commercial products used successfully to increase the permeability of the skin for insulin delivery in animal experiments (Figure 2.4) [62].

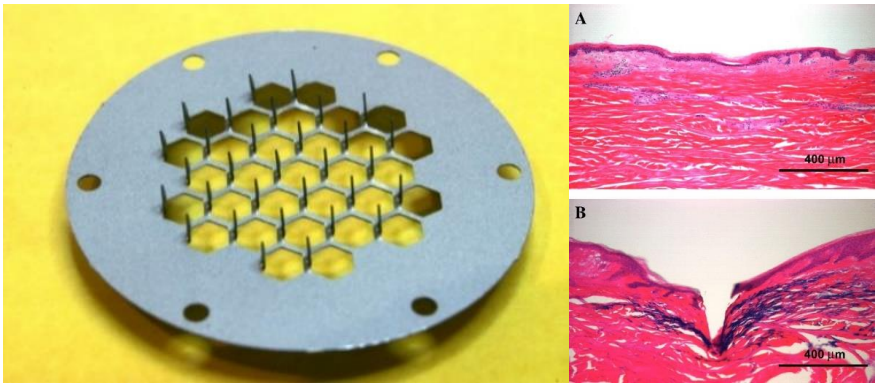

Figure 2.4. AdminPatch® 1500 microneedle array (AdminMed, Sunnyvale, CA, USA) contains 31 microneedles with the length of 1400 µm, made from medical-grade SS316L stainless steel [63]. In second figure, working principle of microneedle is shown with the given histological images of human cadaver skin, (A) untreated (B) treated with microneedle [64].

Sonophoresis is an ultrasound-assisted method (Figure 2.6b). Low frequency ultrasound (<100 kHz) is generally used for transdermal applications to increase the permeability of the skin due to being more efficient than high frequency [55, 56]. There are three basic mechanisms of iontophoresis responsible for increasing the permeation of the skin. The first one is based on the generation of microbubbles, which is induced by the pressure difference in the field of oscillating low frequency waves. Those generated microbubbles disrupt the lipid bilayer conformation of SC, either by causing a shock effect (collapsing of microbubbles) or by causing imperfection with stable microbubbles in the media. Another mechanism is acoustic streaming. Simply, ultrasound-driven flow of fluid increases the drug diffusion. The last mechanism is thermal effect. Absorbed ultrasound waves by the skin increase temperature, and this leads to increase in absorption coefficient of skin eventually. Thermal effect is limited due to damages in deep tissues [46, 47, 57, 58].

Electroporation is the well known method used in the transfection as well as TTDS. This active method relies on the formation of transient micropores on the lipid bilayer of SC, which increase the permeability of the layer (Figure 2.5). It involves the application of a high voltage electric pulse (5 to 500 V) with a short time interval (microsecond to millisecond) on the skin, in order to achieve efficient delivery without the possible damage for the deeper tissues [45, 59].

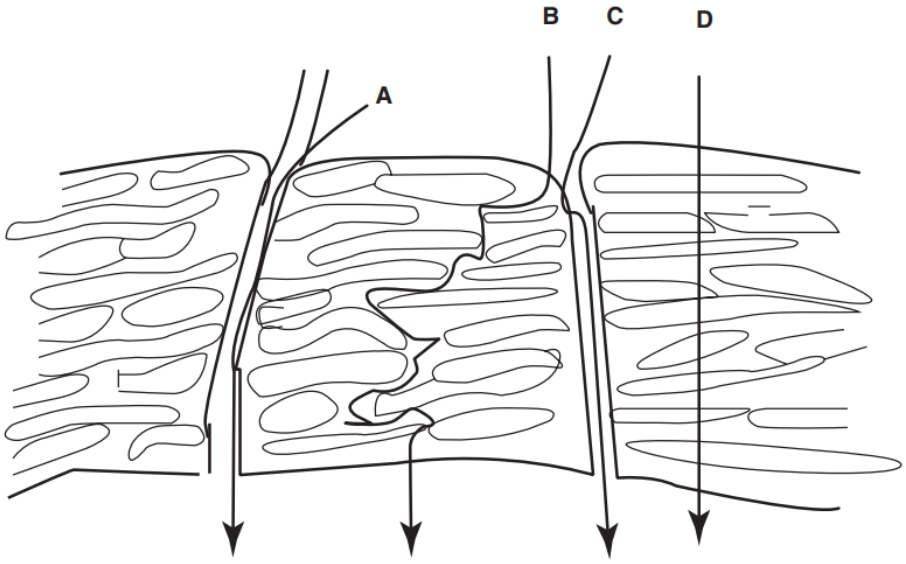

Figure 2.5. Possible drug diffusion pathways through hair follicles (A), intercellular lipid bilayers (B), the sweat ducts (C) are demonstrated, besides the formed channels (D) induced by the electroporation method [69].

Iontophoresis is another active method using low intensity electrical current to enhance TDDS (Figure 2.6d). Generally, this method requires two electrodes, namely anode and cathode, which are placed on the skin. There are three mechanisms present behind iontophoresis which are responsible for increasing the permeability of SC. The first mechanism is the transport of the charged drug molecules via electrophoresis. The second one is electro-osmosis. Simply the bulk flow induces transport for both uncharged and charged drug molecules arises from the movement of cationic ions in the media (e.g. Na+). The third mechanism is electroporation, the formation of pores in the lipid bilayer [46, 60].

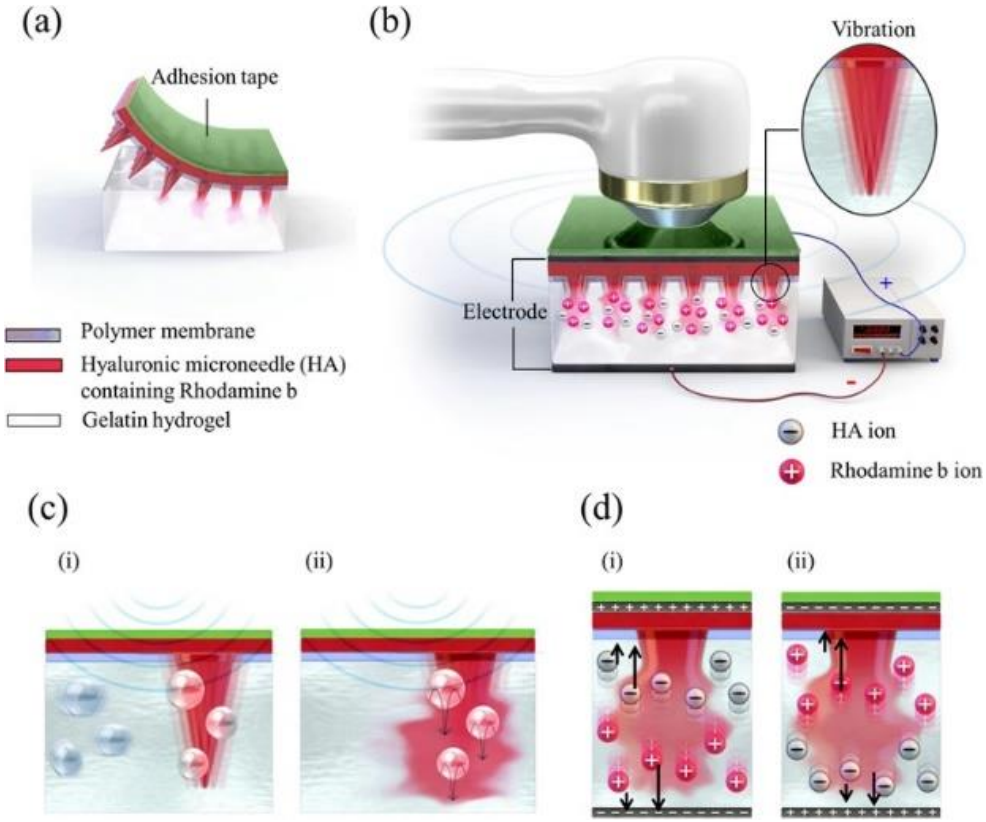

Figure 2.6. Comprehensive study includes the application of the four active methods, (a) microneedle, (b) sonophoresis (c) dissolving of needles and (d) iontophoresis [28].

Jet injectors are devices capable of generating high pressure streams for drug formulations, sufficiently enough to penetrate those into the skin. As a power source, spring and compressed gas are commonly used for rapid loading of drug compartments. Jet injectors enable it to transport liquid as well as powder formulations into the skin. They generally compromise power source, piston and drug comportment. In powder jet injectors, differently, drug particles move with compressed gas (e.g. helium) to the skin [61, 62].

Thermal ablation is based on the removal of SC by heating to increase the permeability of the skin for diffusion of the drug molecules. For the selective evaporation of SC, the heating process can be carried out with two ways: long time heating with moderate temperature (<100°C) or short time with high temperature (>100°C). The time interval varies between 1 μs and 100 ms. Laser, radiofrequency and chemical-based heating are used for thermal ablation [63, 64].

2.4. Microneedles

Microneedle technology was addressed with respect to historical and classification aspects in the following chapters.

2.4.1. History of Microneedles

In 1926, the term of 'microneedle' was used firstly by Ropert Chamber for microdissection studies related to insertion of microneedle into nucleus of echinoderm egg [75]. However, in 1971 (Application Granted in 1976), the idea of microneedle-based drug delivery system was introduced first-time with the patent by Gerstel and Place [76]. The first coated microneedle was introduced with the patent in 1974 (Application Granted in 1975) by Pistor Michel Louis Paul [77]. In 1998, Henry et al. [78] published first microneedle study for the literature, in which microneedles were produced by black silicone method. This study was important not only for being the first published manuscript but also proof of concept by showing the increase in the permeability of skin for calcein within *in vitro* as well as showing that it is painless method within *in vivo*. In 2002, Mikszta et al. [79] used microneedles for the delivery of naked plasmid DNA, which was the first report for genetic materials. In 2003, the delivery of macromolecules; insulin and albumin as well as nanoparticles; 100 nm sized latex beads were reported first-time by solid and hollow microneedles by McAllister et al.[80]. In 2005, sugar-made microneedles appeared as the first reported dissolving microneedles by Miyano et al.[81]. In 2012, the first hydrogel forming microneedles were reported by Donnelly et al. [82]. Different area as sampling from biological fluid (dermal interstitial fluid) by microneedles is introduced for glucose monitoring in 2015 by Wang et al. [83]. Also, in the same year, microneedle containing roller was used for collagen induction therapy and reported to improve skin texture, which became the first cosmetic study in the literature by Fernandes [84].

2.4.2. Classifications of Microneedles

In literature, microneedles are classifed with different aspects according to the alignment of microneedles, materials and drug delivery approaches.

2.4.2.1. In-plane and Out-of-plane Microneedles

One of the common classification is made on the alignment of microneedles on substrate. The two types of microneedles are included in this classification; 'in-plane' and 'out-of-plane' (Figure 2.7). The difference is that while in-plane microneedles are vertically aligned to the substrate, out-of-plane microneedles are parallelly aligned to the substrate resembling fork structure [85]. In-plane microneedles have a lack of needle density and are fragile relatively to out-of-plane. It is easier to manipulate the length and shape of microneedles. In-plane microneedles are produced from metals (e.g. stainless steel and titanium) and silicon with etching and laser cutting methods. Out-of-plane microneedles have denser, robust, furthermore versatile in materials and production methods according to the reports in literature. Generally, since out-of-plane microneedles are denser for needles, they are used for drug delivery or fluid. However, it is harder to achieve microneedles with high aspect ratio. [85–88].

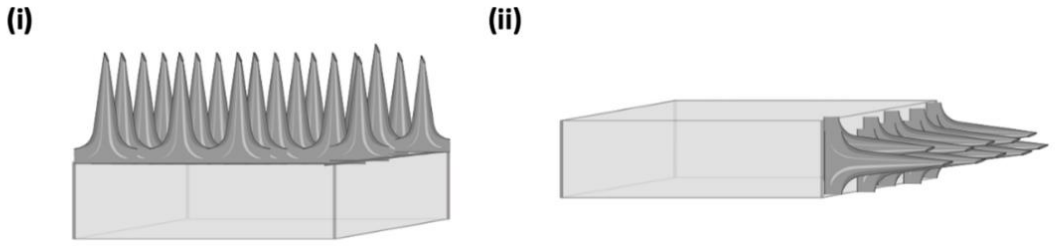

Figure 2.7. Out-of-plane (i) and in-plane microneedles (ii) [85].

2.4.2.2. Materials in Microneedle Fabrication

Microneedles can be produced from various materials such as silicon, metal ceramic, glass, and polymers. Material selection is one of the important criteria; it should have sufficient mechanical properties to penetrate the skin as well as biocompatible, cost-efficient and less corrosive [89,90].

Silicon

Silicon is anisotropic crystalline material, commonly involved in the fabrication of microelectromechanical systems due to its various advantages [91]. The Young's modulus of silicon varies between 50 GPa and 180 GPa with respect to orientation of crystalline lattice [90, 92]. The first reported microneedle was made of silicon using dry etching by

Henry et al. [78]. In this study, 20 by 20 solid microneedle array (the length of 150 μm and base diameter of ≅ 80 μm) were produced with deep reactive ion etching on silicon substrate. Chromium as masking material was deposited on silicon, then patterned into dots by UV-photolithography. Silicon with the patterned chromium was subjected to deep reactive ion etching (fluorine/oxygen was used). Microneedles were formed in the areas protected by chromium [78]. Dervisevic et al. [93] produced silicon microneedles using UV-photolithography and deep reactive etching (≅ 9500 microneedle per cm^{-2}, the lenght of ≅ 250 μm and base dimeter of ≅ 50 μm) for glucose monitoring. O'Mahony et al. [94] produced hollow silicon microneedles (the length of 500 μm and aspect ratio of ≅ 1.5) with the incorporation of wet etching, dry etching and photolithography. In the study, the patterning of deposited front and back sides of silicon wafer was achieved by dry etching and photolithography methods. Then, wet etching with KOH was applied to front and back sides subsequently to achieve convex corner undercut and bore formation inside the microneedle. Aluminium was used to stop etching after the bore formation. Lastly, glass reservoir has the volume of 1.1 μL, etched in 49% HF acid for the incorporation with hollow silicon microneedles (Figure 2.8) [94]. As advantages, silicon has sufficient physical properties for penetration; furthermore, the production methods allow to precise geometry for microneedles. However, poor biocompability, high-cost and complex production process as well as brittleness which may lead to the fracturing of microneedles inside the skin, are the primary drawbacks of silicon [90, 95, 96].

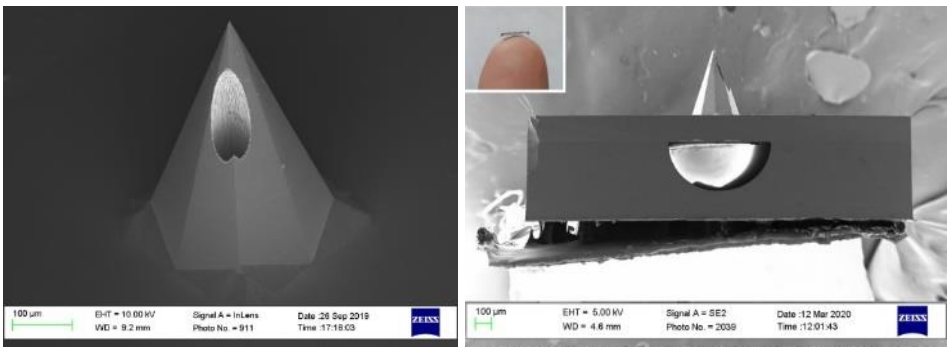

Figure 2.8. Scanning electron microscope images of a hollow silicon microneedle. Left image shows single silicon microneedle whereas right image represents the microneedle with its reservoir [94].

Metal

Metals, are commonly used in hypodermic needles (stainless steel) and medical products such as implants (e.g. titanium and its alloys). Up to date, the various kind of metals was used to produce microneedles, such as stainless steel, titanium, palladium, nickel, alloys, and gold. But, stainless steel and titanium are generally used for metallic microneedles [90, 95, 97]. Direct metal laser sintering, laser cutting, laser ablation, etching techniques, electrodeposition, hot embossing, metal injection molding are production methods of metallic microneedles [98]. Li et al. [99] produced porous titanium microneedles (the length of ≅ 500 μm, porosity of 30.1%, average pore diameter of 1.3 μm) using metal injection molding (Figure 2.9). Polydimethylsiloxane (PDMS) was used to transfer negative mold for titanium slurry which forms master microneedles by filling the mold. Finally, titanium microneedles were exposed to metal sintering to achieve porous titanium microneedles [99]. Metal has sufficient mechanical properties for skin penetration.

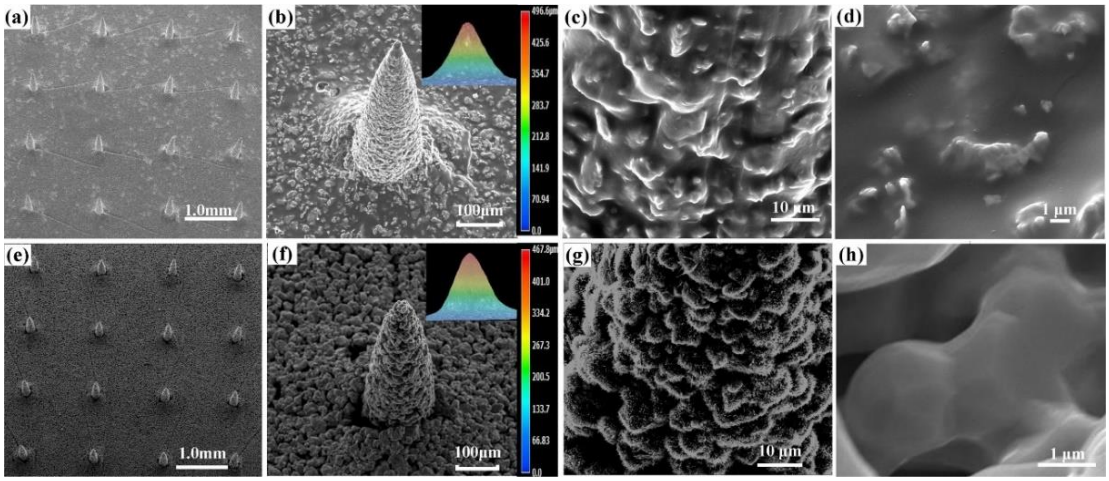

Figure 2.9. Scanning electron microscope images of titanium microneedles (a-d) and porous titanium microneedles (e-h) [99].

Compared to material of silicon, metals have higher toughness, which make metals less likely to be fractured inside the skin. Besides, some metals offer good biocompatible such as stainless steel grade 316L and titanium alloys [95,97]. Corrosion rate is high for some metals (e.g. stainless steel) so titanium alloys may be preferred instead of the others. In addition, some metals (generally nickel) are allergic for humans, so the selection of the type of metal should be evaluated carefully for microneedle fabrication [100].

Ceramic

Ceramic is also used for the production of microneedles. Alumina (Al_2O_3) and zirconia (ZrO_2) as well as novel composite material, Ormocer® (organically modified ceramic) are ceramics commonly used for microneedle fabrication. Micromolding and two-photon polymerization are the methods used to produce ceramic microneedles [101–103]. Bystrova et al. [104] produced ceramic microneedles (the lengths of microneedles are 560 μm in Figure 2.10a-e and 300 μm in Figure 2.10f-i) using micromolding. Simply, the silicon master was produced by photolithography and etching processes. Polydimethylsiloxane replicate was achieved from silicon master, then used to achieve the second PDMS replicate, which was used as negative mold for the casting of ceramic slurry. After the sintering process, ceramic microneedles were achieved [104]. Ceramics such as alumina and zirconia are biocompatible and corrosion resistant [97, 105, 106]. In addition, it is possible to achieve desired shapes of microneedles with the methods discussed above. However, alumina microneedles were shown to be brittle under tensile stress with manual application [104]. Zirconia has higher fracture toughness relative to alumina, so the combination of those ceramics may be used for the production of microneedles [101].

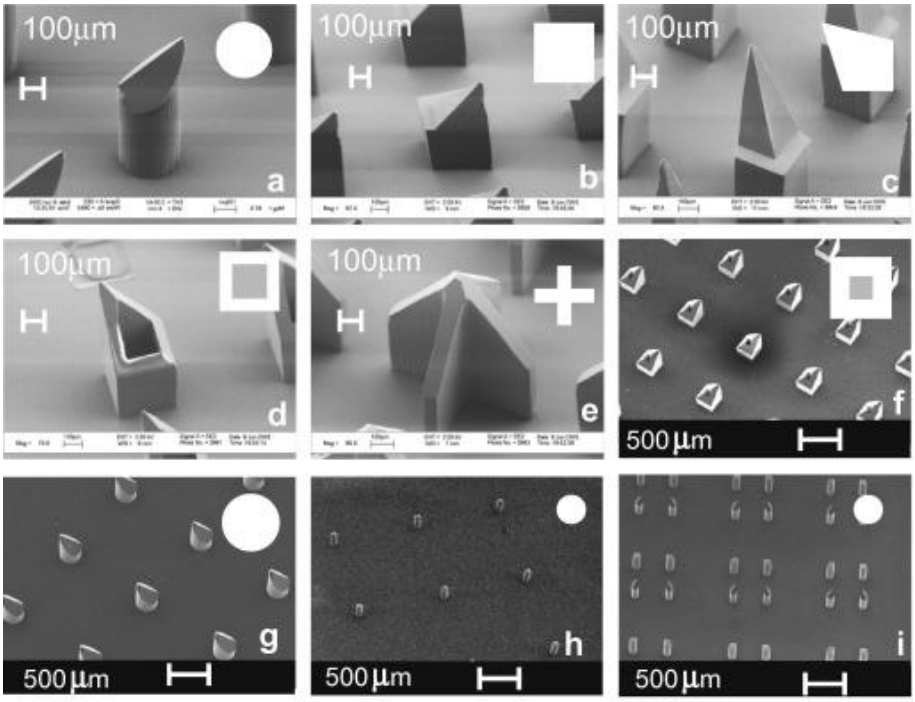

Figure 2.10. Scanning electron microscope images of the different shapes of ceramic microneedles produced with micromolding method [104].

Glass

Glass microneedles also present in literature. Generally, pulling pipette is applied to produce glass microneedles, which are hollow used for infusion studies. [64,107,108] Glass takes advantage of inert, and sufficient mechanical properties as well as easy sterilization due to its endurance for high temperature and pressure [96,109]. Silica glass is brittle (the value of fracture toughness close to ceramics), so has potential to break off into the skin which may result in pain and silica granulomas [90,110]. In addition, pulling pipette method is time-consuming and requires intense optimization [96,111]. Borosilicate glass may be considered in microneedle studies due to being more elastic and biocompatible relatively to silica glass [89,90]. Gupta et al. [107] achieved borosilicate microneedles (the lengths of 1000 μm, tip angel of 30°) from borosilicate glass pipettes by pulling pipette method using micropipette puller and beveler (Figure 2.11). These microneedles are used for the delivery of insulin to Type 1 diabetic patients.

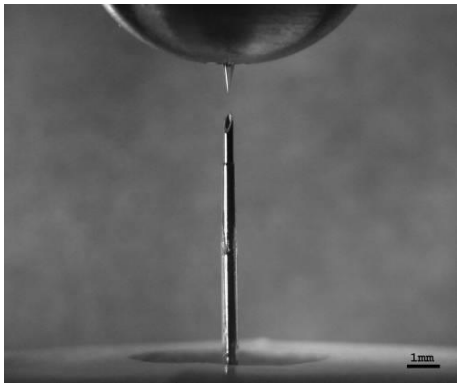

Figure 2.11. Size comparison between Single hollow borosilicate microneedles (top) and subcutaneous insulin catheter (9 mm) [107].

Polymer

Polymers are drawing interest for microneedle production due to their superior features to the materials discussed above. Considering economic and safety aspects, polymers have many advantages such as allowing easy and inexpensive large-scale production as well as being biocompatible, biodegradable, resistant to corrosion and flexibility [112, 113]. However, polymeric microneedles suffer from lower mechanical properties which may result unsuccessful skin penetration [114]. There are various kinds of polymers used in the literature for the production of microneedles such as poly (methyl methacrylate)

(PMMA) [115], poly (lactic-co-glycolic acid) (PLGA) [116], poly (vinylpyrrolidone) (PVP) [117], poly (lactic acid) (PLA) [118], poly (vinyl alcohol) (PVA) [119] , hyaluronic acid (HA) [120], polysaccharides (e.g. maltose and chitosan) [121], silk fibroin [122]. Micromolding, droplet-born air blowing, micro-electromechanical systems (MEMS) based techniques, additive manufacturing (3D printing) are the methods used to produce polymeric microneedles [95].

Micromolding is a well known method to produce polymeric solid and dissolving besides, ceramic microneedles. Conventionally, micromolding requires the negative mold (generally made of PDMS) to be filled with the polymer melt or polymer solution (in this case method also called solvent casting in literature). Solidification step takes place by the evaporation of solvent, polymerization in mold or lowering the temperature [95, 118, 123–128]. In addition to centrifugation and vacuuming steps, atom spraying and piezo-based inkjet printing can also be used to fill microcavities inside a mold [129, 130].

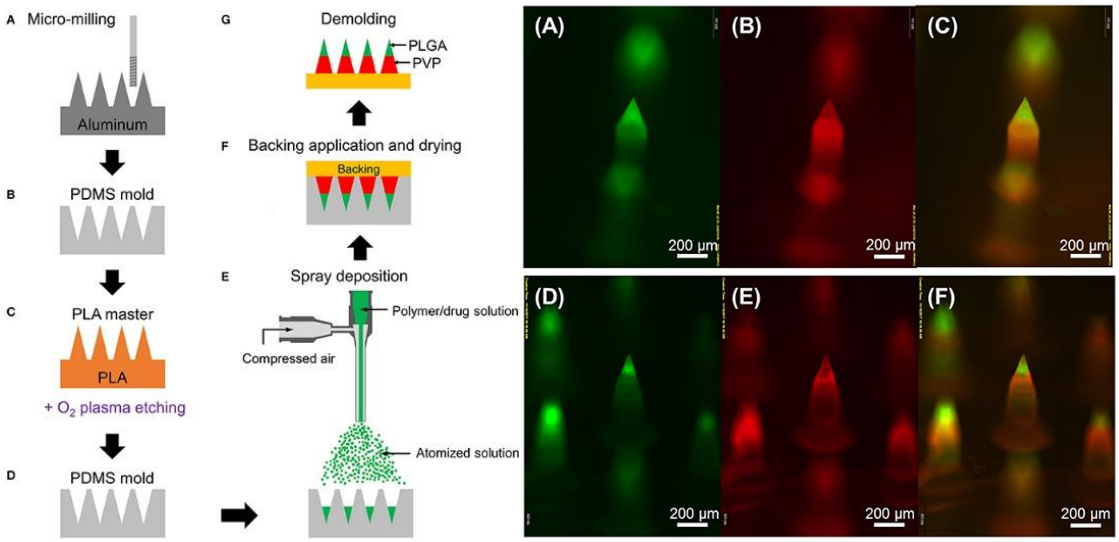

Figure 2.12. Schematic representation of the micromolding process (left) and multilayered microneedles fabricated (right) (green and red fluorescence represents PLGA and PVP, respectively) [131].

Kim et al. [131] produced multilayer microneedles with obelisk shape, which consists of PVP and PLGA, by micromolding method (Figure 2.12). Master mold was fabricated from aluminum by micromilling. First negative PDMS mold was achieved from the master and then filled with PLA melt. The PLA master was exposed to dry etching to

sharpen tips. Second female mold was achieved from this PLA master. Atomized spray technique was applied to fill the second negative mold with a drug containing PVP solution and PLGA, respectively. After the incorporation of the backing layer, the solidified microneedle array was removed from the second negative mold [131]. Micromolding takes advantageous of being simple and cost-efficient method for the large scale production [102, 132]. As disadvantages, drug loss during molding and time-consuming multi-step can be given [133].

Droplet-born air blowing (DAB) is a drawing-based lithography method, first introduced by Kim et al. [134] This method basically relies on the drawing of the polymer droplet upward by physical contact of the moveable probe, air blowing step for solidification of shaped polymer droplet and separation from the neck side of the two attached microneedles, respectively. As advantages, DAB prevents drug loss resulting from micromolding and offers the platform to produce the microneedles fastly in gentle conditions [95,134]. Kim et al. [134] produced insulin containing dissolving microneedles from the polymers of PVP, carboxymethyl chitosan (CMC) and hyaluronic acid (HA) within less than 10 min with the condition of 4–25°C. Comparison of mechanical properties for materials addressed in the section, was given in Figure 2.13.

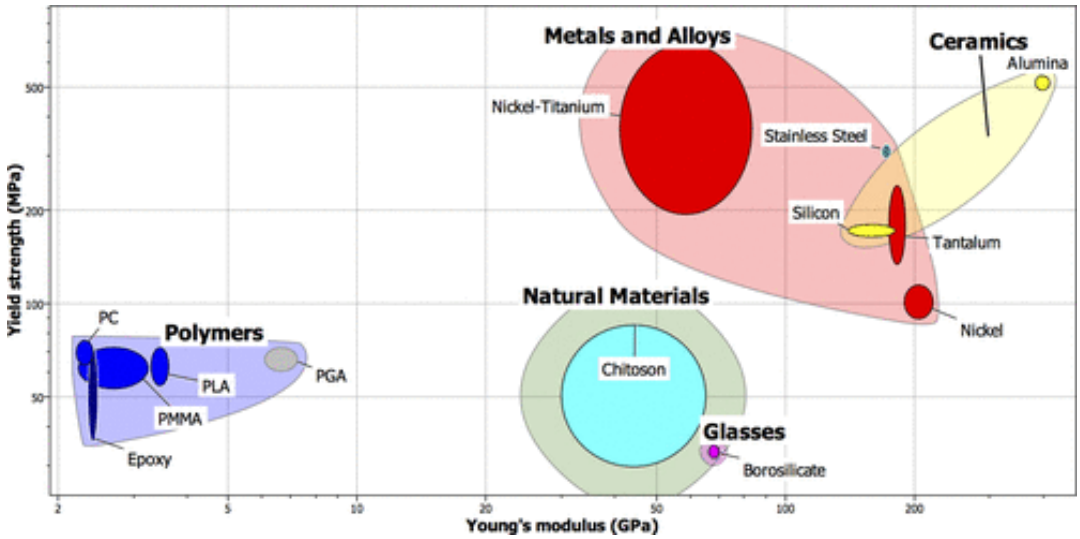

Figure 2.13. Mechanical properties of different types of materials used for microneedle fabrication [135].

MEMS based techniques including the following steps of deposition, patterning and etching are used to produce microneedles. Deposition is the thin film formation on substrate carried out via chemical or physical vapor- based deposition as well as spin coating. Patterning is carried out with photolithography (UV exposure). Etching is a development step using dry or chemical etching. MEMS based fabrication enables the production of hollow and solid microneedles with high precision in geometry, but it is an expensive method and requires clean room facility. Polymeric microneedles made of SU-8 are produced with MEMS based techniques [90, 95, 97].

2.4.2.3. Drug Delivery Approaches

Another classification is made on drug delivery approaches which require five different types of microneedles (Figure 2.14), each of which was addressed in this section by highlighting polymeric microneedles.

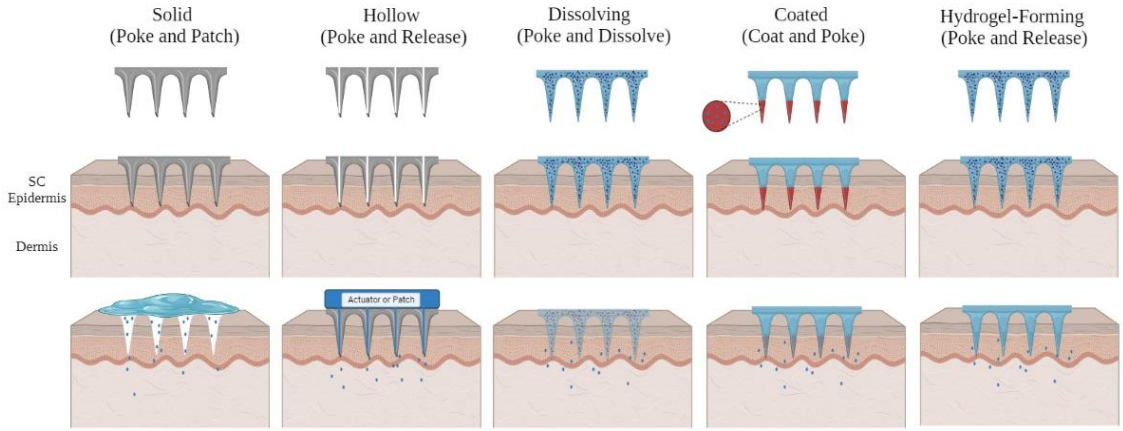

Figure 2.14. Microneedle drug delivery approaches (it is created in Biorender.com).

Solid

Solid microneedles function in a way of poke and patch approach which aims to create micro-channels through the SC by piercing to get the skin ready for the topically application of the drug-loaded patches or creams. Not surprisingly, first microneedle studies of transdermal delivery was carried out with solid microneedles due to the simplicity of this approach [78, 96, 102]. Li et al. [118] produced PLA made conical solid microneedles (the length of 600, 700 and 800 μm) by micromolding method.

Polydimethylsiloxane negative mold was created by laser drilling. Melt casting of PLA pellets was carried out by heating and vacumming (200°C, -85 kPa) [118].

Dissolving

These types of microneedles are produced from biodegradable or water-soluble polymers. They function in a poke and dissolve approach in which microneedles dissolve inside the skin after their penetration. Drug molecules are encapsulated in the polymer which forms the microneedles, so drug molecules are released as long as microneedles dissolve. That is why, drug delivery profile depends on the rate of dissolution or degradation of microneedles. Generally, the micromolding method is used to produce dissolving microneedles [102].

Coated Microneedles

Coated microneedles have a drug containing layer on the surface of microneedles. These types of microneedles function in a way of coat and poke approach in which solid microneedles are coated, and then, penetrated to the skin. Coating layer dissolves and releases drug molecules [102].

Hydrogel-forming

Hydrogel-forming microneedles rely on a poke and release approach. Microneedles are made of cross-linked polymer. After the penetration, microneedles swell due to the intake of interstitial fluid. Swelling forms the conduits inside the polymer, which enables drug molecules to pass through and released [102].

Hollow

Hollow microneedles are the miniature form of hypodermic needles. These types of microneedles using poke and flow approach, have a lumen inside the shaft together with tip or side opening holes, which enable the passage of drug molecules into the skin. Actuator (e.g. micropump and injector) is commonly used with hollow microneedles for the infusion. Delivery of the large amount of drug is possible with hollow microneedles. However, due to relatively more complex structure than other type of microneedles, hollow microneedles are generally produced with MEMs based techniques, which require expensive and multi-step fabrication [102].

Table 2.1. The list of different types of polimeric microneedles with their production methods.

Authors and year	Material	Type	Method	The use of purpose	References
Ju et al. 2020	PMMA	Hollow-Coated	Micromolding (Casting polymerization)	Blood glucose level monitoring	[115]
Pawley et al. 2021	PLGA	Solid, Dissolving and Coated	Micromolding (Solvent Casting)	Intracochlear delivery of dexamethasone	[116]
Ramadon et al. 2023	PVP	Dissolving	Micromolding (Solvent Casting)	The delivery of lidocaine hydrochloride	[117]
Kim et al. 2013		Dissolving	Droplet-born air blowing	The delivery of insulin	[134]
Li et al. 2017	PLA	Solid	Micromolding (Melt casting)	Pretreatment for insulin delivery	[118]
Oh et al. 2022	PVA	Hydrogel-forming	Micromolding	Microneedle Patch	[119]
Castilla et al. 2021	Chitosan	Dissolving	Micromolding	The delivery of meloxicam for cattle	[121]
Wang et al. 2019	Silk fibroin	Hydrogel-forming	Micromolding (Solvent Casting)	The delivery of insulin	[122]

2.5.3. Poly Lactic Acid (PLA)

Poly lactic acid is a biodegradable aliphatic polyester obtained from natural feedstocks (e.g. corn and sugarcane) or by the process of recycling (Figure 2.15). In 1970, PLA was approved by the US Food and Drug Administration (FDA) to be used in the applications

involving its interaction with body fluid. It has two isomers as L-lactide and D-lactide [136]. Isomeric compounds of PLA have their own distinct properties which is given in Table 2.2. It is biocompatible and has attractive mechanical properties (efficient Young's modulus and high toughness), which lead to be used in microneedle production [118].

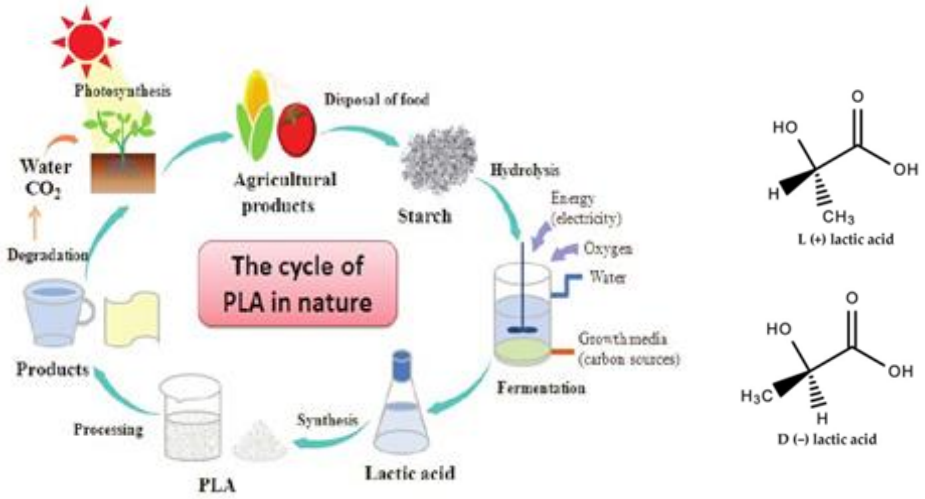

Figure 2.15. The cyle of PLA in nature and its isomers [136].

Table 2.2. Physicochemical properties of PLA.

Properties	Poly(L-lactide) (PLLA)	Poly(D-lactide)	Poly(D-L-lactide)
Solubility	All of these are soluble in benzene, chloroform, tetrahydrofuran etc. but insoluble in ethanol, methanol as well as aliphatic hydrocarbons.		
Crystaline Structure	Semi-crsytalline	Crystaline	Amorphous
Melting Point, Tm (°C)	170~180	170~180	No melting
Glass Transition point, Tg (°C)	50-60	55-60	50-60
% Fracture strain	20-30	20-30	Variable

2.6. Micropump Systems

Micropumps, the miniature devices, are capable of pumping fluid or liquid in small volumes ranging from microscale to nanoscale. Micropumps are used with a wide range of applications such as drug delivery, micro analysing, and the propulsion of space crafts.

2.6.1. Classification

Micropumps are divided into two primary groups as mechanical (displacement) and non-mechanical micropumps (Figure 2.16). Mechanical pumps have a moving part such as an oscillating diaphragm or rotor, which exerts pressure on the fluid for pumping. Non-mechanical pumps benefit from electrical or magnetic induction of fluid as well as chemical processes and ultrasonic driven flow.

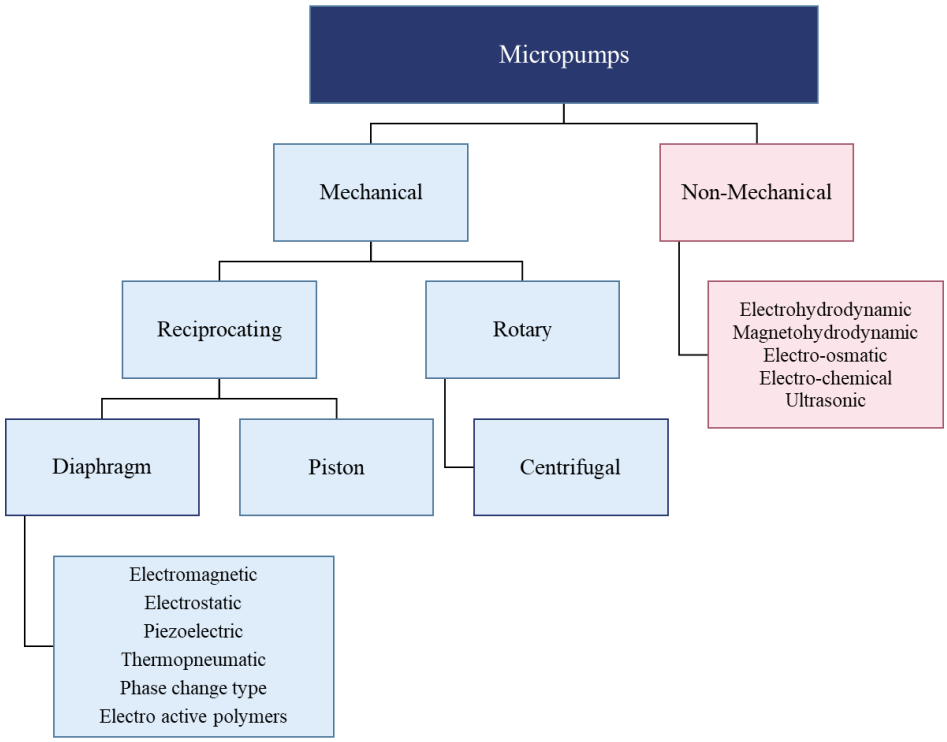

Figure 2.16. Classification of micropumps [137].

According to the action of moving parts, mechanical micropumps are divided into two sub-categories: rotating and reciprocating. In rotary types, the pumping of fluid occurs by the circulation of the rotor. In reciprocating types, there is a diaphragm or piston that makes the action of oscillation for pumping [137].

2.6.2. Diaphragm/ Membrane- Based Micropumps

In this part, micropumps using diaphragm/ membrane were addressed in the scope of their mechanism and properties.

2.6.2.2. Piezoelectric Micropumps

Piezoelectric materials have the ability of converting electrical energy to mechanical strain and conversely. This property, called 'Piezoelectric effect', makes these materials to be used in micropump systems. In these systems, piezoelectric material is sandwiched between two flexible material (e.g. PDMS) to form diaphragms. Oscillation of diaphragm occurs by application of electrical energy. Piezoelectric micropumps enable fast response and large actuation, but deflection is low and requires high voltage [137,138]. The transduction effectiveness of these piezoelectric actuators can be expressed by the piezoelectric coupling factor which is the ratio of the converted energy to the supplied energy is given below (Equation 2.3).

$$k^2 = \frac{U_{converted}}{U_{supplied}} \tag{2.3}$$

where, k^2 is piezoelectric coupling factor.

2.6.2.3. Electrostatic Micropumps

Electrostatic micropumps are another type of diaphragm/ membrane-based pumping systems. The principle of these micropumps is based on the electrostatic attraction forces (also known Coulomb attraction force). In these systems, there are two electrode plates: one is attached on a flexible diaphragm and the other one is located parallel to the first one. There is an air gap between them. Applying electrical potential leads to the attraction of the plates and then the deflection of diaphragm as a result. Electrostatic micropumps take the advantage of requiring low energy and fast response to operate. However, the deflection is low in these systems [137, 138].

The attraction force between two plates, can be expressed by Equation 2.4 given below.

$$F = \frac{dW}{dX} = \frac{1}{2}(\kappa A \frac{V^2}{X^2}) \tag{2.4}$$

Where, F is attraction force (N), W is the stored energy (J), X is the distance between two plates (m), κ is relative permittivity, A is area of the plates (m^2), V is the applied voltage (V).

2.6.2.4. Thermopneumatic and Phase Change Type

The operating principle of thermopneumatic micropumps is based on thermal expansion of air, which imparts the pressure on the diaphragm. The heater is used to cause thermal expansion of air. Similarly to thermopneumatic systems, phase-change type micropumps rely on the gas pressure, but firstly phase-change of liquid to gas is required. For these systems, in some cases, the body may serve as an actuator itself. For example, methyl perfluoropropyl ether passes to the gas phase in the temperature of the skin. These two systems enable the high deflection on the diaphragm with the low applied voltage. However, they are slow response systems, which reduce the frequency of pumping [137].

2.6.2.5. Electro Active Polymers

Electro active polymers have the ability to change their shape under the electrical field. During the change of their shape, the volume of the liquid reservoir is reduced, so pumping the liquid out. Ion conductive polymer film and dielectric elastomers are electro active polymers, which are used in micropump systems. Electrode plates were used for the actuation. Ion conductive polymer film operates in low voltage (2-5V) and fast response is possible, but the production of these polymers is difficult. Dielectric elastomers require a high voltage to operate (3-4500 V). Commonly, fast response and high deflection are the advantages of the electro active polymers[137, 139].

2.6.2.1. Electromagnetic Micropumps

In this part, micropumps systems using electromagnetic actuation for drug delivery were highlighted. Electromagnetic actuation relies on the oscillation of diaphragm or membrane by magnetic forces (also known as Lorent forces) which are created by electromagnetic induction. The relation between the exerted magnetic field and force by electromagnet is given with Equation 2.5 below.

$$\vec{F} = \vec{I}L \; x \; \vec{B} \tag{2.5}$$

where, F is force (N), I is current (A), L is lenght of coil (m) and B is magnetic field (T).

These devices commoly include diaphragm, liquid reservoir (chamber) and actuator. The number of diaphragm and reservoir could vary according to the design of process. For diaphragm, permanent magnet is embedded into flexible material (e.g. PDMS) or magnetic composite can be used. Electromagnetic micropumps have such advantages as high force/deflection and fast response. However, requiring high voltage is the main disadvantage [137–139].

Jayaneththi et al. [140] produced a micropump device which has one diaphragm (made of iron-PDMS composite) and two chambers (the reservoir volume of 0.5 mL). The device includes a stainless steel microneedle with a length of 1000 μm for pumping out water. Commercial magnetic pulser was used as an actuator. In that study, zero-order delivery was achieved at 108 ± 2.6 μL/min and 9.07 ± 0.28 μL/min.

2.6. Dexamethasone for COVID-19 treatment

Dexamethasone is a corticosteroid drug used in the treatment of COVID-19 due to its anti-inflammatory and immunosuppressive effects [141]. It is recommended by the World Health Organization (WHO) for the treatment of COVID 19. Dexamethasone can be taken by tablets or intravenous injection. Six mg of dexamethasone is recommended intravenously for adult COVID 19 patients once a day.

3. MATERIALS AND METHODS

In this thesis, it was aimed to develop a micropump based microneedle array for the benefit of COVID-19 patients. In this direction, a hollow polymeric microneedle array was fabricated from PLLA by solvent casting method. For actuation of the micropump, a thin magnetic membrane was fabricated from PDMS / Fe_3O_4 particles with a hand-made spin coater. Fluid reservoir was 3D printed from ABS polymer. Before the assembly of these 3 components (microneedle array, membrane and reservoir), characterization studies were conducted for each component. After the assembly of all components, dosing performance of a micropump system was investigated. The main experimental steps in this thesis were schematically summarized in Figure 3.1.

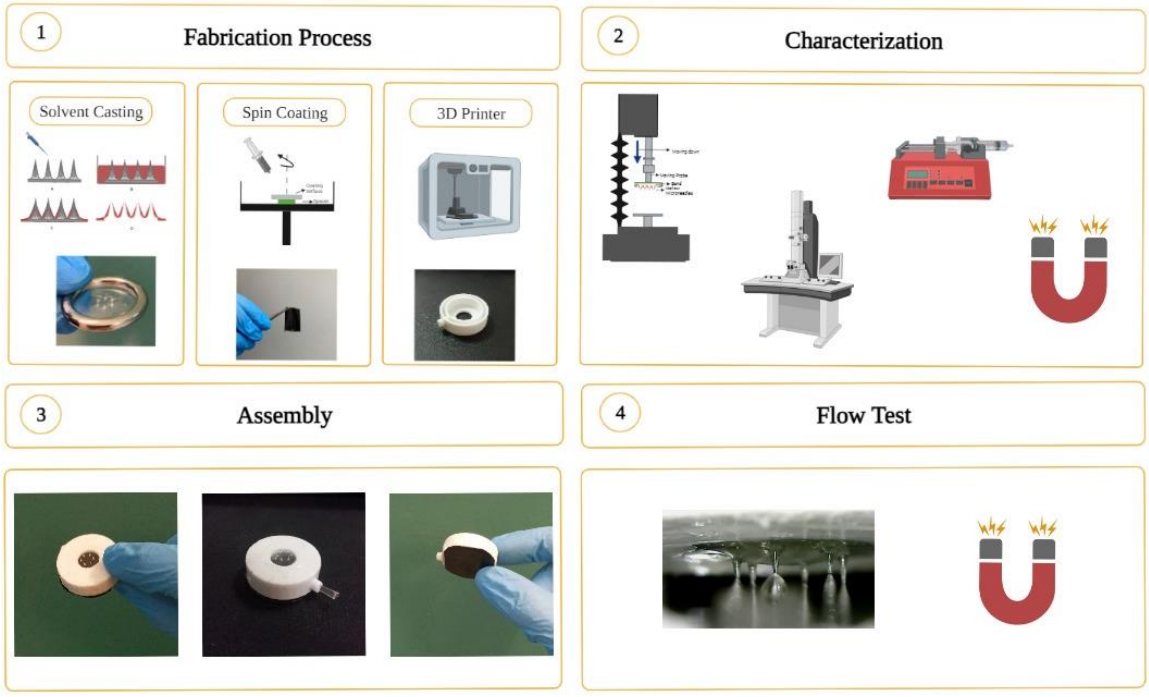

Figure 3.1. Schematic illustration of the main experimental steps in this thesis.

3.1. Materials

Poly-L-lactic acid (PLLA) (Mw = 217−225 kDa) was gifted from Corbion (Netherlands), poly(dimethyl siloxane) (PDMS; Sylgard-184) from Dow Corning (USA), polyvinyl alcohol (PVA)) (Mw= 31,000-50,000, 98-99% degree of hydrolysis) was obtained from Sigma-Aldrich (Germany). Other chemicals were iron (II) chloride tetrahydrate ($FeCl_2.4H_2O$), iron (III) chloride hexahydrate ($FeCl_3.6H_2O$), chloroform,

dichloromethane, acetone, hydrochloric acid (HCl) and sodium hydroxide (NaOH) and Parafilm M® (Brand Bermis, Wertheim, Germany) was purchased from Sigma-Aldrich (Germany). Dexamethasone 21 phosphate DEKORT 8 mg/2 mL I.M./I.V was obtained from Deva (Turkey).

3.2. Fabrication Process

Fabrication processes were mainly divided into three parts; i) microneedle array, ii) magnetic membrane and iii) fluid reservoir.

3.2.1. Fabrication of Microneedles

Hollow microneedle array was produced from PLLA using solvent casting method. Positive mold, which enables single and cost efficient fabrication, was designed to be used in solvent casting process. Solvent casting method relys on wetting of positive mold, and then, microneedle formation by the removal of solvent.

3.2.1.1. Preperation of Positive Mold

Before casting of polymer solution, a hand-made reservoir was prepared to serve as a mold. The components of the reservoirs are shown in Figure 3.2. A commercial Dermapen cartridge has 9 needles made of stainless steel with the length of 2.7 mm. Three needles of cartridge located in the middle were removed in order to ensure that each needle has equal distance away from the metal ring (diameter = 20 mm) served as a boundary. The mold reservoir, which is composed of the modified Dermapen cartridge, nickel ring and 3d printed PLA spacer, was prepared for solvent casting. Aluminum foil and teflon tape were used to prevent the contact of chloroform with the plastic parts of the cartridge and PLA spacer. Binder clips were used to fix components as well as to prevent leakage of polymer solution away from the reservoir. The final appearance of the mold is shown in Figure 3.2b.

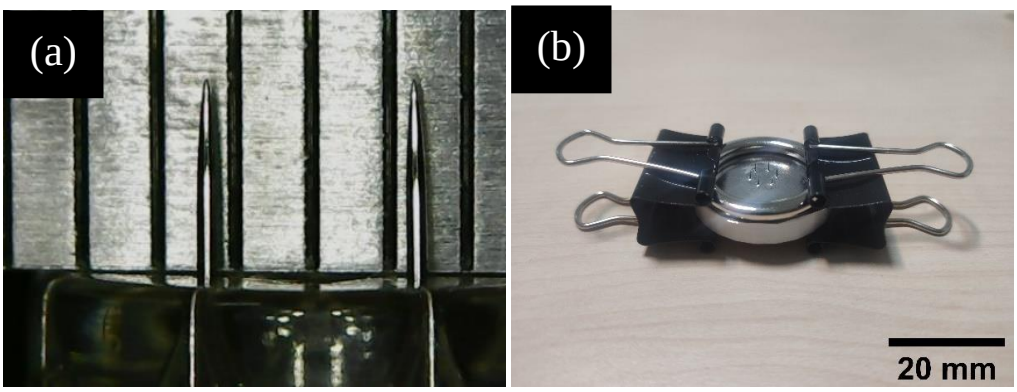

Figure 3.2. (a) Side view of Dermapen cartridge and (b) the assembly of positive mold.

3.2.1.2. Solvent Casting Process

Polymer pellets were dissolved in chloroform at 80 rpm at room temperature to obtain 15% (mass/vol %; m/v%) solution. Then, 0.5 mL of polymer solution was poured into the reservoir carefully without the coating of Dermapen microneedles, and then, left to dry in room temperature for 3 days (Figure 3.3a). Drying process leads to both solvent removal (solidification) as well as microneedle formation (Figure 3.3b). To prevent any deformation and achieve easy separation, microneedles were kept at -20°C for 30 min.

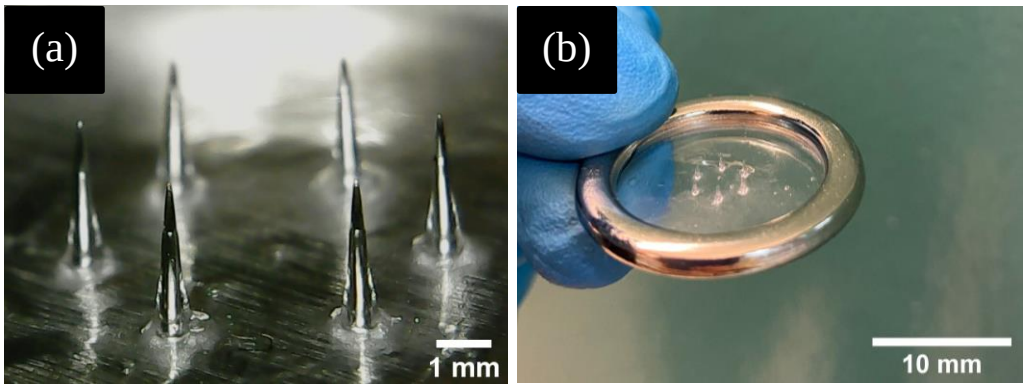

Figure 3.3. (a) Dried polymer present on the surface of stainless steel microneedles after solvent casting, (b) microneedle array removed from the positive mold.

3.2.2. Polymer Coating of Hollow Microneedle Array

In this thesis, dip coating method was applied for the coating of the surface of microneedles. In coating formulations shown in Table 3.1, PVA was used as a viscosity enhancer to be deposited on the microneedles. Tween 20 is a surfactant added into

formulation to decrease surface tension of aqueous PVA solution. Methylene blue is for a staining agent to better visualise the surface coating.

Table 3.1. Formulations used for the preparation of the coating solution.

	Viscosity Enhancer	**Surfactant**	**Visualizing Agent**
Sample no.	PVA, (w/v %)	Tween 20, (v/v %)	Methylene Blue, (w/v %)
1	10	0.1	0.1
2	15		
3	20		

For the immersion, the microneedles were fixed with double-sided tape on the movable probe of the Texture Analyzer (Stable Micro Systems, UK). The probe was then lowered to the reservoir containing the coating solution. The microneedles were kept in this solution for 15 s and then pulled upwards at a speed of 20 mm/s. After coating, the microneedles were left to dry at room temperature overnight.

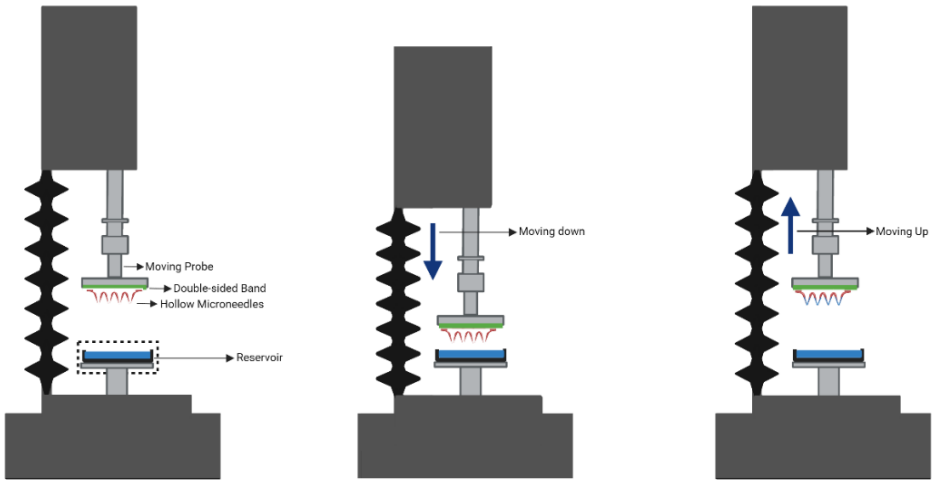

Figure 3.4. Dip coating process for PLLA microneedle array (it is created in Biorender.com).

3.2.3. Fabrication of Magnetic Membrane

This part includes the fabrication process of magnetic membrane.

3.2.3.1. Synthesis of Fe_3O_4 particles

Iron oxide particles are synthesized by co-precipitation method [142]. The solution of 5 g iron (II) chloride tetrahydrate ($FeCl_2 \cdot 4H_2O$) in 10 mL HCl (2 M) and 11 g iron (III) chloride hexahydrate ($FeCl_3.6H_2O$) in 40 mL HCl (2 mL) were prepared and then mixed with each other in the glass volumetric flask to achieve the mass ratio of Fe (II) / Fe (III) as 1:2. After complete dissolution, 50 mL of NaOH (5M) were added to the iron solution slowly for the precipitation process. At the end of the process, the color of solution was turned into black. The iron oxide nanoparticles (Fe_3O_4) were then precipitated at the bottom of the glass balloon with a magnet. The precipitate were washed with deionized water (20 mL, 3x), ethanol (20 mL, 3x) and water (20 mL, 3x) after centrifugation at 5000 rpm for 5 min, respectively. Finally, Fe_3O_4 particles were dried and crushed with mortar to obtain powders.

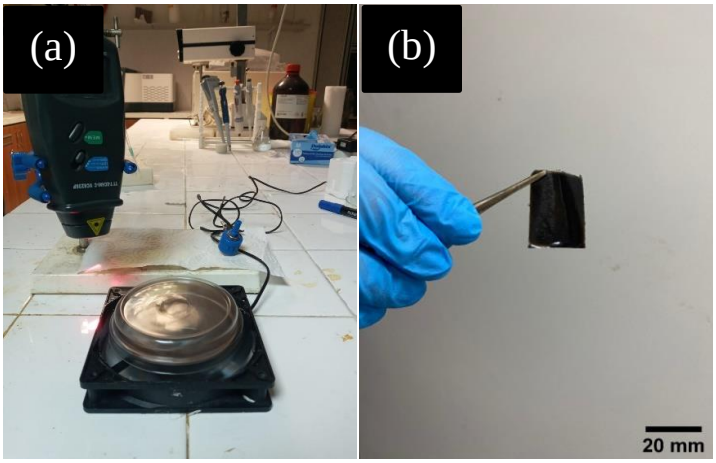

Figure 3.5. (a) Set up of the spin coater: a laser tachometer, potentiometer and fan, (b) thin magnetic membrane obtained after curing process.

3.2.3.2. Fabrication of Fe_3O_4-PDMS composite membrane

Polydimethylsiloxane was preferred as membrane material due to its high elasticity and easy molding. Iron oxide powders and base elastomer were dispersed with a high speed homogenizer (Ultra-turrax T18, IKA, Germany), at scale 3 (~ 11.500 rpm) in an ice bath for 30 min. Then, the curing agent was added to the dispersion and mixed with a spatula for 15 min to achieve 10, 20, 30% w/w Fe_3O_4/membrane nanocomposite. Liquid

composite is then degassed. Dynamic spin coating method was applied to produce thin magnetic membrane. For the coating surface, 30x20 mm glass covered with aluminum foil was used. Aluminum foil helps for the easy removal of the membrane without any deformation.

While a hand-made spin coater rotates at 500 rpm, 1 mL of nanocomposite dispersion was poured on the surface of the glass and held at that speed for 20 s to achieve complete coating. The coating was cured at 90ºC for 3 h in the oven. After curing, the membrane was removed from the coating surface easily (Figure 3.5).

3.2.4. Fabrication of Fluid Reservoir and Assembly of its Components

Two different models were prepared as the drug reservoir of the micropump. In model 1, ABS mold was printed by 3D printer. Then, to achieve PDMS reservoir, 5:1 base/curing agent of PDMS was vacuumed to remove air bubbles and then poured into ABS mold for curing at 90ºC for 3 hours. Once the curing process was completed, ABS mold was removed from PDMS by dissolving it in the acetone bath for 2 days. Magnetic membrane was attached to the PDMS reservoir with the partial curing method. Thin PDMS (10:1 base/curing agent) interface on the bonding area, was partially cured at 60ºC for 35 min. Then, the magnetic membrane was kept contacting to this partially cured area and left curing together overnight at 60ºC (Figure 3.6). Microneedle array, which is attached to the PLA ring by solvent bonding, was interlocked with the PDMS reservoir.

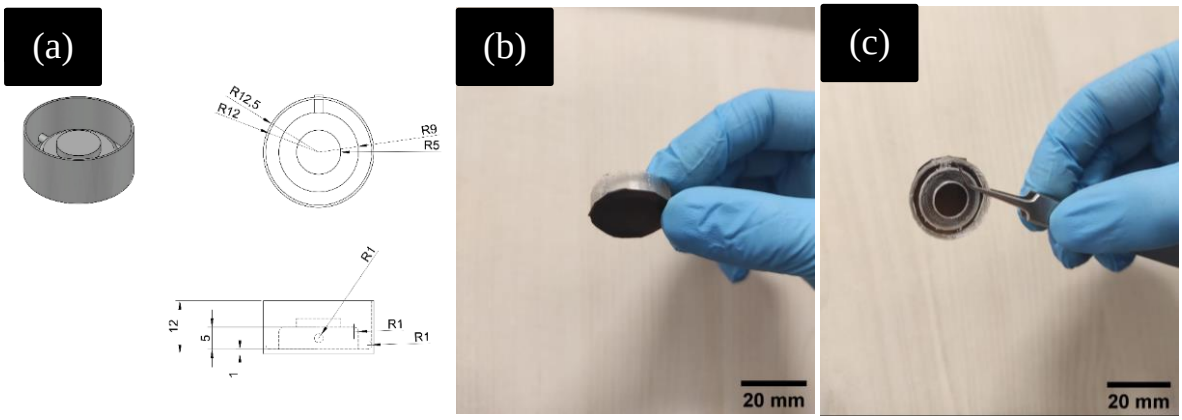

Figure 3.6. (a) The 3D model of ABS mold, (b) and (c) the final assembly of the PDMS reservoir with magnetic membrane.

In model 2, 3D printed ABS mold was directly used as a fluid reservoir. Before the assembly, the reservoir was kept in the acetone bath for 30 s for smoothing the filaments which make the reservoir water-proof to prevent any pressure loss.

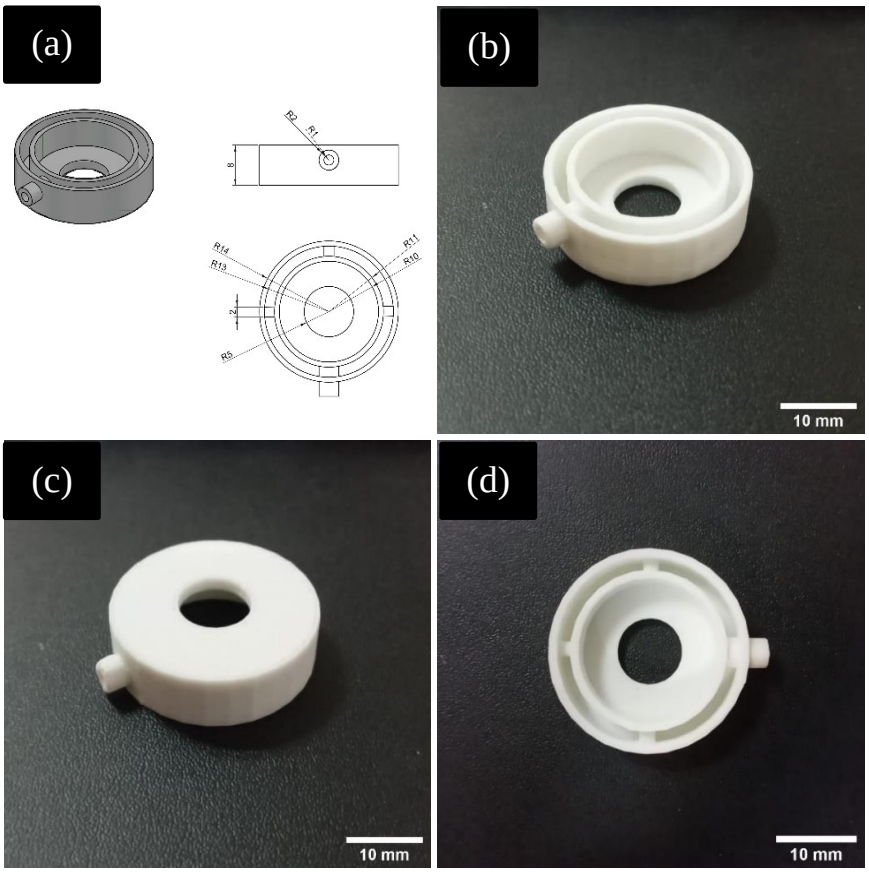

Figure 3.7. (a) The 3D model of ABS reservoir, (b), (c) and (d) the images of 3D printed ABS reservoir from different angles.

For the assembly of magnetic membrane to ABS reservoir, the hollow side of the reservoir (Figure 3.7b and d) was filled with degassed PDMS. Then, partial curing (30 min at 65^{o}C) was applied to PDMS. Magnetic membrane was attached to partially cured areas without the stretching of the membrane, and then all these parts left overnight at 65^{o}C to achieve complete curing. Microneedle array was attached to fluid reservoir by solvent bonding. The assembly of all components is shown in Figure 3.8.

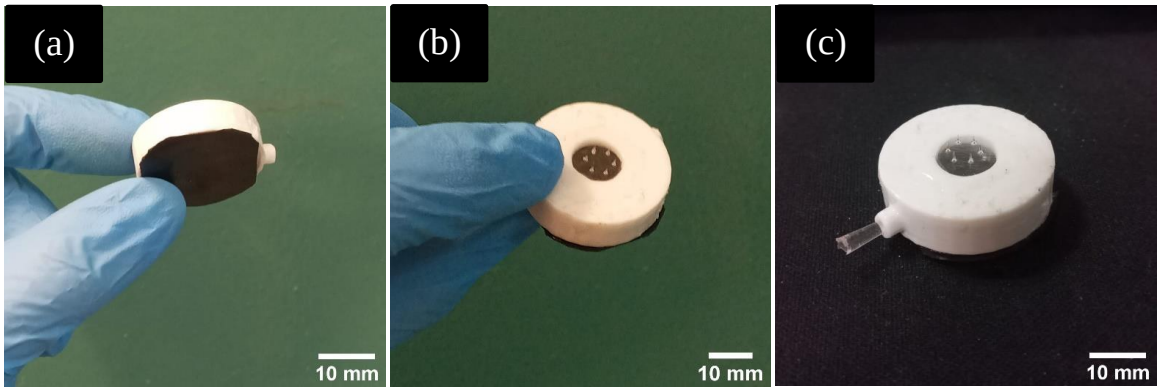

Figure 3.8. Images of the micropump based microneedle array from different angles.

Due to PDMS' low elastic modulus, Model 1 is more susceptible to the deformation which could arise from the pressure exerted when the micropump system was pressed into skin. This scenario may result in accidental dosing. However, ABS is more rigid and resistant to deformation. That is why, Model 2 was chosen for the final assembly.

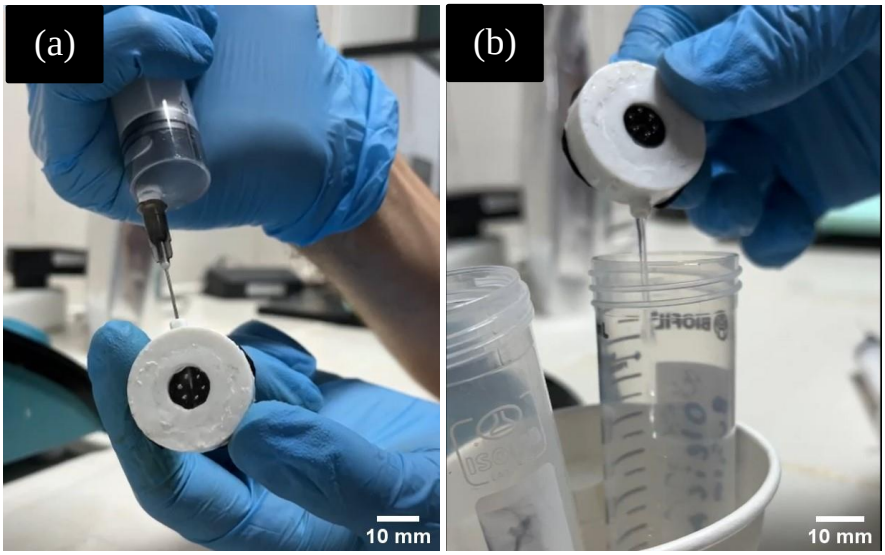

Figure 3.9. Filling (a) and draining (b) of a liquid from drug reservoir.

Simplicity of filling and draining process is important criteria for easy use. Model 2 was designed with the opening large enough to be filled with hypodermic needle easily. Also, Model 2 allows to drain a liquid out of the reservoir in a fast and simple way (Figure 3.9). In Model 1, the filling process would be performed with an injection through the PDMS reservoir, but filling would be harder than Model 2 because of high pressure inside the reservoir. In Model 1, draining would be more problematic. Removing of interlocked ring would be required to drain a liquid.

3.3. Characterization Studies

Characterization was conducted for the microneedle array, magnetic membrane and the final assembly, respectively.

3.3.1. Microneedle Array

Morphological analysis was conducted to define the shape of the microneedle array. In mechanical analysis, failure force and % height reduction, were characterized. For penetration studies, a microneedle array was inserted into Parafilm®. Leakage test was conducted with a syringe adaptor to detect any liquid leakage from the array.

3.3.1.1. Differential Scanning Calorimetry

In order to characterize the physical properties of PLLA, differential scanning calorimetry (DSC, Perkin Elmer, USA) was used. The percent crystallinity (Xc%), melting temperature (Tm), glass transition temperature (Tg) of the samples were analyzed from PLLA pellets and fabricated microneedle array. Samples were heated from 30 to 200°C with a rate of 10°C min−1 under nitrogen gas. Equation 3.1 used for the calculation of Xc % was given below

$$\text{Xc}\ (\%) = \frac{\Delta H}{\Delta Hm0} \times 100 \qquad (3.1)$$

ΔH_m (J/g) represents the area under the thermogram between 65 and 200°C, ΔH^0_m represents the enthalpy of melting of a fully crystallized PLLA sample (93.1 J/g) [143].

3.3.1.2. Morphological Analysis

The morphology of PLLA microneedles was examined by digital microscope and scanning electron microscope (SEM) (GAIA3, TESCAN, Czechia). Geometric parameters were measured with a digital microscope for multi-repetitive examination. Only the difference between tip outer diameter and inner diameter was measured from SEM images due to higher precision. The length of coating were visualized and measured from the SEM images using ImageJ software (NIH, USA).

3.3.1.3. Mechanical Analysis

Mechanical analysis was conducted with Texture Analyzer (Stable Micro Systems, UK) to determine the maximum axial force that microneedle can withstand before the failure. According to force-displacement curve, failure force or 'buckling force' is determined with the point at which the resistance force starts to reduce or reach to saturation due to buckling [144]. Three single microneedles were taken from the same array. In total of 9 microneedles were tested with the arrays fabricated from different batches.

Each single microneedle was placed on metal block on the ground with double-sided adhesive tape. The cylindrical moving probe (10 mm in diamater) made of Delrin® was lowered to microneedle with the test speed of 0.1 mm/s. Trigger force was 0.003 N, pre and post test was 1 mm/s. In one of the study, 32 N was found as the the maximum average force applied by human volunteers for 30 s [145]. Therefore, once the exerted force has reached to 32 N, it was hold for 30 s. Height reduction (%) of the microneedles was also examined with the same method and parameters (n=3). Height reduction (%) was calculated with Equation 3.2 given below.

$$\text{Height reduction (\%)} = \frac{\text{HB}-\text{HA}}{\text{HB}} \times 100 \qquad (3.2)$$

HB represents the height before the compression whereas HA represents the height after the compression.

3.3.1.4. Insertion Studies on Parafilm®

Parafilm M® (Brand Bermis, Wertheim, Germany) has the thickness of 127 μm and was used as an artificial skin [145]. Polystyrene foam was used to mimic soft tissue under the skin [146]. Eight layers of Parafilm® were placed on the polystyrene foam. Microneedle array was placed on the metal moving probe of the Texture analyzer with double-sided adhesive tape. The moving probe was lowered to Parafilm® layers. All parameters of Texture analyzer were the same with the mechanical analysis (target force = 32 N for 30 s, test speed = 0.1 mm/s, trigger force = 0.003 N). Percentage of holes created by microneedle penetration for each layer of Parafilm® were then analyzed. In addition, microneedles were viewed after insertion to detect any deformation present on microneedles.

3.3.1.5. Leakage Test

Leakage test was carried out to be sure that there is no leaking liquid from the microneedles or its base, instead of the lumen. Appropriate syringe adapter was designed with Autocad and printed with a 3D printer from PLA filament (Figure 3.10). In order to smooth the PLA surface, the syringe adaptor was kept in an acetone bath for 3 min. The microneedle array was solvent bonded to a syringe adaptor with dichloromethane. This technique is advantageous in that it allows strong bonding and does not require any adhesive. Aqueous solution of methylene blue was pumped through the adapter using a syringe pump with a flow rate of 20 mL/min for better visual investigation.

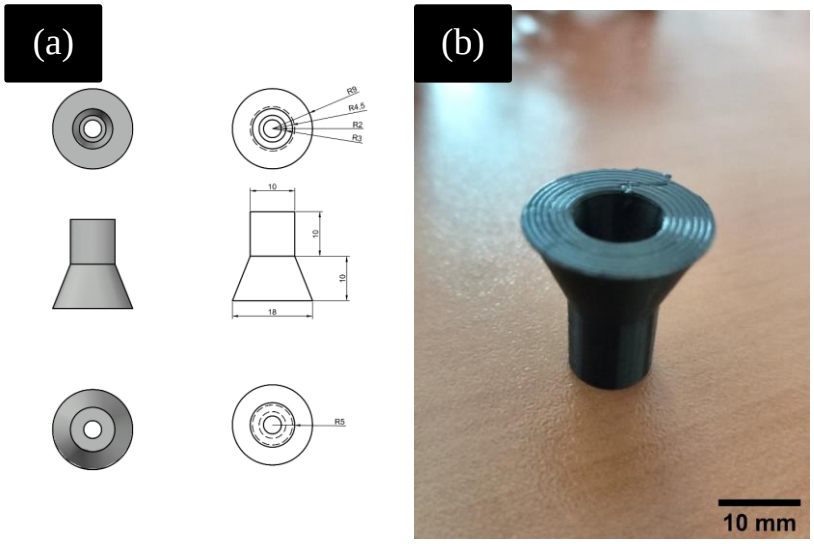

Figure 3.10. (a) The 3D model of the syringe adaptor and (b) its 3D printed image.

3.3.2. Magnetic Membrane

Characterization of magnetic membrane via magnetic properties and thicknesses was explained in this part.

3.3.2.1. Vibrating Sample Magnetometer (VSM)

Magnetic field dependent magnetization of iron oxide particles and magnetic membranes were measured with a quantum design vibrating sample magnetometer (VSM; QD-PPMS, USA) at room temperature within ±2 T magnetic field strength.

3.3.2.2. Membrane Thickness

To analyze the thickness of the magnetic membranes, they were placed between two microscope slides. A digital microscope and ImageJ software were applied as tools for the measurement.

3.3.2.3. Leakage Test

Leakage test was conducted before the assembly of microneedle array to reservoir to be sure that any leakages take place from the membrane side. Dry reservoir with a magnetic membrane was filled with 2.5 mL distilled water and then followed carefully every hour for a total of 5 hours to detect any leakage (Figure 3.11).

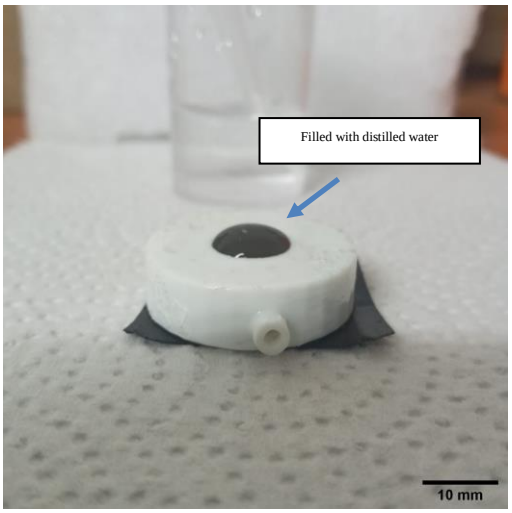

Figure 3.11. Leakage test applied to the reservoir.

3.3.3. Electromagnetic Characterization

Magnetic characterization of electromagnet and deflection of magnetic membranes under applied voltage was described in this part.

3.3.3.1. Actuator

A power supply is provided (Digital DC Power Supply, OWON, China) for the actuation of electromagnet, which can apply voltage in the range of 0 – 60 V and current in the range of 0 – 3 A. The variation of magnetic flux density created at the level of electromagnet (d = 0) with applied voltages was investigated by the Gaussmeter. In the following studies, magnetic flux densities as a function of distance from the electromagnet surface were investigated at different voltage values applied to the

electromagnet. The voltages of 5 to 60 V and distance of 0 to 5 cm were investigated. The setup used for the magnetic characterization of the electromagnet is shown in Figure 3.12.

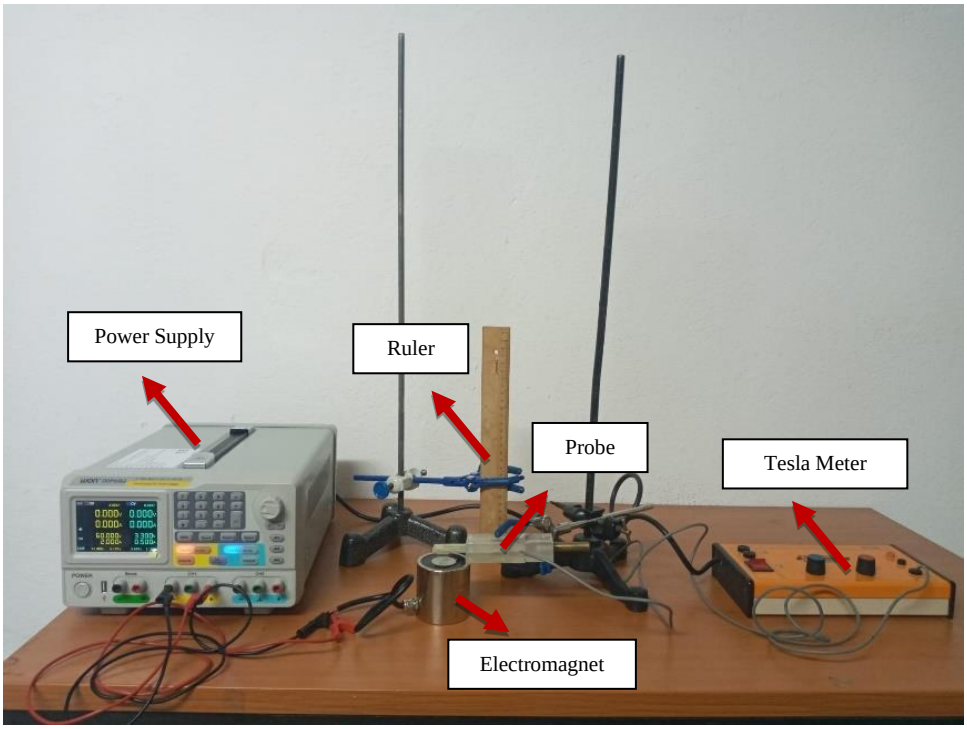

Figure 3.12. The setup used to determine magnetic flux density of the actuator.

3.3.3.2. Deflection of Magnetic Membrane

Before the assembly of the system, displacement of magnetic membranes fabricated with different amounts of Fe_3O_4 particles (10, 20 and 30% by mass) was investigated under the voltage of 20, 40, 60 V. To do this, each magnetic membrane is attached to a metal ring, which has the same diameter with the pumping area of Model 2 (20 mm), by double-sided band. The membrane, which showed higher deflection, was chosen for the pumping studies of fluid. The measurements of deflection was performed with a time interval of 3 s. The setup used for the deflection measurements of magnetic membranes is shown in Figure 3.13.

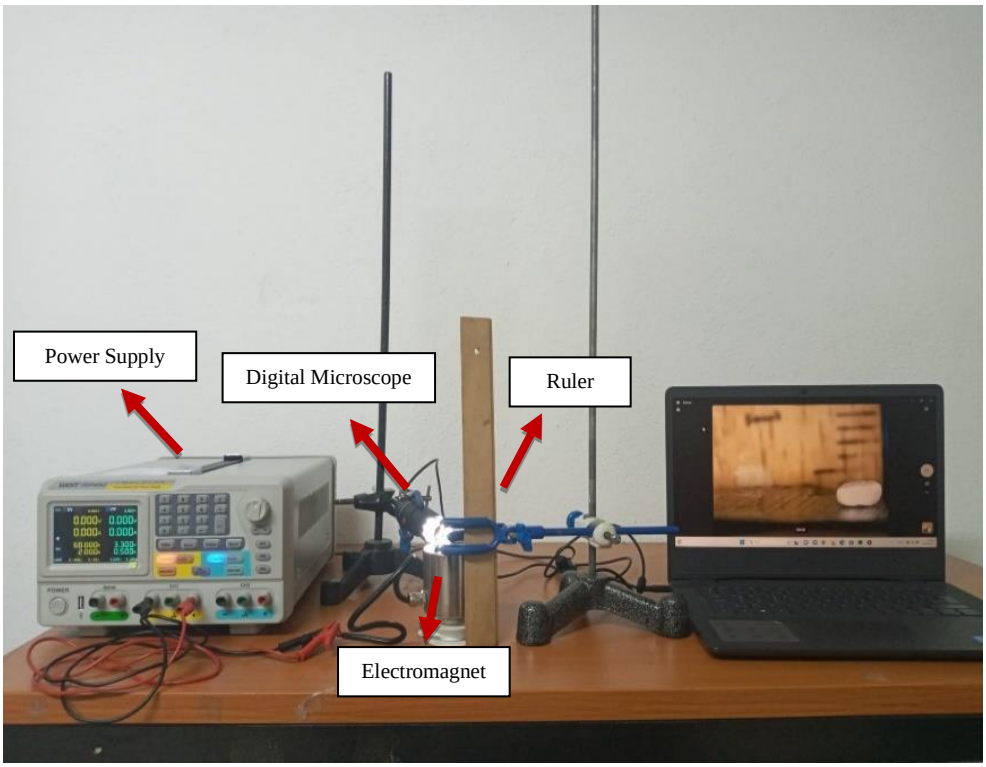

Figure 3.13. The setup used to determine membrane deflection.

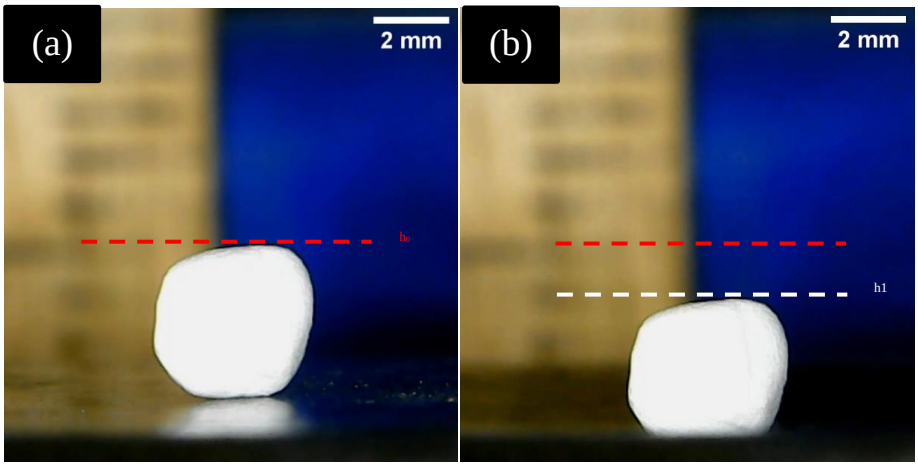

Figure 3.14. Polystyrene foam placed on the center of the membrane; level before (a) and after magnetic deflection (b).

To determine deflection and response time (deflection time plus return time of the membrane), a piece of polystyrene foam which weighs less than 0.01 mg, was placed on the center of the magnetic membrane to be used as a marker (Figure 3.14). Response time (deflection plus return time) was measured from the recorded videos during the voltage application.

3.3.4. Dosing Performance of Micropump System

To determine the dosing ability of micropump based microneedle array, aqueous solution of Dexamethasone 21 phosphate was used. To achieve the stock solution, Dekort®, 8mg/2ml was diluted to 0.2 mg/mL with distilled water. Measured density of stock solution was 1.8 g/mL. Fluid reservoir was filled with 2 ml solution by a syringe. Dosing performance of membrane was analyzed with different voltages (30,40,50 and 60 V) with constant current (2 A).

In another study, a cylinder neodymium magnet (10x1.5 and 1.3 g) was placed on the middle of the membrane, and then, dosing ability was characterized. Since magnet attracts electromagnet, distance at which magnetic flux density of magnet is zero, was measured with tesla meter. This value of distance was used as a total space between magnet and electromagnet in order to avoid unintented dosing of magnet due to attraction to electromagnet. Also, the actuation process was followed up with a USB microscope to be sure that dosing/pumping was stopped after power was cut-off.

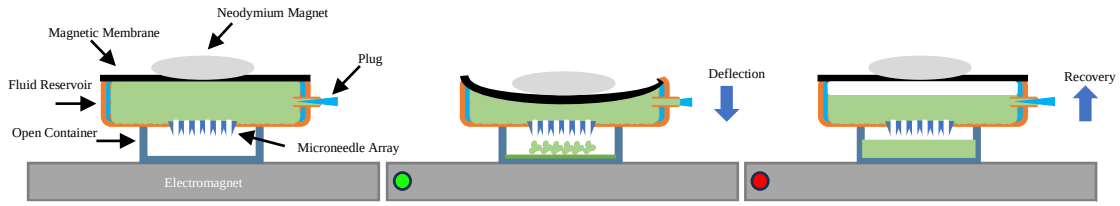

Figure 3.15. The setup for multible dosing is shown above.

The working principle of micropump relies on the oscillation of the magnetic membrane, which increases the fluidic pressure inside the reservoir (Figure 3.16). Fluid reservoir was filled with 1.3 ml solution, instead of 2 ml because the weight of magnet imparts pressure on liquid, so it results in accidential flow. Dosing performance with programmed single and multiple actuations was separately analyzed by weighting the solution, which is pumped into a open container. Power supply which was programmed according to response time, which was achieved from the deflection study in section 3.3.3.2. Parameters of programmed power supply were created after the approximate response time of the membrane was determined in deflection studies.

In micropump systems, membrane actuation is defined as periodic reciprocating movement of membrane. Thus, Equation 3.3 was used to calculate flow rate as given below.

$$\text{Flow rate } \left(\frac{\mu L}{s}\right) = \frac{\text{Pumped Volume}(\mu L)}{\text{Pumping Time } (s)} \quad \text{(Equation 3.3)}$$

Graphs of flow rate and accumulated drug release over time were provided. Besides, % dead volume was calculated as Equation 3.4 given below.

$$\%\ \text{Dead volume} = \frac{\text{Initial Volume}(\mu L) - \text{Pumped Volume}(\mu L)}{\text{Initial Volume}(\mu L)} \times 100 \quad \text{(Equation 3.4)}$$

According to these data, the dosing ability and pumping efficiency of the system were evaluated.

4. RESULT AND DISCUSSION

In this thesis, PLLA hollow microneedles were successfully fabricated by a one-step solvent casting method. Subsequently, a drug reservoir was developed with a novel design using a 3D printer and a magnetic membrane supported by a cylindrical magnet, which acts as a micropump in this system, was successfully combined with the reservoir. The pumping capacity of the developed micropump based microneedle array was investigated at different voltages and it was shown that it could perform a successful pumping process. The results obtained within the scope of the thesis are given here in four sections with detailed characterizations as: i) microneedle array, ii) magnetic membranes, iii) electromagnetic characterization and iv) micropump system.

4.1. Microneedle Array

4.1.1. Fabrication of Microneedles

In the literature, hollow microneedles, which are produced by solvent casting, requires additional processes such as tip-opening procedures to make microneedles suitable for the poke and flow approach [147,148]. As such additional processes make the overall process, laborious, time-consuming and costlyIn this thesis, hollow microneedles are produced from positive mold, which enabled the single step-production of hollow polymeric microneedles without any additional process on microneedles. PLLA is chosen as a material for the production of microneedles since it is biocompatible, biodegradable and has sufficient mechanical properties for the penetration [118]. In addition, PLA is approved by FDA in the studies, which requires its contact with body fluid.

4.1.2. Differential Scanning Calorimetry

Differential scanning calorimetry thermogram is presented in Figure 4.1. According to the thermogram, no glass transition or cold crystallization temperature was detected for PLLA microneedle array. However, the melting temperature was detected as 179°C indicating that the material is semi-crystalline. This result is compatible with the related literature (170~180°C) [147]. The enthalpy of melting was measured as 35.4 J/g for PLLA microneedle array and 77.8 J/g for PLLA pellets. Percent crystallinity of the PLLA microneedle array was calculated as 38 %, which is almost half of the PLLA pellets. This results are also summarized in Table 4.1.

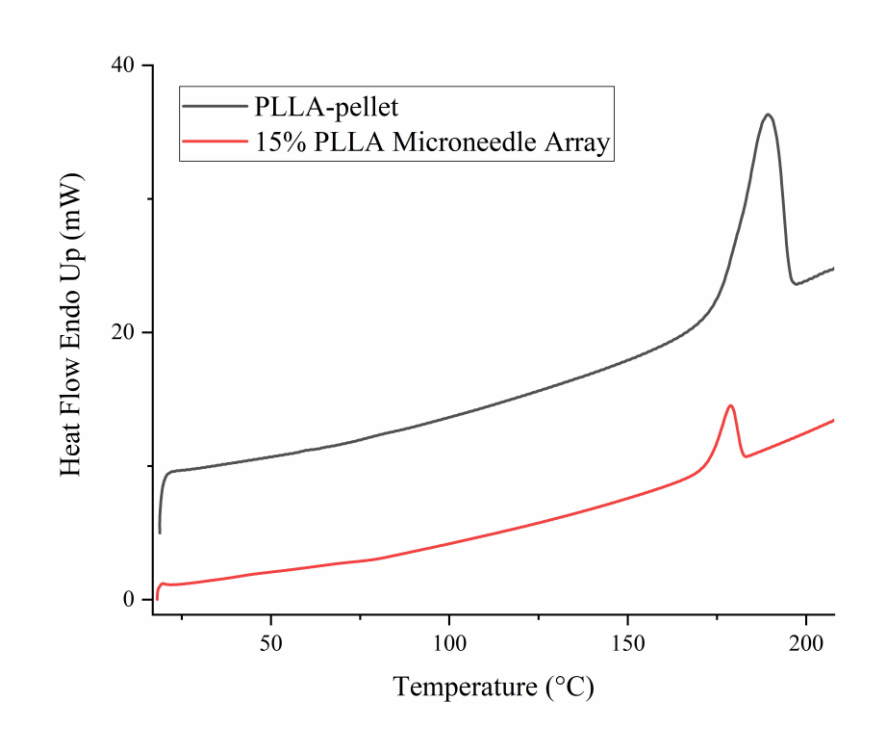

Figure 4.1. Thermograms of PLLA pellet and microneedle array.

Table 4.1. The summary of the DSC results.

	Tm (°C)	**Xc (%)**	**ΔHm (J/g)**	**Tg (°C)**
PLLA-pellet	189.0	84	77.8	-
%15 PLLA	179.0	38	35.4	-

4.1.3. Morphological Analysis

Morphological analysis was conducted with SEM and USB digital microscope. As seen in Figure 4.2, there are 6 microneedles present in the array as expected. Microneedles are truncated-cone-shaped with a cavity inside the shaft and the openings are located at the tip and base. The summary of the results belonging to the geometric results is given in Table 4.2. The length, width and tip diameter (OD) of the microneedles were measured as 1.4 ± 0.2, 0.9 ± 0.1 and 0.20 ±0.03 mm, respectively. These parameters are compatible with the reported studies in literature [149–151]. The PLLA microneedles have a flat tip with interfacial area of approximately 1,600 μm2, which is lower than solid microneedle with a tip diameter of 50 μm. Tip inner diameter and the area of array are appropriate with components of the reservoir (metal microneedle and the ring). Due to wetting of

solution, polymer deposition on the surface of stainless steel increased the interspace of base and tip as well as tip area compared to metal microneedle.

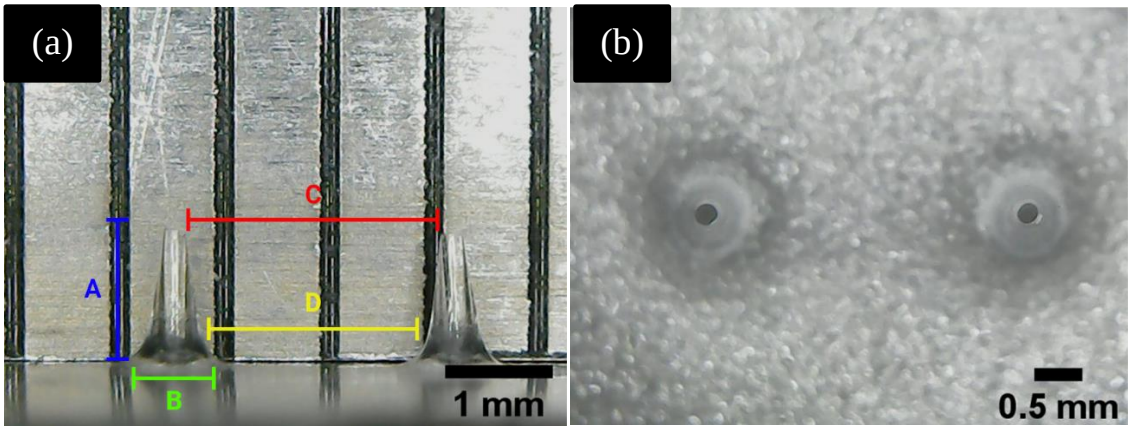

Figure 4.2. Digital microscope images of PLLA microneedles. Geometric parameters of microneedles (a): A: Length, B: Width, C: Interspace of Tip, D: Interspace of Base, and the top view (b).

Table 4.2. Geometric parameters of PLLA microneedles (n=14). The results are given as mean ± standard deviation.

Length (mm)	**Width (mm)**	**Interspace of Base (mm)**	**Interspace of Tip (mm)**
1.4 ± 0.2	0.9 ± 0.1	1.8 ± 0.1	2.4 ± 0.1
OD (mm)	**Wall thickness (µm)**	**Aspect Ratio**	**Density (needle per mm²)**
0.20 ± 0.03	2.4 ± 0.1	1.5 ± 0.2	0.019

*OD: Tip Outer Diameter, ID: Tip Inner diameter.

The length of PLLA microneedles are smaller than the skin thickness (epidermis and dermis) of tight, waist, suprascapular and deltoid sites of the human body [152]. Therefore, PLLA microneedle array developed in this thesis is a suitable candidate for use at these anatomical sites for the purpose of intradermal delivery of dexamethasone.

Pain is strongly related with the length of microneedles because of the excitement in the increased number of sensory nerves in the skin. Gill et al.[153] reported that the length of

microneedle between 450 to 1450 μm can reduce the pain score between 20 to 3-fold compared to 26 G needle. According to this, it may be expected that PLLA microneedle array is going to cause less pain in patients compared to 26 G needle.

Laurent et al. [154] assessed the performance of BD Soluvia™ injection system, which contains one 30-gauge microneedle with the length of 1.5 mm. According to that study, some adverse effects such as small drops of blood, itching and redness were reported for humans but they noted that all these effects were reversed in 20- 30 min. Considering this information and the length of PLLA microneedles fabricated, similar adverse effects may be expected for PLLA microneedles, too. Even these reported adverse effects, as indicated in the same study, PLLA microneedle array is expected to be advantages over standard intradermal administration, called 'Mantoux technique', with respect to being safe, painless and self administrable.

'A bed of nail' is the distribution of force on microneedles, which results insufficient force to break elasticity of skin. This phenomenon has adverse effects on the penetration of microneedle arrays [155]. To avoid a bed of nail effect, microneedle array can be designed. Olatunji et al. [156] analyzed the insertion forces of each microneedle array with different interspaces of base. It was reported that a bed of nail effect is observed on microneedle arrays, which has interspace of base with a range of 30-150 μm. When considering the interspace of PLLA microneeedle arrays fabricated here as 1.8 ± 0.1 mm, this value is more than 10-times greater than 150 μm, so a bed of nail effect is not expected for the PLLA microneedle array.

Figure 4.3 shows the SEM images of the PLLA microneedle array. As seen in these images, PLLA array with 6 needles were successfully fabricated. Moreover, the channels with ID of 0.2 mm (wall thickness = 2.4 μm) were very distinct and it can be said that aqueous drug solutions can easily flow throughout these channels. Besides, no porosity was observed on the surface of PLLA microneedles, so it is interpreted that microneedles are resistant to the liquid leakage or infusion of any clogging agent through the surface.

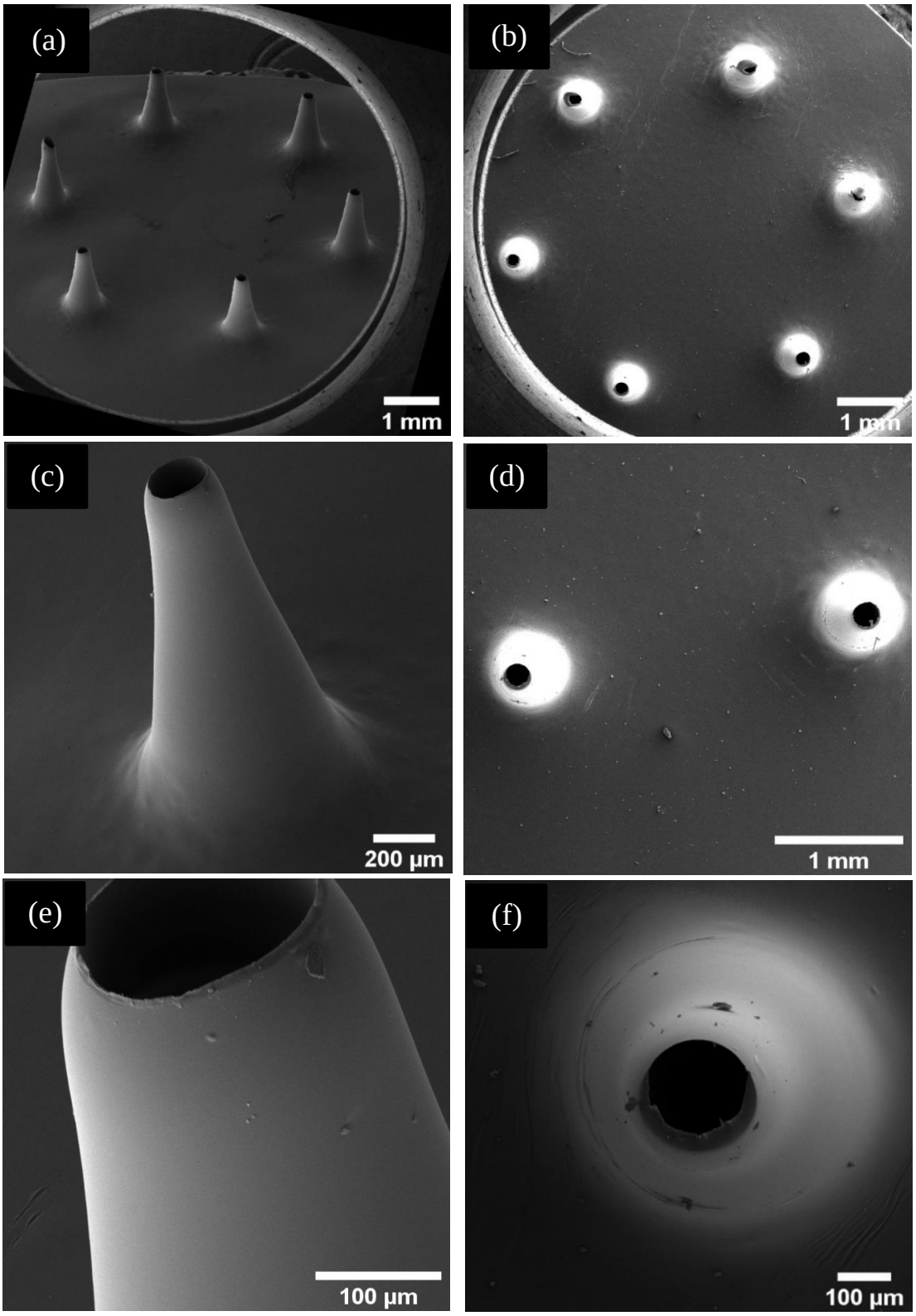

Figure 4.3. Scanning electron microscobe images; (a) general view of the PLLA microneedle array with 45° angle, (b) top view of the array showing the channels, and (c), (d), (e) and (f) shows the close-up images related to single or two microneedles.

4.1.4. Mechanical Analysis

A relationship between the force applied on a microneedle and the probe displacement is shown in Figure 4.4a. Once the probe touched the tip of the microneedle, the force started to increase up to some point at which failure occurs (Figure 4.4b). At this point, the force decreased to some extent and then increased again until 32 N force achieved. This represents the typical stress-displacement relationship seen in microneedles. As calculated from force-displacement curves, failure or fracture force was found as 2.9 ± 0.4 N for a single microneedle. Percent height reduction (%) was calculated as 58 ± 4 %. Moreover, failure occurred by buckling as expected.

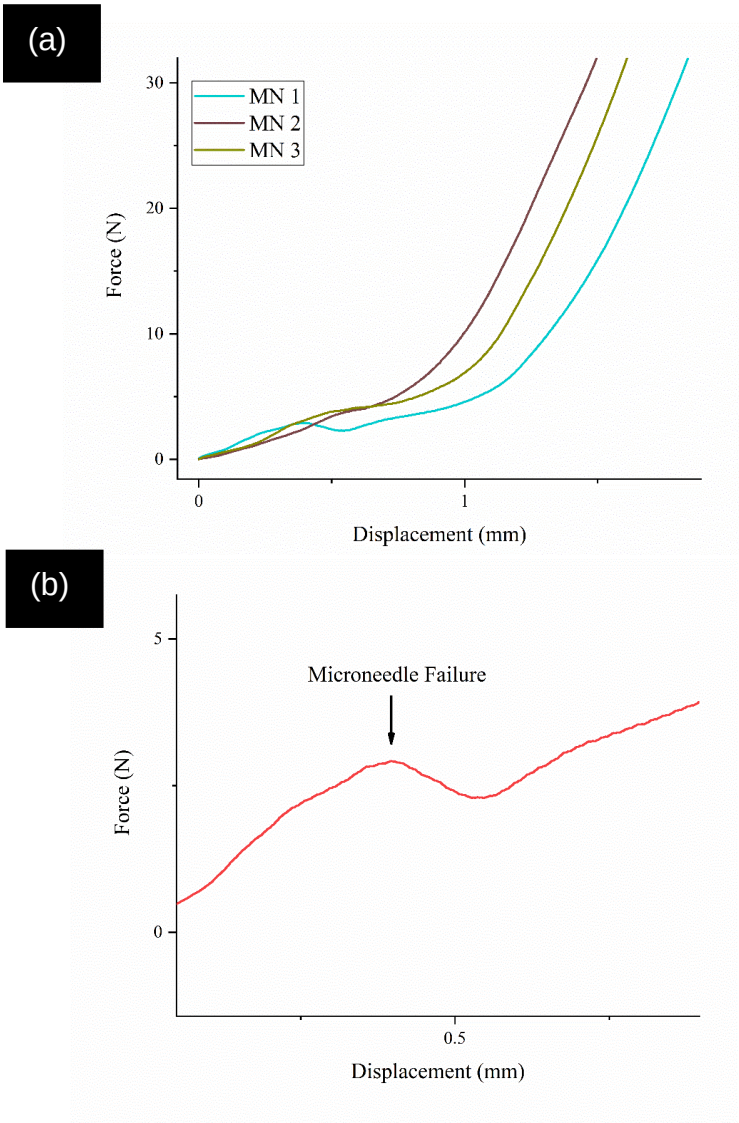

Figure 4.4. (a) Force-displacement curve of the PLLA microneedle from different batches, (b) representative scale-extended force-displacement curve showing the point where failure occurs.

To ensure penetration into skin, microneedles should have higher failure force than the insertion force. Margin of safety, the ratio of failure force to insertion force, is a useful index to consider the suitability of microneedles for biological applications. The interfacial area of microneedle tip has significant impact on its insertion force while other parameters are less significant [157]. Ye et al. [151] produced polymethyl methacrylate hollow microneedles which has a tip diameter of 0.2 mm (similar value with PLLA microneedles) and reported the insertion force per needle as 0.025 N in rabbit skin. Fracture force of PLLA microneedle here is approximately 100-fold of this insertion force.

In another study, Kochhar et al. [158] reported that insertion force of 2 N per a needle which has tip diameter of 0.276 mm and spacing of 1.6 mm. Fracture force of PLLA microneedle fabricated in this thesis is approximately 1.5-fold than this insertion force. When considering these reported insertion forces, it is interpreted that PLLA microneedles should have sufficient failure force for successful penetration into human skin.

Cárcamo-Martínez et al. [159] produced 5x5 microneedle array from the aqueous mixture of 25 % Gantrezs S-97 and 10% PEG. Then, the compression test was conducted on the the array with the same target force applied in this thesis (32 N). Height reduction (%) for the array was reported as 25%. This value is slightly higher than 2-fold of PLLA array. Considering the force per needle, while each microneedle from 5x5 array was subjected to 1.3 N, PLLA microneedle was subjected to 5.3 N, which is 4-fold higher than the reported values in the literature.

To ensure penetration into skin, microneedles should have higher failure force than the insertion force. Margin of safety, the ratio of failure force to insertion force, is a useful index to consider the suitability of microneedles for biological applications. The interfacial area of microneedle tip has significant impact on its insertion force while other parameters are less significant [157]. Ye et al. [151] produced polymethyl methacrylate hollow microneedles which has a tip diameter of 0.2 mm (similar value with PLLA microneedles) and reported the insertion force per needle as 0.025 N in rabbit skin. Fracture force of PLLA microneedle is approximately 100-fold of this insertion force.

In another study, Kochhar et al. [158] reported that insertion force of 2 N per a needle which has tip diameter of 0.276 mm and spacing of 1.6 mm. Fracture force of PLLA microneedle is approximately 1.5-fold than this insertion force. When considering these reported insertion forces, it is interpreted that PLLA microneedles should have sufficient failure force for successful penetration into human skin.

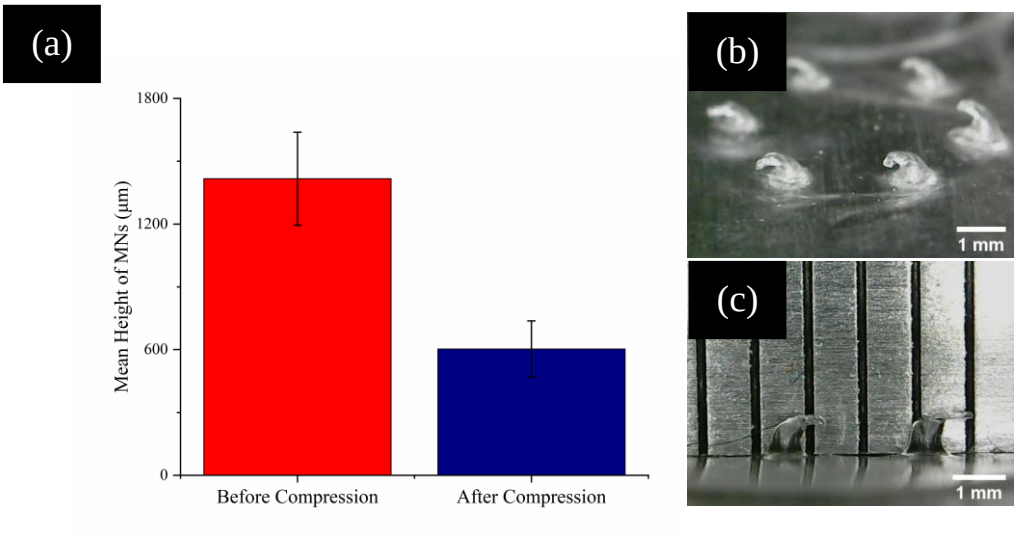

Figure 4.5. (a) Comparison of the height of microneedles before and after compression, and (b) and (c) shows their corresponding digital images.

Cárcamo-Martínez et al. [159] produced 5x 5 microneedle array from the aqueus mixture of 25 % Gantrezs S-97 and 10% PEG. In study, the compression test was conducted on the the array with the same target force (32N). Height reduction (%) for the array was reported as 25%. This value is slightly higher than 2-fold of PLLA array. Considering the force per needle, while each microneedle from 5x5 array was subjected to 1.3 N, PLLA microneedle was subjected to 5.3 N, which is 4-fold higher than the reported values in the literature.

4.1.5. Insertion Study on Parafilm®

In insertion test, PLLA microneedle array was compressed on an 8-fold Parafilm® layer. The percentage of created holes for each layer is given in Figure 4.6. Larrañeta et al. [145] regarded the effective penetration for the percentage which is higher than %20. According to this, PLLA microneedle arrays provide effective penetration up to the 7th layer (~ 900 µm). After the insertion, no deformation was detected on the microneedle array (Figure 4.7). While the holes up to 5th layer were large enough to detect easily, a close

examination was required to 6, 7 and 8th layers with a digital microscope due to small holes and elastic properties of parafilm. Digital images of all 8 parafilm® layers are given in Figure 4.7.

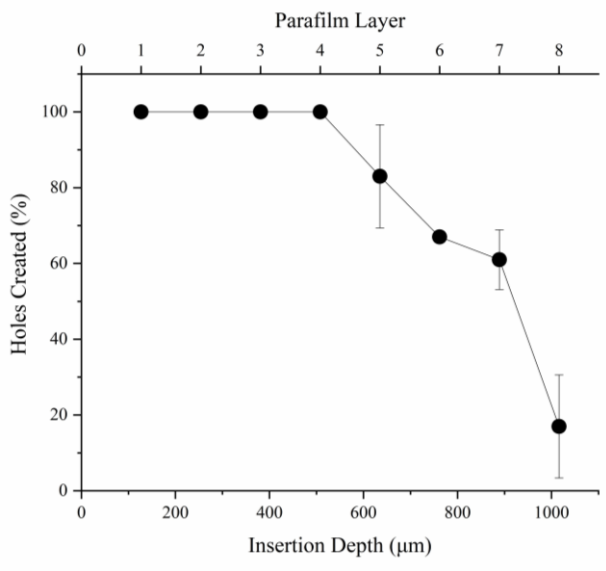

Figure 4.6. The percentage of holes created in each layer of Parafilm® after the PLLA microneedle array insertion.

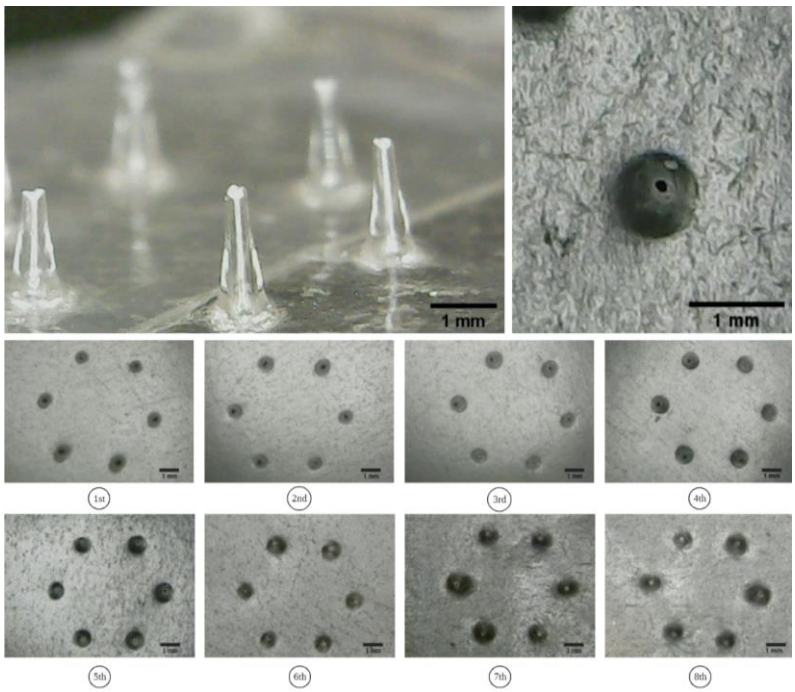

Figure 4.7. The image on top left shows the morphology of the microneedles after insertion. No any deformation was observed. The other images represent the holes created in each Parafilm® layer after the PLLA microneedle array insertion.

Figure 4.8 represent the mechanical analysis results of Parafilm® insertion test with the zones present at different states of force-displacement curve. In zone 1, microneedle array on the moving probe does not touch the Parafilm®. The resistance force, therefore, is not observed. In zone 2, microneedles penetrate into Parafilm® and travel through the lenght of microneedle (~1.5 mm). In zone 3, the base of microneedle array touches the Parafilm® layers. Thus, all compression force acts on the area of the base.

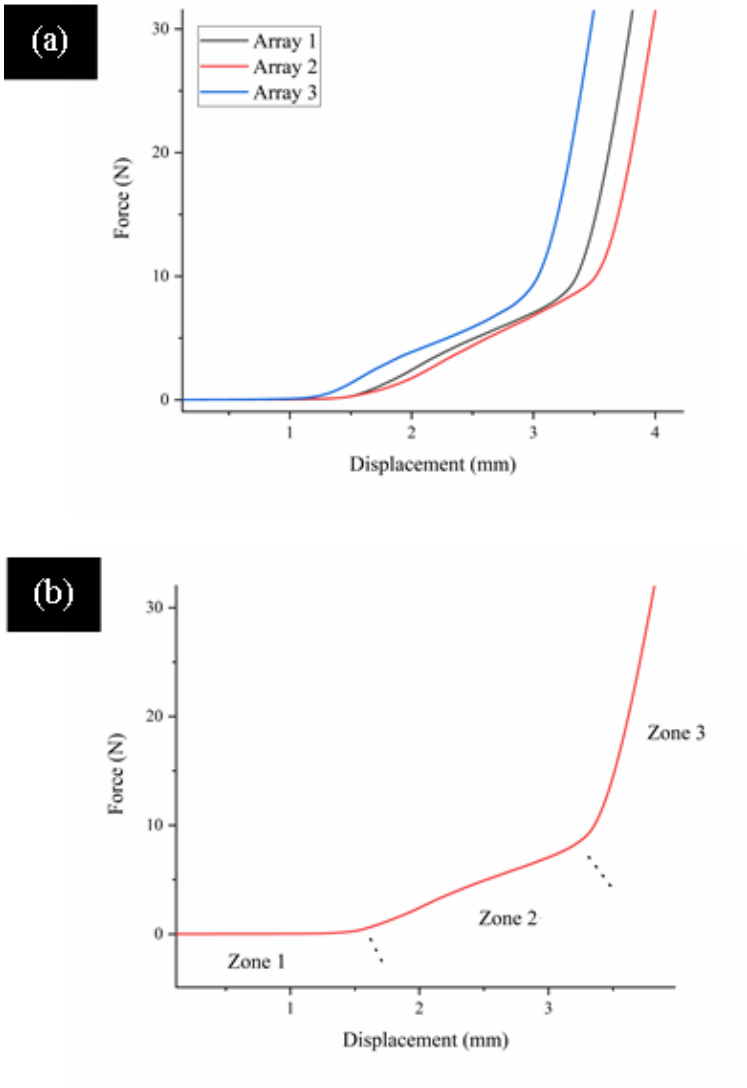

Figure 4.8. (a) Force-displacement curve of the Parafilm® insertion study, (b) zones present at different states of force-displacement curve.

4.1.6. Leakage Test

Since the drug will be released via the poke and flow approach, it is important to be sure that there is not any leakage during the application. Thus, the flow study was conducted

with a syringe adaptor to ensure that only flow occurs from the tip openings. During the study, possible leakage from the PLLA microneedle array and the syringe was followed. As seen in Figure 4.8, it was not detected any leakage from the array and syringe with a flow rate of 20 mL/min. Only flow was observed from the microneedle tips as requested. According to this, it is concluded that PLLA microneedle array is convenient for dosing via micropump.

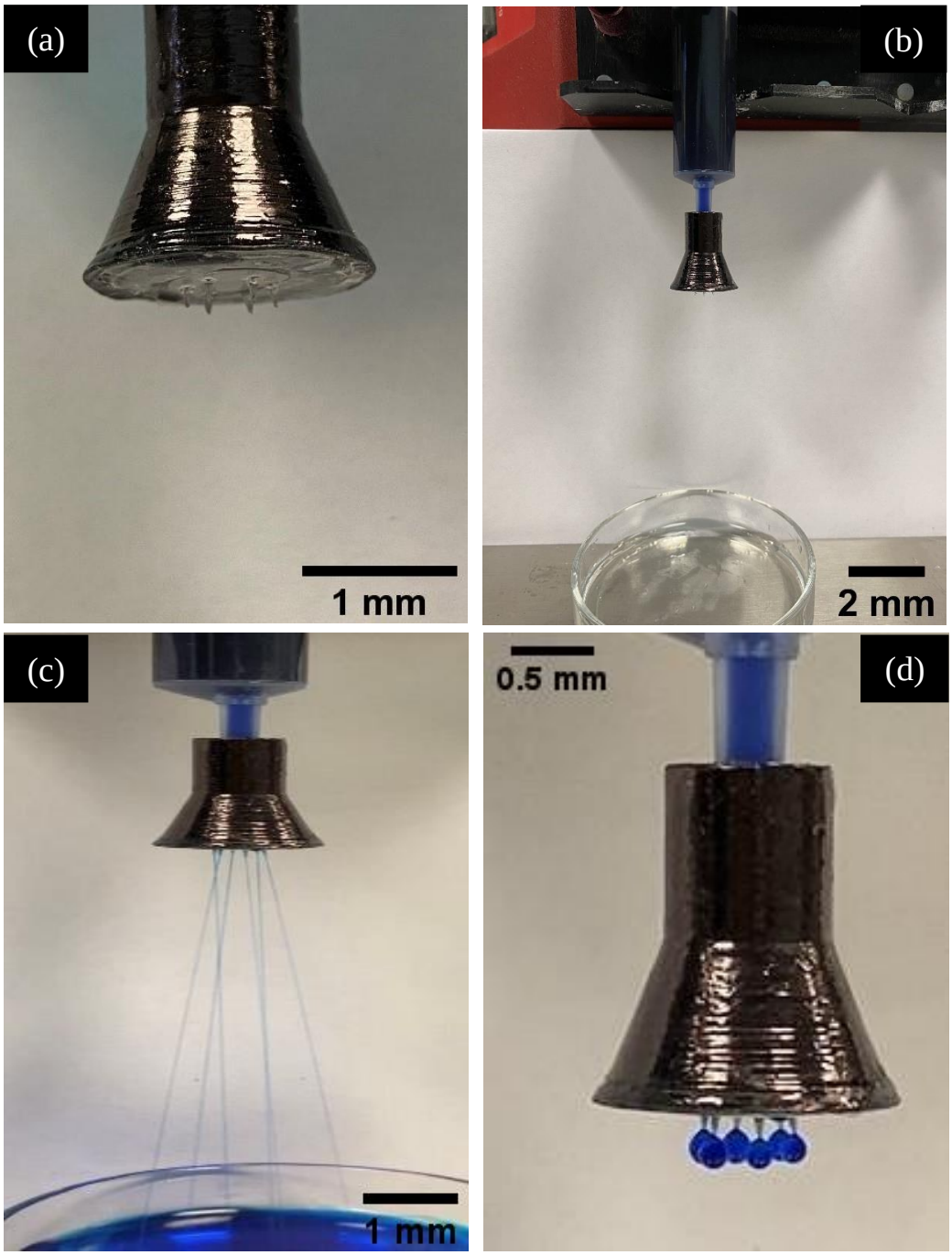

Figure 4.9. PLLA microneedle array with syringe adaptor (a, b), during (c) and after (d) the flow.

4.1.7. Polymer Coating

In the beginning, the purpose of coating of the PLLA microneedles was to close the tip openings for minimizing the risk of clogging. As seen in Figure 4.9, coating solution was succesfully deposited on microneedles for each concentration. However, polymer deposition did not close the tip opennings completely for each coating formulation. Thus, the planned experiments for the drug delivery over the polymer coating layer was not conducted.

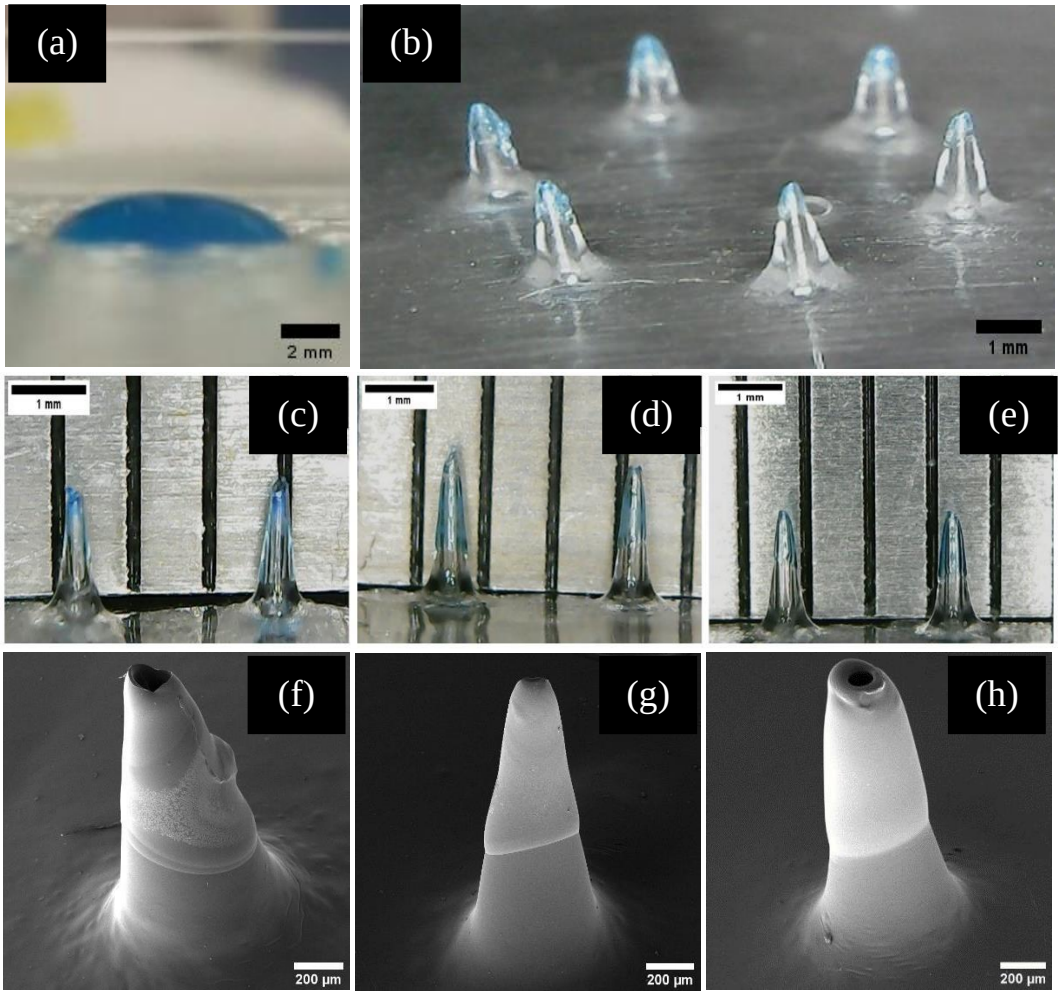

Figure 4.10. The side view of the coating solution (a), general view of the coated array (b), digital microscope and SEM images of PVA coated microneedles with the different concentrations: 10 % (c, f), 15 % (d, g), 20% (e, h) PVA.

The length of coating at different positions of the microneedle shaft is summarized in Table 4.3. Inward-facing surface was slightly higher than outward. The reason of this was that the solution is not flat but convex on the center (Figure 4.10a). As seen in Figure

4.10f, g and h, in the highest concentration (20% PVA; w/v), the coating is thicker than the lower concentrations due to higher polymer deposition.

Table 4.3. The lenght of coating on inward and outward surface of the microneedle shaft (n=18).

Average coating length	**10 % PVA**	**15 % PVA**	**20% PVA**
Inward-facing surface (mm)	0.65 ± 0.1	0.65 ± 0.14	0.62 ± 0.15
Outward-facing surface (mm)	0.51 ± 0.06	0.55 ± 0.09	0.55 ± 0.19

4.2. Magnetic Membranes

4.2.1. Vibrating Sample Magnetometer (VSM)

The saturation magnetization of the iron oxide particles was found as 62.5 emu/g. This magnetization value is compatible with the related literature [160]. Magnetization of PDMS membranes decreased to lower values as expected (Figure 4.11). Saturation magnetization of the magnetic membranes with highest Fe_3O_4 content was found as 15.3 emu/g. This value decreased to 10.7 emu/g for PDMS-20% Fe_3O_4 and 5.5 emu/g for PDMS-10% Fe_3O_4 (Table 4.4). Higher iron oxide content in membranes results in higher magnetization as expected [161]. The remanence and coercivity of all samples are zero, which indicates that magnetic membrane have superparamagnetic properties.

Table 4.4. The saturation magnetization values of the iron oxide particles and magnetic membranes.

Sample Name	**Saturation Magnetization (emu/g)**
Bare	62.5
PDMS-30% Fe_3O_4	15.3
PDMS-20% Fe_3O_4	10.7
PDMS-10% Fe_3O_4	5.5

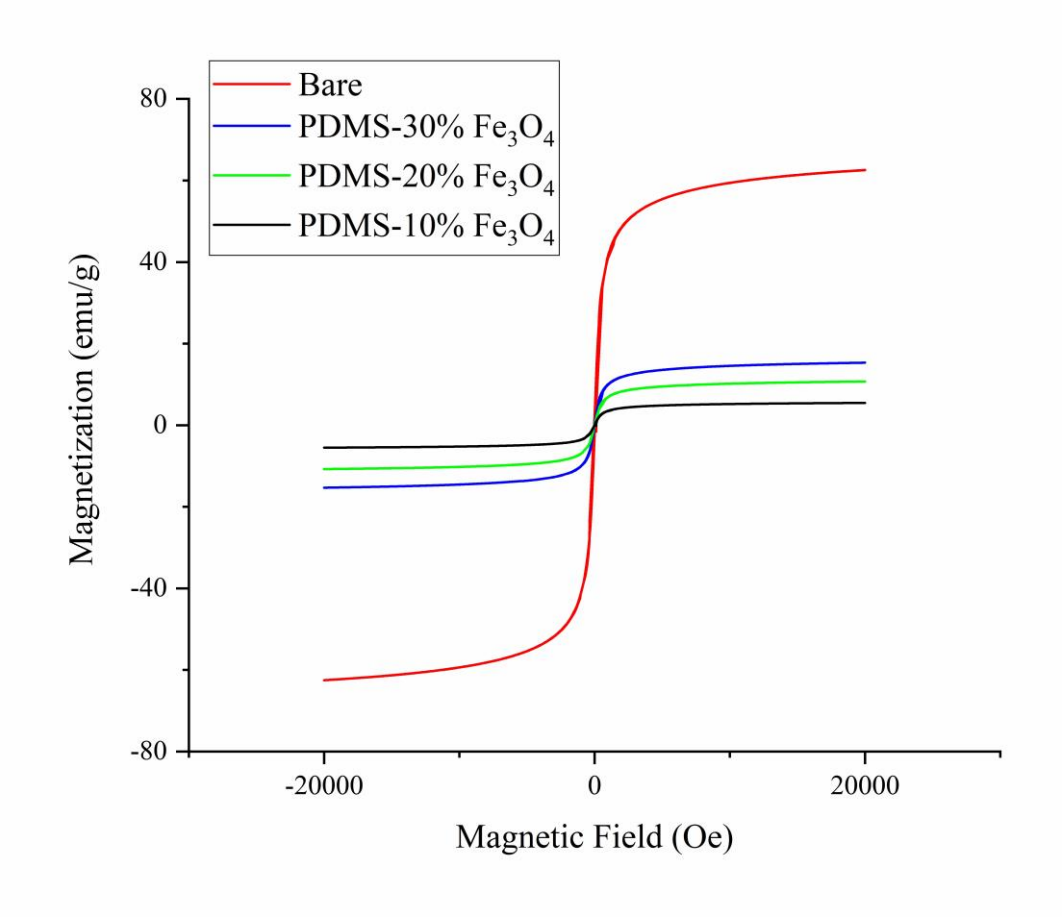

Figure 4.11. Hysteresis curves of Fe_3O_4 particles and magnetic membranes.

4.2.2. Membrane Thickness

The thickness of the spin-coated magnetic membranes is shown in Figure 4.11. It can be seen from Figure 4.11b that PDMS-30% Fe_3O_4 was the thickest and PDMS-10% Fe_3O_4 was the thinnest one. The reason is that the increased concentration of Fe_3O_4 in the membrane results in higher viscosity of fluid composite. That is why, higher concentration has more resistance against the movement and membrance became thick. In other words, centrifugal forces, which are acting during the spinning, have less impact on spreading of composite. The range of thickness varied from 0.74 to 0.44 mm.

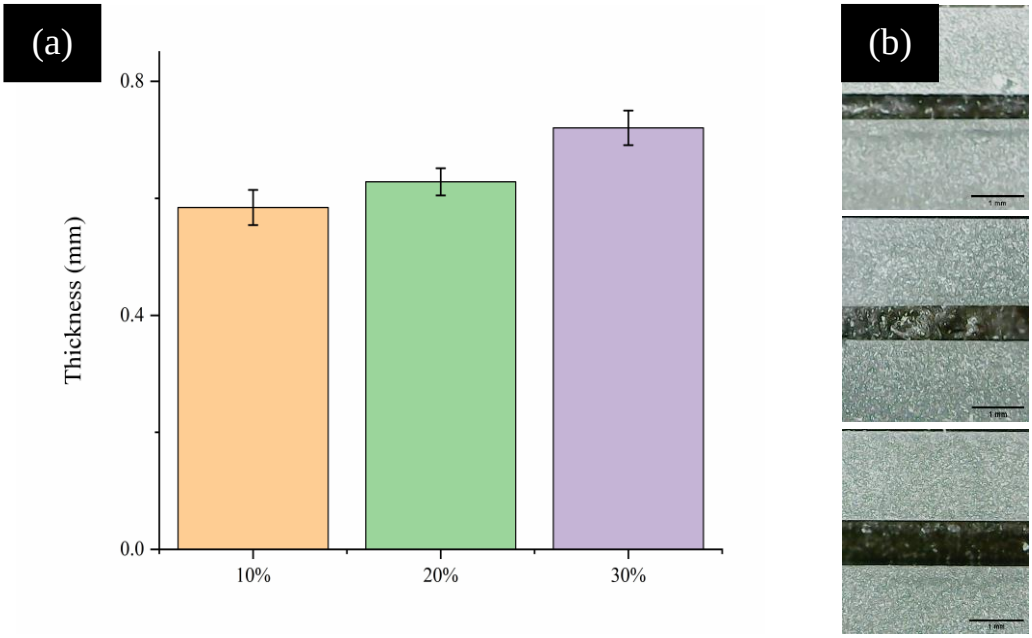

Figure 4.12. (a) Magnetic membrane thicknesses for different Fe_3O_4 concentration and (b) their corresponding digital images - from the top to the bottom belong to the PDMS-10% Fe_3O_4, PDMS-20% Fe_3O_4, and PDMS-30% Fe_3O_4, respectively.

4.2.3. Leakage Test

After 5 h of observation, no liquid leakage from either the membrane or reservoir was detected (Figure 4.13). This result was important to expand the studies through the dosing.

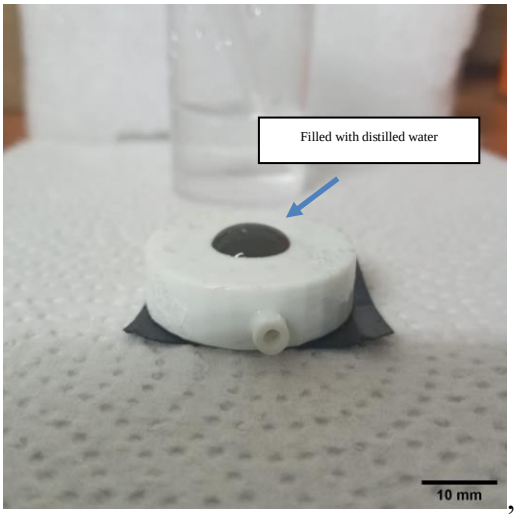

Figure 4.13. Leakage test applied to the reservoir.

Generally in the literature, attaching PDMS to ABS requires complex preocedures such

as oxgen plasma and silanization [162]. In our design, PDMS was assembled to ABS reservoir by using another PDMS layer. This technique was interpreted as effective and easy for the assembly of micropump components.

ABS is a well known material which is resistant to water. But, leakage of water may occur through filaments. Smoothing of filaments was interpreted as an effective and simple process for micropump fabrication.

4.3. Electromagnetic Characterization

4.3.1. Actuator

Magnetic flux density of the electromagnet was measured as a function of distance between 5 – 60 V to determine the supplied magnetic field. Magnetic flux density is the function of applied voltage and distance, which can be formulated as Equation 4.1 derived from Ampere's Law for constant current.

$$B = \frac{\mu_0 V}{2\pi r R} \tag{4.1}$$

Where, B is magnetic flux density (T), $\mu 0$ is permeability of free space, V is applied voltage (V), r is distance from the wire (m), R is resistance (Ω). Even though, this is the formula given for single wire, it provides the framework to interpret the results. Formula indicates that while the strength of magnetic field is proportional to applied voltage, it is inversely proportional to the distance away from the source. As seen in Figure 4.14a, applied voltage and magnetic flux density are linearly proportional.

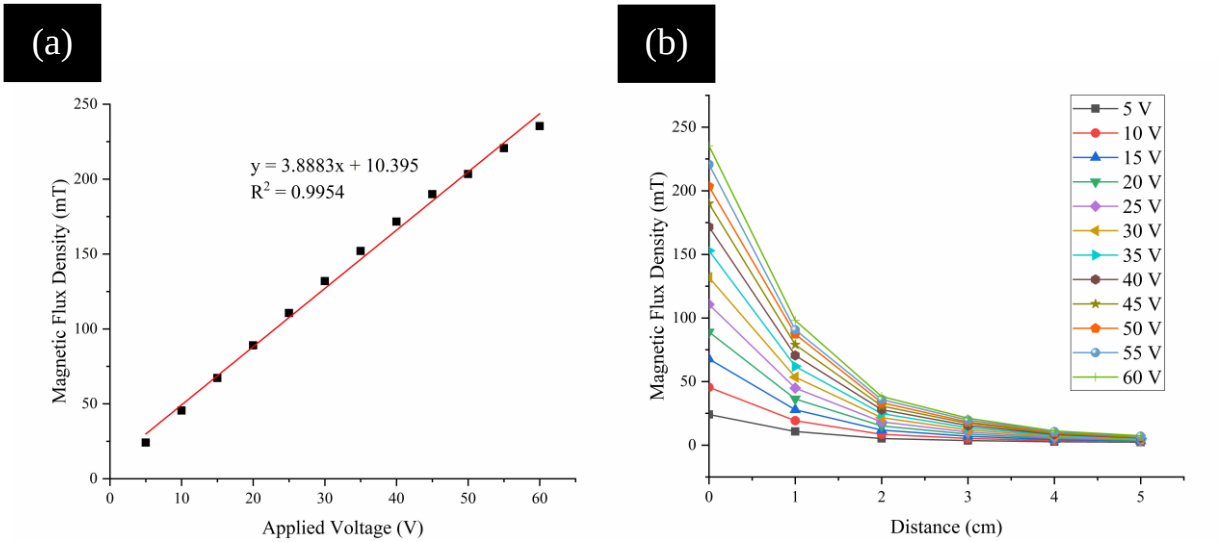

Figure 4.14. (a) Measured magnetic flux density of the electromagnet surface (d= 0) at different voltages applied, (b) Measured magnetic flux density of the electromagnet at different distances under 5 – 60 V applied.

Higher applied voltage results in higher magnetic flux density. In addition, Figure 4.14b shows that as the probe moves away from the source, the strength of magnetic flux density decreases. These results are convenient with Ampere's law. According to graphs, it is seen that electromagnet has capacity of creating magnetic flux density up to ~ 235 mT. However, considering the length of micropump (L = 7 mm) as well as microneedle array between electromagnet and magnetic membrane, the strength of magnetic flux is expected to be lesser than 235 mT.

4.3.2. Membrane Deflection

During deflection study, it is seen that the membrane has the ability of returning to its initial position for all iron oxide concentrations when the power supply is turned off (Figure 4.15a, e). As expected, the increase in voltage resulted in higher magnetic field, consequently higher deflection. The range of deflection varied from 0.17 ± 0.01 to 1.13 ± 0.1. As seen in Figure 4.16, PDMS-20% Fe_3O_4 showed the higher deflection for each applied voltage. The increase in the composition of iron oxide from 10 % to 20 wt% caused the higher deflection. However, deflection was decreased when the concentration was increased to 30 wt%. The reason for this might be the decrease in the elasticity of the membrane. Similar results were also reported in the literature. Paknahada et al. [161] produced PDMS-Fe_3O_4 composite and reported that deflection of membrane was proportional to concentrations (up to 5 wt%), but inversely proportional for higher

concentration due to decreasing elasticity of membrane. As a result, the PDMS-20% Fe_3O_4 membrane was chosen for the dosing studies due to its highest deflection.

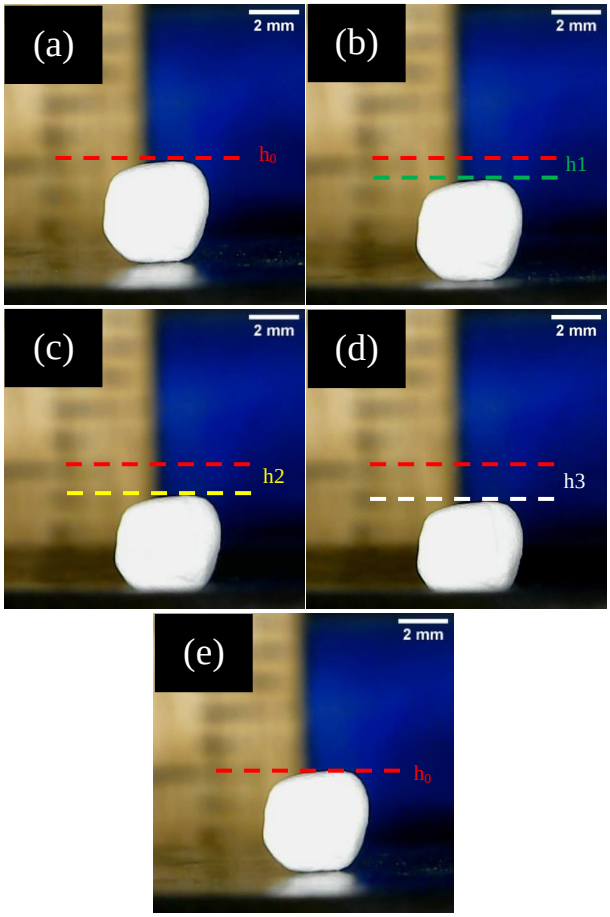

Figure 4.15. The deflection of membrane of 30 % wt Fe_3O_4 under different voltage: (a) V= 0, (b) 20 V, (c) 40 V, (d) 60 V, (e) V=0.

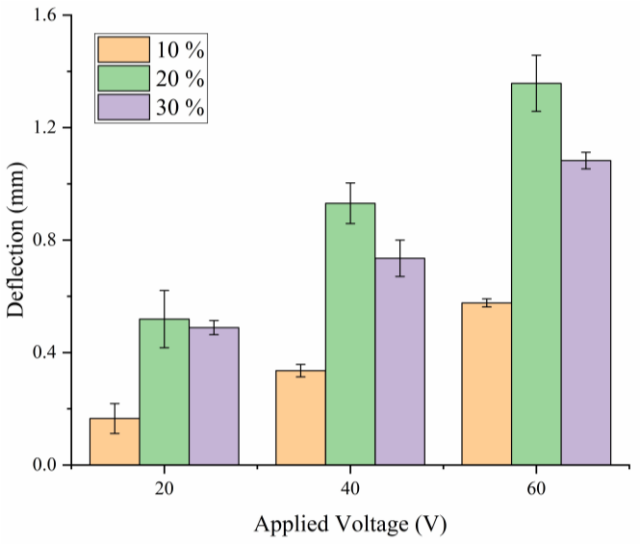

Figure 4.16. Deflection of different membranes were given under certain applied voltage.

Deflection profile was achieved for the all concentrations following the order of h3 > h2 > h1 (Figure 4.15)**.** When analyzing the recorded videos of the membrane, it was seen that the membrane reaches the maximum deflection and returns to its initial position in less than 2 s. Thus, the response time (return time plus deflection) was interpreted as less than 4 s. Paknahada et al. [161] reported the response time as 10 s for 5 wt% Fe_3O_4/PDMS magnetic membrane. In this work, response time was less than 10 s for all magnetic membranes. The reason of this may be higher Fe_3o_4 concentration lead to stronger magntic forces. Laser displacement meters may be used for further studies to determine the response time and deflection more precisely.

4.4. Micropump System

Dosing performance of micropump based microneedle array and its general properties was reported in this section. Firstly, the results of magnetic membrane were presented Then, a membrane with neodymium magnet was reported.

4.4.1. Dosing performance

Magnetic membrane itself (PDMS-20% Fe_3O_4) was unable to pump the liquid out of the reservoir. Even at 60 V, pressure exerted by membrane was not sufficient. Considering the similar studies in the literature, Jayaneththi et al. [140] used magnetic membrane (30 % wt) for pneumatic actuation to achieve flow through one microneedle (outer and bore diameter as 235, 108, the length of 1000 μm). In their study, flow rates were reported as 9.07 to 108 μL/min according to different actuations.

In another study, Wang et al [163] fabricated magnetic iron oxide-PDMS membrane (50 % wt) with dimension of 1.1 x 1.1 mm for electromagnetic actuation. The aperture with the diameter of 0.2 mm was used to exit the flow. They reported the pumped volume of drug solution as 0.05 μL, 0.1 μL and 0.27 μL for the magnetic fields of 70, 109 and 181 mT, respectively.

To compare our design paremeters with the literature mentioned above, Darcy–Weisbach equation (Equation 4.2) may provide an insight about pressure loss. In our study, there are 6 microneedles with the bore diameter of 200 μm and length of 1400 μm. According to the equation, more microneedles and their higher length may result in higher pressure

loss, and therefore unable to pump-out. In addition to pressure loss, the height of the reservoir plus the length of the microneedle, represents the total distance (~ 10 mm) between electromagnet and membrane which reduce the magnetic field (Figure 4.14b). Also, considering electromagnetic absorption of PLA and ABS, the effective magnetic field was less than 100 mT (60V) as seen in Figure 4.14b.

$$hf = f_d \frac{L \times v^2}{D \times 2g} \tag{4.2}$$

Where hf is pressure loss (m), f_d is darcy friction factor, L is length of pipe (m), D hydrodynamic diameter of pipe (m), v is velocity of fluid (m/s), g is acceleration due to gravity (m/s^2).

Design of the system can be improved to enable dosing with the membrane itself. For example, distance between membranes and power source may be reduced to impart higher pressure and the number of microneedles in the array may be decreased to lessen the resistance to flow. To benefit higher magnetic fields, instead of positive pressure, negative pressure can be used by addition of a second fluid reservoir.

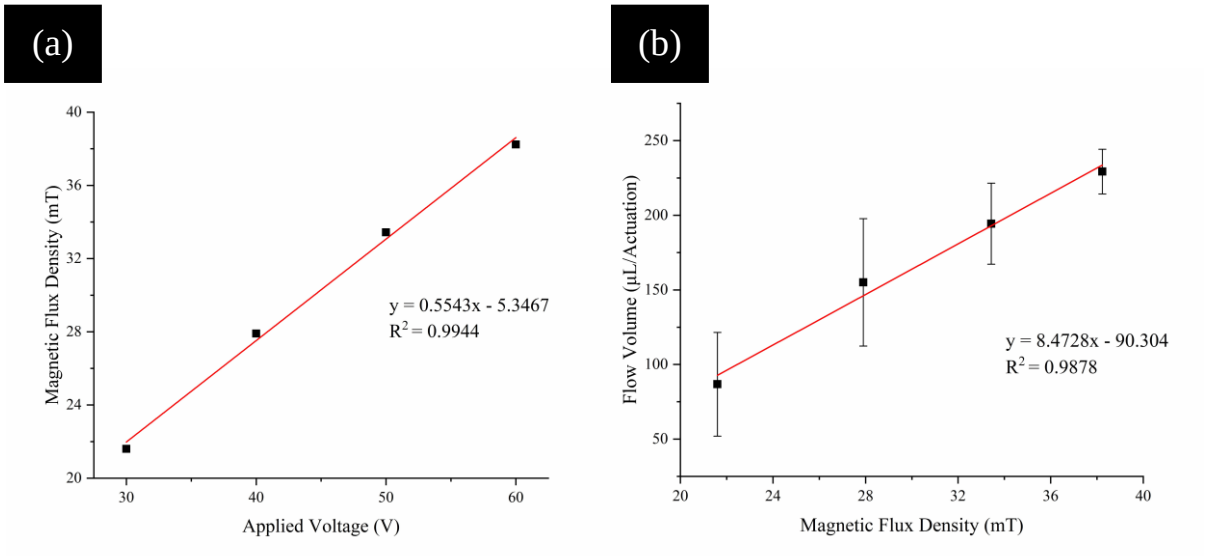

Figure 4.17. (a) Magnetic flux density of the micropump system according to the applied voltage, (b) the flow rate received with respect to the magnetic field for single actuation.

Magnetic membrane with neodymium magnet was successfully managed to pump liquid

at different voltages. In single actuation study, system was able to pump the liquid out of the reservoir with flow rates of 87 to 230 µL/actuation (43 ± 17 and 115 ± 8 µL/s) at 30-60 V. As expected, maximum flow rate was achieved for the highest applied voltage (60 V). System was not functional at 20 V, so 30 V was prefered as a start point of actuation. Flow rate profile was linear over the magnetic field as seen Figure 4.17.

Said et al [164] incorporated magnetic particles with PDMS to fabricate a thin 6 % NdFeB/PDMS composite for single actuation. The flow rate of 6.523 nL/min was reported for 0.63 mT. Gidde et al [165] placed a magnet on the bare PDMS membrane for actuation. Their system was composed of three chamber such as inlet, pumping and outlet. Working design relied on negative pressure for pumping. Maximum flow rate was reported as 441 µL/min (30 µL/s) for 5.3 Vrsm. This value is slightly higher than the minimum reported flow rate (22 µL/s) in this study for single actuation.

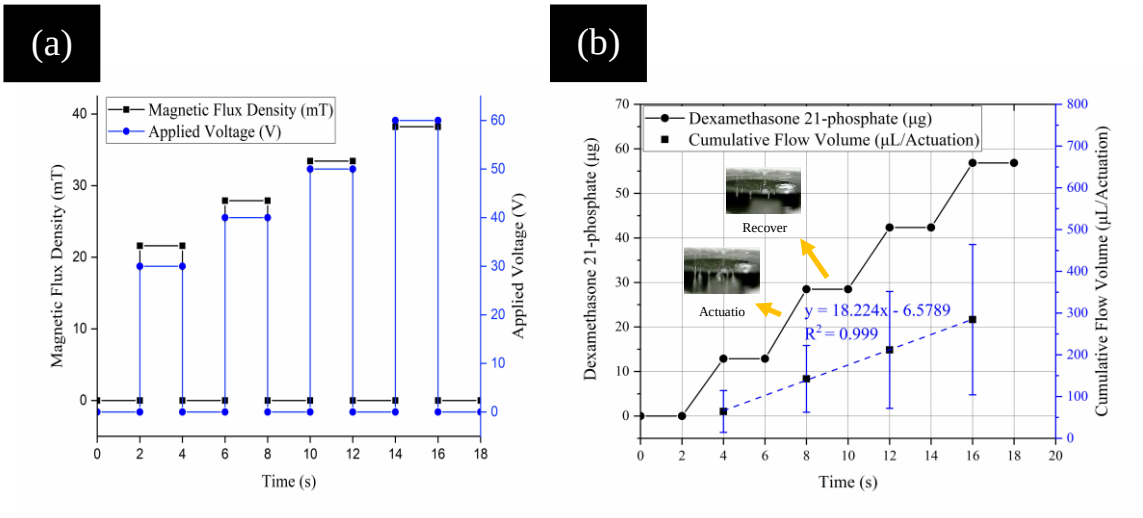

Figure 4.18. (a) The parameters of programmed actuation (voltage over time) together with measured magnetic fields, (b) the cumulative dexamethasone release and cumulative flow volume over time.

In a repeated actuation study, the micropump system managed adjustable dosing over time as seen in Figure 4.18. Dosing profile over time was linear. Total pumped volume was measured as 0.28 ± 0.09 mL. Final dead volume (%) was calculated as 78 ± 7.5. System has the ability of delivering about 62 µg dexamethasone in 16 seconds. Dosing was achived by gradual increase in voltage. Adjustable flow rate was varied between 32

± 12 and 142 ± 45 µL/s. Distinctly, the micropump system does not require any check valve or another reservoir to balance pressure after its actuation. As such, system takes advantageous of simple and portable (a total weight of system is 4.6 g).

Percent dead volume of 78 ± 7.5 is high, but it is an expected scenario for a single micropump system. To decrease dead volume, the height of the reservoir can be reduced to the distance at which the membrane touches the base of the reservoir due to deflection. Besides, the system can be converted to pneumatic design to balance pressure inside the reservoir by using a check valve.

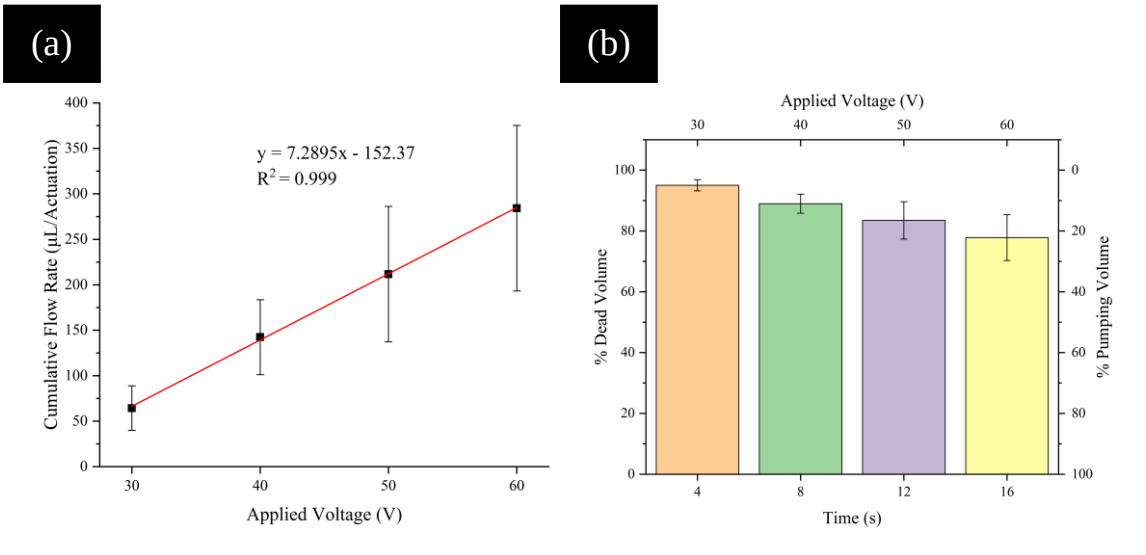

Figure 4.19. (a) cumulative flow rate with respect to actuation, (b) the change of dead volume (%) over time.

Table 4.5. The general properties of the micropump developed in this thesis.

Type of Actuation	**Design of Working**	**Type of Displacement**	**The number of Chamber**	**Volume of Reservoir (mL)**
Electromagnetic	Unidirectional	Positive	One	2
Membrane	**Flow Rate (**µL/s)	**Response Time(s)**	**Weight of System (g)**	**Adjustable Dosing**
Nd magnet+ 20 %	32 ± 12 and 142 ± 45 µL/s	< 4	4.6	Yes

In summary (Table 4.5), an electromagnetically actuated micropump can deliver an aqueous drug solution through PLLA hollow microneedles with flow rates between 43 ± 17 and 115 ± 8 μL/s for single dosing or 32 ± 12 and 142 ± 45 μL/s for programmed actuation at 30 – 60 V range. It is overall 4.6 g with a response time less than 4 s.

5. CONCLUSION

In literature, hollow microneedles fabricated by solvent casting methods require additional steps to make them suitable for infusion. Besides, MEMs fabrication methods are also used but process steps are expensive and complex. In this thesis, a positive mold was developed for direct fabrication of hollow microneedles. Microneedles fabricated by this technique have the ability of skin penetration. Moreover, the proposed microneedle fabrication method is simple and cost efficient, so it appeals to industry as a feasible process for the large-scale fabrication of hollow polymeric microneedles. Not only PLLA but also other polymers can be used with this technique to fabricate microneedle arrays. As a disadvantage of this method, the differences in the length of microneedles may be problematic. While longer microneedles damage the deeper tissues, smaller microneedles are unable to reach the dermis. Therefore, the fabrication process can be improved to achieve more homogenous and repeatable microneedles.

The fabricated micropump system provides adjustable dosing over time. Single or repeated dosing are possible with the system. It is not only for dexamethasone but also other therapeutics can be used with the micropump for dosing. Since the micropump includes simple and low-cost fabricated components, design criterias can be easily improved to increase its efficiency or to adapt for other applications.

In the future, this micropump assisted microneedle array may be a promising device since it benefits from advantages of microneedles and micropumps. It is expected in the near future that a number of commercial microneedle and micropump products will be presented to the market. That is why, the development of novel and feasible fabrication methods is crucial to make these products easily reachable.

6. REFERENCES

[1] J.E. Lai-Cheong, J.A. McGrath, Structure and function of skin, hair and nails, Medicine (United Kingdom). 49 (2021) 337–342.

[2] J.V. Sullivan, S. Myers, Skin Structure and Function, Wound Healing and Scarring, Plastic Surgery - Principles and Practice. (2022) 1–14.

[3] Human skin | Definition, Layers, Types, & Facts | Britannica, (n.d.). https://www.britannica.com/science/human-skin (accessed March 25, 2023).

[4] J. Hou, Paracellular Channel in Organ System, The Paracellular Channel. (2019) 93–141.

[5] S. Nafisi, H.I. Maibach, Skin penetration of nanoparticles, Emerging Nanotechnologies in Immunology: The Design, Applications and Toxicology of Nanopharmaceuticals and Nanovaccines. (2018) 47–88.

[6] J. Calonje, T. Brenn, A. Lazar, S. Billings, McKee's Pathology of the Skin, 2 Volume Set E-Book, 2018. https://books.google.com/books?hl=en&lr=&id=pMN1DwAAQBAJ&oi=fnd&pg=PP1&dq=Calonje,+J.+E.,+Brenn,+T.,+Lazar,+A.+J.,+%26+Billings,+S.+(2018).+McKee%27s+Pathology+of+the+Skin,+2+Volume+Set+E-Book.+Elsevier+Health+Sciences.&ots=OF3LeN2cYk&sig=P4SGch-EMCjjTOr5VJJVw1raSQc (accessed March 25, 2023).

[7] H. Yousef, M. Alhajj, S. Sharma, Anatomy, Skin (Integument), Epidermis, StatPearls. (2022). https://www.ncbi.nlm.nih.gov/books/NBK470464/ (accessed March 25, 2023).

[8] W.M. Woo, Skin Structure and Biology, Imaging Technologies and Transdermal Delivery in Skin Disorders. (2019) 1–14.

[9] B. Yan, N. Liu, J. Li, J. Li, W. Zhu, Y. Kuang, X. Chen, C. Peng, The role of Langerhans cells in epidermal homeostasis and pathogenesis of psoriasis, J Cell Mol Med. 24 (2020) 11646.

[10] I. Cardoso-Daodu, … C.A.-W.J. of B., undefined 2021, Hydrogels for management of chronic wound healing, Wjbphs.Com. (2021).

[11] C. Czekalla, K.H. Schönborn, J. Lademann, M.C. Meinke, Noninvasive Determination of Epidermal and Stratum Corneum Thickness in vivo Using Two-Photon Microscopy and Optical Coherence Tomography: Impact of Body Area, Age, and Gender, Skin Pharmacol Physiol. 32 (2019) 142–150.

[12] Y. Kitajima, Implications of normal and disordered remodeling dynamics of corneodesmosomes in stratum corneum, Dermatologica Sinica. 33 (2015) 58–63.

[13] M.B. Murphrey, J.H. Miao, P.M. Zito, Histology, Stratum Corneum, StatPearls. (2022). https://www.ncbi.nlm.nih.gov/books/NBK513299/ (accessed March 25, 2023).

[14] K.P. Ananthapadmanabhan, S. Mukherjee, P. Chandar, Stratum corneum fatty acids: their critical role in preserving barrier integrity during cleansing, Int J Cosmet Sci. 35 (2013) 337–345.

[15] J.V. Sullivan, S. Myers, Skin Structure and Function, Wound Healing and Scarring, Plastic Surgery - Principles and Practice. (2022) 1–14.

[16] D.T. Woodley, Distinct Fibroblasts in the Papillary and Reticular Dermis: Implications for Wound Healing, Dermatol Clin. 35 (2017) 95–100.

[17] P. Ciarletta, M. Ben Amar, Papillary networks in the dermal–epidermal junction of skin: A biomechanical model, Mech Res Commun. 42 (2012) 68–76.

[18] T.W. Mak, M.E. Saunders, Mucosal and Cutaneous Immunity, The Immune Response. (2006) 583–609.

[19] V. Falanga, Bioengineered skin constructs, Principles of Tissue Engineering. (2020) 1331–1352.

[20] M. Bonmarin, F.A. Le Gal, Thermal Imaging in Dermatology, Imaging in Dermatology. (2016) 437–454.

[21] D.A. Yanez, R.K. Lacher, A. Vidyarthi, O.R. Colegio, The role of macrophages in skin homeostasis, Pflugers Arch. 469 (2017) 455–463.

[22] S. Adepu, S. Ramakrishna, Controlled Drug Delivery Systems: Current Status and Future Directions, Molecules. 26 (2021).

[23] T. Ramasamy, H.B. Ruttala, B. Gupta, B.K. Poudel, H.G. Choi, C.S. Yong, J.O. Kim, Smart chemistry-based nanosized drug delivery systems for systemic applications: A comprehensive review, J Control Release. 258 (2017) 226–253.

[24] F. Gensdarmes, Methods of Detection and Characterization, Nanoengineering: Global Approaches to Health and Safety Issues. (2015) 55–84.

[25] N. Tangboriboon, Carbon and Carbon Nanotube Drug Delivery and Its Characterization, Properties, and Applications, Nanocarriers for Drug Delivery: Nanoscience and Nanotechnology in Drug Delivery. (2019) 451–467.

[26] N.J. Kohrs, T. Liyanage, N. Venkatesan, A. Najarzadeh, D.A. Puleo, Drug delivery systems and controlled release, Encyclopedia of Biomedical Engineering. 1–3 (2019) 316–329.

[27] K. Moffatt, R.F. Donnelly, Microneedle technology, Drug Delivery Devices and Therapeutic Systems. (2021) 345–366.

[28] M. Bok, Z.J. Zhao, S. Jeon, J.H. Jeong, E. Lim, Ultrasonically and Iontophoretically Enhanced Drug-Delivery System Based on Dissolving Microneedle Patches, Sci Rep. 10 (2020).

[29] J.F. Liu, B. Jang, D. Issadore, A. Tsourkas, Use of Magnetic Fields and Nanoparticles to Trigger Drug Release and Improve Tumor Targeting, Wiley Interdiscip Rev Nanomed Nanobiotechnol. 11 (2019) e1571.

[30] H.R. Rezaie, M. Esnaashary, A.A. Arjmand, A. Öchsner, The History of Drug Delivery Systems, SpringerBriefs in Applied Sciences and Technology. (2018) 1–8.

[31] S. Adepu, S. Ramakrishna, Controlled Drug Delivery Systems: Current Status and Future Directions, Molecules 2021, Vol. 26, Page 5905. 26 (2021) 5905.

[32] SUSTAINED RELEASE DRUG DELIVERY SYSTEM : A CONCISE REVIEW | PharmaTutor, (n.d.). https://www.pharmatutor.org/articles/sustained-release-drug-delivery-system-concise-review?page=3%2C2 (accessed March 25, 2023).

[33] J.S. Silva, D. Marques-da-Silva, R. Lagoa, Towards the Development of Delivery Systems of Bioactive Compounds With Eyes Set on Pharmacokinetics, Modeling and Control of Drug Delivery Systems. (2021) 125–144.

[34] C.N. Cheaburu-Yilmaz, H.Y. Karasulu, O. Yilmaz, Nanoscaled Dispersed Systems Used in Drug-Delivery Applications, Polymeric Nanomaterials in Nanotherapeutics. (2019) 437–468.

[35] J. Kim, O. De Jesus, Medication Routes of Administration, StatPearls. (2023). https://www.ncbi.nlm.nih.gov/books/NBK568677/ (accessed March 25, 2023).

[36] B. Zorec, V. Préat, D. Miklavčič, N. Pavšelj, Active enhancement methods for intra- and transdermal drug delivery: a review, Slovenian Medical Journal. 82 (2013). https://vestnik.szd.si/index.php/ZdravVest/article/view/657 (accessed March 25, 2023).

[37] M.E. Ruiz, S. Scioli Montoto, Routes of Drug Administration, ADME Processes in Pharmaceutical Sciences. (2018) 97–133.

[38] D. Nunes, S. Andrade, M.J. Ramalho, J.A. Loureiro, M.C. Pereira, Polymeric Nanoparticles-Loaded Hydrogels for Biomedical Applications: A Systematic Review on In Vivo Findings, Polymers 2022, Vol. 14, Page 1010. 14 (2022) 1010.

[39] A. Advankar, R. Maheshwari, V. Tambe, P. Todke, N. Raval, D. Kapoor, R.K. Tekade, Specialized tablets: ancient history to modern developments, Drug Delivery Systems. (2019) 615–664.

[40] S.K. Bardal, J.E. Waechter, D.S. Martin, Pharmacokinetics, Applied Pharmacology. (2011) 17–34.

[41] S.G. Antimisiaris, A. Marazioti, M. Kannavou, E. Natsaridis, F. Gkartziou, G. Kogkos, S. Mourtas, Overcoming barriers by local drug delivery with liposomes, Adv Drug Deliv Rev. 174 (2021) 53–86.

[42] W. Leppert, M. Malec-Milewska, R. Zajaczkowska, J. Wordliczek, Transdermal and Topical Drug Administration in the Treatment of Pain, Molecules 2018, Vol. 23, Page 681. 23 (2018) 681.

[43] F. Sabbagh, B.S. Kim, Recent advances in polymeric transdermal drug delivery systems, J Control Release. 341 (2022) 132–146.

[44] D. Choudhary, H. Goykar, K. Rajpoot, R.K. Tekade, Chronopharmacokinetics, Biopharmaceutics and Pharmacokinetics Considerations: Volume 1 in Advances in Pharmaceutical Product Development and Research. (2021) 163–194.

[45] A.Z. Alkilani, M.T.C. McCrudden, R.F. Donnelly, Transdermal Drug Delivery: Innovative Pharmaceutical Developments Based on Disruption of the Barrier Properties of the stratum corneum, Pharmaceutics. 7 (2015) 438–470.

[46] M.R. Prausnitz, R. Langer, Transdermal drug delivery, Nature Biotechnology 2008 26:11. 26 (2008) 1261–1268.

[47] D. Ramadon, M.T.C. McCrudden, A.J. Courtenay, R.F. Donnelly, Enhancement strategies for transdermal drug delivery systems: current trends and applications, Drug Deliv Transl Res. 12 (2022) 758–791.

[48] A. Arora, M.R. Prausnitz, S. Mitragotri, Micro-scale devices for transdermal drug delivery, Int J Pharm. 364 (2008) 227–236.

[49] H. Benson, Transdermal Drug Delivery: Penetration Enhancement Techniques, Curr Drug Deliv. 2 (2005) 23–33.

[50] T.H.-J.S.C. Chem, undefined 1960, Physical chemical analysis of percutaneous absorption process from creams and ointments, Cir.Nii.Ac.Jp. (n.d.). https://cir.nii.ac.jp/crid/1570572700008379776 (accessed March 26, 2023).

[51] K. Moser, K. Kriwet, A. Naik, Y.N. Kalia, R.H. Guy, Passive skin penetration enhancement and its quantification in vitro, European Journal of Pharmaceutics and Biopharmaceutics. 52 (2001) 103–112.

[52] D.I.J. Morrow, P.A. Mccarron, A.D. Woolfson, R.F. Donnelly, Innovative Strategies for Enhancing Topical and Transdermal Drug Delivery, The Open Drug Delivery Journal. 1 (2007) 36–59.

[53] S. Zsikó, E. Csányi, A. Kovács, M. Budai-Szűcs, A. Gácsi, S. Berkó, Methods to Evaluate Skin Penetration In Vitro, Scientia Pharmaceutica 2019, Vol. 87, Page 19. 87 (2019) 19.

[54] M. Markovic, S. Ben-Shabat, A. Dahan, Prodrugs for Improved Drug Delivery: Lessons Learned from Recently Developed and Marketed Products, Pharmaceutics. 12 (2020) 1–12.

[55] B.W. Barry, Novel mechanisms and devices to enable successful transdermal drug delivery, European Journal of Pharmaceutical Sciences. 14 (2001) 101–114.

[56] M. Cristofoli, C.P. Kung, J. Hadgraft, M.E. Lane, B.C. Sil, Ion Pairs for Transdermal and Dermal Drug Delivery: A Review, Pharmaceutics 2021, Vol. 13, Page 909. 13 (2021) 909.

[57] K.M.B. Mackay, A.C. Williams, B.W. Barry, Effect of melting point of chiral terpenes on human stratum corneum uptake, Int J Pharm. 228 (2001) 89–97.

[58] A. Akbarzadeh, R. Rezaei-Sadabady, S. Davaran, S.W. Joo, N. Zarghami, Y. Hanifehpour, M. Samiei, M. Kouhi, K. Nejati-Koshki, Liposome: classification, preparation, and applications, Nanoscale Res Lett. 8 (2013) 102.

[59] E. Larrañeta, R.E.M. Lutton, A.D. Woolfson, R.F. Donnelly, Microneedle arrays as transdermal and intradermal drug delivery systems: Materials science, manufacture and commercial development, Materials Science and Engineering: R: Reports. 104 (2016) 1–32.

[60] A. Trautmann, G.L. Roth, B. Nujiqi, T. Walther, R. Hellmann, Towards a versatile point-of-care system combining femtosecond laser generated microfluidic channels and direct laser written microneedle arrays, Microsystems & Nanoengineering 2019 5:1. 5 (2019) 1–9.

[61] A.S. Rzhevskiy, T.R.R. Singh, R.F. Donnelly, Y.G. Anissimov, Microneedles as the technique of drug delivery enhancement in diverse organs and tissues, J Control Release. 270 (2018) 184–202.

[62] K. Cheung, T. Han, D.B. Das, Effect of Force of Microneedle Insertion on the Permeability of Insulin in Skin, J Diabetes Sci Technol. 8 (2014) 444.

[63] AdminPatch® 1500 microneedle array | AdminMed, (n.d.). http://www.adminmed.com/array1500 (accessed March 25, 2023).

[64] W. Martanto, J.S. Moore, O. Kashlan, R. Kamath, P.M. Wang, J.M. O'Neal, M.R. Prausnitz, Microinfusion using hollow microneedles, Pharm Res. 23 (2006) 104–113.

[65] A. Boucaud, M.A. Garrigue, L. Machet, L. Vaillant, F. Patat, Effect of sonication parameters on transdermal delivery of insulin to hairless rats, Journal of Controlled Release. 81 (2002) 113–119.

[66] A. Tezel, A. Sens, J. Tuchscherer, S. Mitragotri, Frequency dependence of sonophoresis, Pharm Res. 18 (2001) 1694–1700.

[67] A. Azagury, L. Khoury, G. Enden, J. Kost, Ultrasound mediated transdermal drug delivery, Adv Drug Deliv Rev. 72 (2014) 127–143.

[68] J. Manikkath, A.R. Hegde, H.S. Parekh, S. Mutalik, Peptide Dendrimers in Delivery of Bioactive Molecules to Skin, Nanoscience in Dermatology. (2016) 89–97.

[69] B.M. Medi, B. Layek, J. Singh, Electroporation for dermal and transdermal drug delivery, Percutaneous Penetration Enhancers Physical Methods in Penetration Enhancement. (2017) 105–122.

[70] K. Jinturkar, M. Rathi, … A.M. delivery of therapeutic genomics and, undefined 2011, Gene delivery using physical methods, Elsevier. (n.d.). https://www.sciencedirect.com/science/article/pii/B9780123849649000037 (accessed March 25, 2023).

[71] A. Arora, Liquid and powder jet injectors in drug delivery: Mechanisms, designs, and applications, Percutaneous Penetration Enhancers Physical Methods in Penetration Enhancement. (2017) 221–230.

[72] R. Diotti, V. Caputo, G.S.-P.A. of V. Development, undefined 2022, Conventional and nontraditional delivery methods and routes of vaccine administration, Elsevier. (n.d.). https://www.sciencedirect.com/science/article/pii/B9780128143575000064 (accessed March 25, 2023).

[73] J.W. Lee, P. Gadiraju, J.H. Park, M.G. Allen, M.R. Prausnitz, Microsecond thermal ablation of skin for transdermal drug delivery, Journal of Controlled Release. 154 (2011) 58–68.

[74] R. Parhi, A. Mandru, Enhancement of skin permeability with thermal ablation techniques: concept to commercial products, Drug Delivery and Translational Research 2020 11:3. 11 (2020) 817–841.

[75] R.C.-T.B. Bulletin, undefined 1921, Microdissection studies, III. Some problems in the maturation and fertilization of the echinoderm egg, Journals.Uchicago.Edu. (n.d.). https://www.journals.uchicago.edu/doi/pdf/10.2307/1536756 (accessed March 28, 2023).

[76] M. Gerstel, 964,482 VA Place - US Patent 3, undefined 1976, Drug delivery device, Google Patents. (n.d.). https://patents.google.com/patent/US3964482A/en (accessed March 28, 2023).

[77] M. Louis Paul Pistor, F. Assignees, E.A. Guerin, P. Pistor, Device for cutaneous therapeutic treatment, (1974).

[78] S. Henry, D. V. McAllister, M.G. Allen, M.R. Prausnitz, Microfabricated Microneedles: A Novel Approach to Transdermal Drug Delivery, J Pharm Sci. 87 (1998) 922–925.

[79] J.A. Mikszta, J.B. Alarcon, J.M. Brittingham, D.E. Sutter, R.J. Pettis, N.G. Harvey, Improved genetic immunization via micromechanical disruption of skin-barrier function and targeted epidermal delivery, Nature Medicine 2002 8:4. 8 (2002) 415–419.

[80] D. V Mcallister, P.M. Wang, S.P. Davis, J.-H. Park, P.J. Canatella, M.G. Allen, M.R. Prausnitz, Microfabricated needles for transdermal delivery of macromolecules and nanoparticles: Fabrication methods and transport studies, 100 (2003) 13755–13760. www.pnas.orgcgidoi10.1073pnas.2331316100 (accessed March 29, 2023).

[81] T. Miyano, Y. Tobinaga, T. Kanno, Y. Matsuzaki, H. Takeda, M. Wakui, K. Hanada, Sugar Micro Needles as Transdermic Drug Delivery System, Biomed Microdevices. 7 (2005) 185–188.

[82] R.F. Donnelly, T.R.R. Singh, M.J. Garland, K. Migalska, R. Majithiya, C.M. McCrudden, P.L. Kole, T.M.T. Mahmood, H.O. McCarthy, A.D. Woolfson, Hydrogel-Forming Microneedle Arrays for Enhanced Transdermal Drug Delivery, Adv Funct Mater. 22 (2012) 4879–4890.

[83] P.M. Wang, M. Cornwell, M.R. Prausnitz, Minimally invasive extraction of dermal interstitial fluid for glucose monitoring using microneedles, Diabetes Technol Ther. 7 (2005) 131–141.

[84] D. Fernandes, Minimally Invasive Percutaneous Collagen Induction, Oral Maxillofac Surg Clin North Am. 17 (2005) 51–63.

[85] R. Maia, V. Carvalho, R. Lima, G. Minas, R.O. Rodrigues, Microneedles in Advanced Microfluidic Systems: A Systematic Review throughout Lab and

Organ-on-a-Chip Applications, Pharmaceutics 2023, Vol. 15, Page 792. 15 (2023) 792.

[86] X. He, J. Sun, J. Zhuang, H. Xu, Y. Liu, D. Wu, Nanotechnology and Microtechnology in Drug Delivery Systems-Review Microneedle System for Transdermal Drug and Vaccine Delivery: Devices, Safety, and Prospects, (n.d.).

[87] T. Lijnse, K. Haider, C. Betancourt Lee, al -, J. Ji, F.E. H Tay, J. Miao, H. Kai, L. Liu, F.E. Tay, Conference Series OPEN ACCESS To cite this article: Jing Ji et al, J. Phys.: Conf. Ser. 34 (2006) 1132.

[88] R. Zhang, P. Zhang, C. Dalton, G.A. Jullien, Modeling of drug delivery into tissues with a microneedle array using mixture theory, Biomech Model Mechanobiol. 9 (2010) 77–86.

[89] S. Dharadhar, A. Majumdar, S. Dhoble, V. Patravale, Microneedles for transdermal drug delivery: a systematic review, Https://Doi.Org/10.1080/03639045.2018.1539497. 45 (2018) 188–201.

[90] E. Larrañeta, R.E.M. Lutton, A.D. Woolfson, R.F. Donnelly, Microneedle arrays as transdermal and intradermal drug delivery systems: Materials science, manufacture and commercial development, Materials Science and Engineering: R: Reports. 104 (2016) 1–32.

[91] O. Paul, J. Gaspar, P. Ruther, Advanced silicon microstructures, sensors, and systems, IEEJ Transactions on Electrical and Electronic Engineering. 2 (2007) 199–215.

[92] M.A. Hopcroft, W.D. Nix, T.W. Kenny, What is the Young's modulus of silicon?, Journal of Microelectromechanical Systems. 19 (2010) 229–238.

[93] M. Dervisevic, M. Alba, L. Yan, M. Senel, T.R. Gengenbach, B. Prieto-Simon, N.H. Voelcker, M. Dervisevic, M. Alba, L. Yan, B. Prieto-Simon, N.H. Voelcker, T.R. Gengenbach, M. Senel, Transdermal Electrochemical Monitoring of Glucose via High-Density Silicon Microneedle Array Patch, Adv Funct Mater. 32 (2022) 2009850.

[94] C. O'Mahony, R. Sebastian, F. Tjulkins, D. Whelan, A. Bocchino, Y. Hu, J. O'Brien, J. Scully, M. Hegarty, A. Blake, I. Slimi, A.J.P. Clover, A. Lyness, A.-M. Kelleher, Hollow silicon microneedles, fabricated using combined wet and dry

etching techniques, for transdermal delivery and diagnostics, Int J Pharm. 637 (2023) 122888.

[95] R. Nagarkar, M. Singh, H.X. Nguyen, S. Jonnalagadda, A review of recent advances in microneedle technology for transdermal drug delivery, J Drug Deliv Sci Technol. 59 (2020) 101923.

[96] T. Waghule, G. Singhvi, S.K. Dubey, M.M. Pandey, G. Gupta, M. Singh, K. Dua, Microneedles: A smart approach and increasing potential for transdermal drug delivery system, Biomedicine & Pharmacotherapy. 109 (2019) 1249–1258.

[97] Á. Cárcamo-Martínez, B. Mallon, J. Domínguez-Robles, L.K. Vora, Q.K. Anjani, R.F. Donnelly, Hollow microneedles: A perspective in biomedical applications, Int J Pharm. 599 (2021) 120455.

[98] P. Madalena Santos, C.O. Rangel-Yagui, A. V Janorkar, L. Luo, N. Sargioti, T.J. Levingstone, E.D. O, H.O. McCarthy, N.J. Dunne, Metallic Microneedles for Transdermal Drug Delivery: Applications, Fabrication Techniques and the Effect of Geometrical Characteristics, Bioengineering 2023, Vol. 10, Page 24. 10 (2022) 24.

[99] J. Li, B. Liu, Y. Zhou, Z. Chen, L. Jiang, W. Yuan, L. Liang, Fabrication of a Ti porous microneedle array by metal injection molding for transdermal drug delivery, PLoS One. 12 (2017) e0172043.

[100] Y. Yoshihisa, T. Shimizu, Metal Allergy and Systemic Contact Dermatitis: An Overview, Dermatol Res Pract. 2012 (2012).

[101] K. Ita, Ceramic microneedles and hollow microneedles for transdermal drug delivery: Two decades of research, J Drug Deliv Sci Technol. 44 (2018) 314–322.

[102] A. Tucak, M. Sirbubalo, L. Hindija, O. Rahić, J. Hadžiabdić, K. Muhamedagić, A. Čekić, E. Vranić, Microneedles: Characteristics, Materials, Production Methods and Commercial Development, Micromachines 2020, Vol. 11, Page 961. 11 (2020) 961.

[103] A. Ovsianikov, B. Chichkov, P. Mente, N.A. Monteiro-Riviere, A. Doraiswamy, R.J. Narayan, Two photon polymerization of polymer-ceramic hybrid materials for transdermal drug delivery, Int J Appl Ceram Technol. 4 (2007) 22–29.

[104] S. Bystrova, R. Luttge, Micromolding for ceramic microneedle arrays, Microelectron Eng. 88 (2011) 1681–1684.

[105] R.L. Rasmussen, J.G. Morse, K.W. Morse, Main Group Elements, Encyclopedia of Physical Science and Technology. (2003) 1–30.

[106] D.V. Shtansky, E.A. Levashov, I.V. Sukhorukova, Multifunctional bioactive nanostructured films, Hydroxyapatite (Hap) for Biomedical Applications. (2015) 159–188.

[107] J. Gupta, E.I. Felner, M.R. Prausnitz, Minimally Invasive Insulin Delivery in Subjects with Type 1 Diabetes Using Hollow Microneedles, Diabetes Technol Ther. 11 (2009) 329.

[108] G. Mahadevan, H. Sheardown, P. Selvaganapathy, PDMS embedded microneedles as a controlled release system for the eye, J Biomater Appl. 28 (2013) 20–27.

[109] S. Bhatnagar, P.R. Gadeela, P. Thathireddy, V.V.K. Venuganti, Microneedle-based drug delivery: materials of construction, Journal of Chemical Sciences. 131 (2019) 1–28.

[110] J. Finley, J. Knabb, Cutaneous silica granuloma, Plast Reconstr Surg. 69 (1982) 340–343.

[111] P.N. Ayittey, J.S. Walker, J.J. Rice, P.P. De Tombe, Glass microneedles for force measurements: A finite-element analysis model, Pflugers Arch. 457 (2009) 1415–1422.

[112] K. Ahmed Saeed AL-Japairai, S. Mahmood, S. Hamed Almurisi, J. Reddy Venugopal, A. Rebhi Hilles, M. Azmana, S. Raman, Current trends in polymer microneedle for transdermal drug delivery, Int J Pharm. 587 (2020) 119673.

[113] M. Azmana, S. Mahmood, A.R. Hilles, U.K. Mandal, K.A. Saeed Al-Japairai, S. Raman, Transdermal drug delivery system through polymeric microneedle: A recent update, J Drug Deliv Sci Technol. 60 (2020) 101877.

[114] G. Du, P. He, J. Zhao, C. He, M. Jiang, Z. Zhang, Z. Zhang, X. Sun, Polymeric microneedle-mediated transdermal delivery of melittin for rheumatoid arthritis treatment, Journal of Controlled Release. 336 (2021) 537–548.

[115] J. Ju, C.-M. Hsieh, Y. Tian, J. Kang, R. Chia, H. Chang, Y. Bai, C. Xu, X. Wang, Q. Liu, Surface Enhanced Raman Spectroscopy Based Biosensor with a Microneedle Array for Minimally Invasive In Vivo Glucose Measurements, 5 (2020) 1777–1785.

[116] D.C. Pawley, S. Goncalves, E. Bas, E. Dikici, S.K. Deo, S. Daunert, F. Telischi, Dexamethasone (DXM)-Coated Poly(lactic-co-glycolic acid) (PLGA) Microneedles as an Improved Drug Delivery System for Intracochlear Biodegradable Devices, Adv Ther (Weinh). 4 (2021).

[117] D. Ramadon, L.F.P. Sutrisna, Y. Harahap, K.S.S. Putri, F. Ulayya, P. Hartrianti, Q.K. Anjani, R.F. Donnelly, Enhancing Intradermal Delivery of Lidocaine by Dissolving Microneedles: Comparison between Hyaluronic Acid and Poly(Vinyl Pyrrolidone) Backbone Polymers, Pharmaceutics 2023, Vol. 15, Page 289. 15 (2023) 289.

[118] Q.Y. Li, J.N. Zhang, B.Z. Chen, Q.L. Wang, X.D. Guo, A solid polymer microneedle patch pretreatment enhances the permeation of drug molecules into the skin, RSC Adv. 7 (2017) 15408–15415.

[119] N.G. Oh, S.Y. Hwang, Y.H. Na, Fabrication of a PVA-Based Hydrogel Microneedle Patch, ACS Omega. 7 (2022) 25179–25185.

[120] H. Du, P. Liu, J. Zhu, J. Lan, Y. Li, L. Zhang, J. Zhu, J. Tao, Hyaluronic Acid-Based Dissolving Microneedle Patch Loaded with Methotrexate for Improved Treatment of Psoriasis, ACS Appl Mater Interfaces. 11 (2019) 43588–43598.

[121] D.A. Castilla-Casadiego, H. Carlton, D. Gonzalez-Nino, K.A. Miranda-Muñoz, R. Daneshpour, D. Huitink, G. Prinz, J. Powell, L. Greenlee, J. Almodovar, Design, characterization, and modeling of a chitosan microneedle patch for transdermal delivery of meloxicam as a pain management strategy for use in cattle, Materials Science and Engineering: C. 118 (2021) 111544.

[122] S. Wang, M. Zhu, L. Zhao, D. Kuang, S.C. Kundu, S. Lu, Insulin-Loaded Silk Fibroin Microneedles as Sustained Release System, ACS Biomater Sci Eng. 5 (2019) 1887–1894.

[123] T.N. Tarbox, A.B. Watts, Z. Cui, R.O. Williams, An update on coating/manufacturing techniques of microneedles, Drug Delivery and Translational Research 2017 8:6. 8 (2017) 1828–1843.

[124] S. Kang, J.E. Song, S.H. Jun, S.G. Park, N.G. Kang, Sugar-Triggered Burst Drug Releasing Poly-Lactic Acid (PLA) Microneedles and Its Fabrication Based on Solvent-Casting Approach, Pharmaceutics 2022, Vol. 14, Page 1758. 14 (2022) 1758.

[125] M. Kim, T. Kim, D.S. Kim, W.K. Chung, Curved Microneedle Array-Based sEMG Electrode for Robust Long-Term Measurements and High Selectivity, Sensors 2015, Vol. 15, Pages 16265-16280. 15 (2015) 16265–16280.

[126] P. Makvandi, A. Maleki, M. Shabani, A.R.J. Hutton, M. Kirkby, R. Jamaledin, T. Fang, J. He, J. Lee, B. Mazzolai, R.F. Donnelly, F.R. Tay, G. Chen, V. Mattoli, Bioinspired microneedle patches: Biomimetic designs, fabrication, and biomedical applications, Matter. 5 (2022) 390–429.

[127] X. Zhang, Y. Wang, J. Chi, Y. Zhao, Smart Microneedles for Therapy and Diagnosis, Research. 2020 (2020).

[128] V. Ghate, A. Renjith, K. Badnikar, S. Pahal, S.N. Jayadevi, M.M. Nayak, P.K. Vemula, D.N. Subramanyam, Single step fabrication of hollow microneedles and an experimental package for controlled drug delivery, Int J Pharm. 632 (2023) 122546.

[129] M.G. McGrath, S. Vucen, A. Vrdoljak, A. Kelly, C. O'Mahony, A.M. Crean, A. Moore, Production of dissolvable microneedles using an atomised spray process: Effect of microneedle composition on skin penetration, European Journal of Pharmaceutics and Biopharmaceutics. 86 (2014) 200–211.

[130] E.A. Allen, C. O'Mahony, M. Cronin, T. O'Mahony, A.C. Moore, A.M. Crean, Dissolvable microneedle fabrication using piezoelectric dispensing technology, Int J Pharm. 500 (2016) 1–10.

[131] M.J. Kim, S.C. Park, B. Rizal, G. Guanes, S.K. Baek, J.H. Park, A.R. Betz, S.O. Choi, Fabrication of circular obelisk-type multilayer microneedles using micro-milling and spray deposition, Front Bioeng Biotechnol. 6 (2018) 54.

[132] D. Huang, J. Li, T. Li, Z. Wang, Q. Wang, Z. Li, Recent advances on fabrication of microneedles on the flexible substrate, Journal of Micromechanics and Microengineering. 31 (2021).

[133] B. Mbituyimana, G. Ma, Z. Shi, G. Yang, Polymer-based microneedle composites for enhanced non-transdermal drug delivery, Appl Mater Today. 29 (2022) 101659.

[134] J.D. Kim, M. Kim, H. Yang, K. Lee, H. Jung, Droplet-born air blowing: Novel dissolving microneedle fabrication, Journal of Controlled Release. 170 (2013) 430–436.

[135] E.M. Cahill, E.D. Ocearbhaill, Toward Biofunctional Microneedles for Stimulus Responsive Drug Delivery, Bioconjug Chem. 26 (2015) 1289–1296.

[136] L. Xiao, B. Wang, G. Yang, M. Gauthier, Poly(Lactic Acid)-Based Biomaterials: Synthesis, Modification and Applications, Biomedical Science, Engineering and Technology. (2012).

[137] S. Mohith, P.N. Karanth, S.M. Kulkarni, Recent trends in mechanical micropumps and their applications: A review, Mechatronics. 60 (2019) 34–55.

[138] M.W. Ashraf, S. Tayyaba, N. Afzulpurkar, Micro Electromechanical Systems (MEMS) based microfluidic devices for biomedical applications, Int J Mol Sci. 12 (2011) 3648–3704.

[139] P. Sritongkham, A. Wisitsoraat, A. Tuantranont, M. Somasundrum, Integration of CNT-Based Chemical Sensors and Biosensors in Microfluidic Systems, (2012) 59–101.

[140] V.R. Jayaneththi, K. Aw, M. Sharma, J. Wen, D. Svirskis, A.J. McDaid, Controlled transdermal drug delivery using a wireless magnetic microneedle patch: Preclinical device development, Sens Actuators B Chem. 297 (2019) 126708.

[141] Dexamethasone in Hospitalized Patients with Covid-19, New England Journal of Medicine. 384 (2021) 693–704.

[142] R. Akçapınar, E. Özgür, V. Goodarzi, L. Uzun, Surface imprinted upconversion nanoparticles for selective albumin recognition, Colloids Surf A Physicochem Eng Asp. 649 (2022) 129301.

[143] F. Hernández Sánchez, J. Molina Mateo, F.J. Romero Colomer, M. Salmerón Sánchez, J.L. Gómez Ribelles, J.F. Mano, Influence of low-temperatue nucleation on the crystallization process of poly(L-lactide), Biomacromolecules. 6 (2005) 3283–3290.

[144] Y.K. Demir, Z. Akan, O. Kerimoglu, Characterization of Polymeric Microneedle Arrays for Transdermal Drug Delivery, PLoS One. 8 (2013) e77289.

[145] E. Larrañeta, J. Moore, E.M. Vicente-Pérez, P. González-Vázquez, R. Lutton, A.D. Woolfson, R.F. Donnelly, A proposed model membrane and test method for microneedle insertion studies, Int J Pharm. 472 (2014) 65–73.

[146] J. Li, Y. Zhou, J. Yang, R. Ye, J. Gao, L. Ren, B. Liu, L. Liang, L. Jiang, Fabrication of gradient porous microneedle array by modified hot embossing for transdermal drug delivery, Materials Science and Engineering: C. 96 (2019) 576–582.

[147] V. Ghate, A. Renjith, K. Badnikar, S. Pahal, S.N. Jayadevi, M.M. Nayak, P.K. Vemula, D.N. Subramanyam, Single step fabrication of hollow microneedles and an experimental package for controlled drug delivery, Int J Pharm. 632 (2023) 122546.

[148] I. Mansoor, Y. Liu, U.O. Häfeli, B. Stoeber, Arrays of hollow out-of-plane microneedles made by metal electrodeposition onto solvent cast conductive polymer structures, Journal of Micromechanics and Microengineering. 23 (2013) 085011.

[149] H.R. Nejad, A. Sadeqi, G. Kiaee, S. Sonkusale, Low-cost and cleanroom-free fabrication of microneedles, Microsystems & Nanoengineering 2018 4:1. 4 (2018) 1–7.

[150] C. Zhou, H. Tang, L. Zhang, H. An, Y. Wu, D. Tang, J. Zhou, Hollow Microneedle Arrays Produced by Low-Cost, High-Fidelity Replication of Hypodermic Needle Tips for High-Dose Transdermal Drug Delivery, Adv Eng Mater. 23 (2021) 2001355.

[151] R. Ye, J. Yang, Y. Li, Y. Zheng, J. Yang, Y. Li, B. Liu, L. Jiang, Fabrication of Tip-Hollow and Tip-Dissolvable Microneedle Arrays for Transdermal Drug Delivery, ACS Biomater Sci Eng. 6 (2020) 2487–2494.

[152] A. Laurent, F. Mistretta, D. Bottigioli, K. Dahel, C. Goujon, J.F. Nicolas, A. Hennino, P.E. Laurent, Echographic measurement of skin thickness in adults by high frequency ultrasound to assess the appropriate microneedle length for intradermal delivery of vaccines, Vaccine. 25 (2007) 6423–6430.

[153] H.S. Gill, D.D. Denson, B.A. Burris, M.R. Prausnitz, Effect of microneedle design on pain in human volunteers, Clin J Pain. 24 (2008) 585–594.

[154] P.E. Laurent, S. Bonnet, P. Alchas, P. Regolini, J.A. Mikszta, R. Pettis, N.G. Harvey, Evaluation of the clinical performance of a new intradermal vaccine administration technique and associated delivery system, Vaccine. 25 (2007) 8833–8842.

[155] G. Yan, K.S. Warner, J. Zhang, S. Sharma, B.K. Gale, Evaluation needle length and density of microneedle arrays in the pretreatment of skin for transdermal drug delivery, Int J Pharm. 391 (2010) 7–12.

[156] O. Olatunji, D.B. Das, M.J. Garland, L. Belaid, R.F. Donnelly, Influence of Array Interspacing on the Force Required for Successful Microneedle Skin Penetration: Theoretical and Practical Approaches, J Pharm Sci. 102 (2013) 1209–1221.

[157] S.P. Davis, B.J. Landis, Z.H. Adams, M.G. Allen, M.R. Prausnitz, Insertion of microneedles into skin: Measurement and prediction of insertion force and needle fracture force, J Biomech. 37 (2004) 1155–1163.

[158] J.S. Kochhar, T.C. Quek, W.J. Soon, J. Choi, S. Zou, L. Kang, Effect of microneedle geometry and supporting substrate on microneedle array penetration into skin, J Pharm Sci. 102 (2013) 4100–4108.

[159] Á. Cárcamo-Martínez, B. Mallon, J. Domínguez-Robles, A.S. Cordeiro, M. Celentano, E. Larrañeta, S.E.J. Bell, R.F. Donnelly, Plasmonic photothermal microneedle arrays and single needles for minimally-invasive deep in-skin hyperthermia, J Mater Chem B. 8 (2020) 5425–5433.

[160] The grafting and release behavior of doxorubincin from Fe 3 O 4 @SiO 2 core-shell structure nanoparticles via an acid cleaving amide bond: the potential for magnetic targeting drug delivery, (2008).

[161] A.A. Paknahad, M. Tahmasebipour, An electromagnetic micro-actuator with PDMS-Fe3O4 nanocomposite magnetic membrane, Microelectron Eng. 216 (2019) 111031.

[162] A. Borók, K. Laboda, A. Bonyár, PDMS Bonding Technologies for Microfluidic Applications: A Review, Biosensors (Basel). 11 (2021).

[163] C. Wang, J.S. Kim, J. Park, Micro check valve integrated magnetically actuated micropump for implantable drug delivery, TRANSDUCERS 2017 - 19th International Conference on Solid-State Sensors, Actuators and Microsystems. (2017) 1711–1713.

[164] M.M. Said, J. Yunas, B. Bais, A.A. Hamzah, B.Y. Majlis, The Design, Fabrication, and Testing of an Electromagnetic Micropump with a Matrix-Patterned Magnetic Polymer Composite Actuator Membrane, Micromachines 2018, Vol. 9, Page 13. 9 (2017) 13.

[165] R.R. Gidde, P.M. Pawar, B.P. Ronge, V.P. Dhamgaye, Design optimization of an electromagnetic actuation based valveless micropump for drug delivery application, Microsystem Technologies. 25 (2019) 509–519.